Coordination Chemistry Reviews 459 (2022) 214454

Contents lists available at ScienceDirect

Coordination Chemistry Reviews

journal homepage: www.elsevier.com/locate/ccr

Review

A comprehensive compendium of literature of 1,8-Naphthalimide based chemosensors from 2017 to 2021

Nisha Jain, Navneet Kaur *

Panjab University, Chandigarh, Punjab, India

ARTICLE INFO

Article history:
Received 20 November 2021
Accepted 1 February 2022

Keywords:
1,8-naphthalimide
Sensors
Metal ions
Anions
Biomolecules
Fluorescence

ABSTRACT

Intensive development of optical (colorimetric/fluorescent) chemosensors is the landmark of successful research efforts made after the advent of supramolecular chemistry. Amongst different types of molecular scaffolds used, the literature of 1,8-naphthalimide is replete due its remarkable optical, photophysical and biological properties unequalled by other types of receptor units. This comprehensive compendium includes development of 1,8-naphthalimide based sensors during the last 5 years ranging from 2017 to 2021 that involve wide and real-world applications for sensing of metal ions, anions and biomolecules. Simultaneously, we hope that gaining insights into the discussed literature reports will assist the research fraternity working in the area of sensing and will facilitate to develop superlative chemosensors possessing improved practical applications in future.

Contents

Abbreviations: ICT, Intramolecular Charge Transfer; PET, photoinduced electron transfer; FRET, fluorescence resonance energy transfer; AIEQ, aggregation-induced emission quenching; AIEE, aggregation-induced emission enhancement; CHEF, chelation enhanced fluorescence; AIE, aggregation induced emission; LOD, limit of detection.

* Corresponding author at: Department of Chemistry, Panjab University, Chandigarh, India.
E-mail address: neet_chem@pu.ac.in (N. Kaur).

https://doi.org/10.1016/j.ccr.2022.214454
0010-8545/

1. Introduction

The research field of design and synthesis of chemosensors has seen brilliant success since the beginning of 21st century for the selective and sensitive tracking of analytes (cations, anions, biomolecules etc.) [1–7]. Chemosensor is basically a chemical probe consisting of receptor, spacer, photoactive units and capable of converting the changes occurring at molecular level (photophysical variations) into a measurable analytical signal (color or fluorescence change) [8]. The major efforts in this research area involve development of optical (colorimetric/fluorescent) chemosensors as vibrant tools for sensing of various analytes because of number of advantages including facile synthesis, spatiotemporal resolution, high sensitivity and selectivity and easy modification of their structures to cover wide range of absorption/ emission characteristics [9,10]. Designing of a molecular probe depends upon number of factors such as sensitivity (detection limit), specificity (ability to distinguish a particular analyte among others), selectivity (analysis of specific ion pool) [11], photostability [12], solvatofluorochromism [13] and membrane permeability [14].

The derivatives of a number of structural motifs including boron dipyrromethene difluoride (BODIPY), cyanine, rhodamine, coumarin, pyrene, squaraine, fluorescein and 1,8- naphthalimide have been used for the detection of a number of analytes [15,16]. Among these, 1,8-naphthalimide and its derivatives are chemically stable and possess excellent optical, photophysical (emission in red/infrared (IR) region, large Stokes shift, high quantum yield, high two-photon absorption cross-section) (Fig. 1), electrochemical, electroluminescent and thermal properties [17–20]. Among these, high two-photon absorption cross-section is peculiarly advantageous for the purpose of imaging of analytes in bioorganisms as it offers a number of advantages in contrast to conventional one-photon probes viz. minimum interference from background fluorescence, light scattering, self-absorption, photobleaching etc., causes less tissue injury along with improved three-dimensional spatial localization, penetration depth, resolution and observation time [21–24]. Furthermore, its photophysical properties can be fine-tuned by varying the substituents on aromatic ring and via π-stacking of the aromatic rings [25,26]. These fascinating properties of 1,8-naphthalimide based derivatives make them excellent candidates for displaying wide variety of applications in the area of bioorganic chemistry, analytical chemistry, materials chemistry, biological and medical science communities etc. [27] and are used as metal ion sensors [28], pH sensors [29,30], cellular imaging agents [31], optoelectronic materials [32], light emitting diodes [33] and solar energy collectors [34]. Various mechanisms responsible for the sensory properties of 1,8-naphthalimide based derivatives include PET [35], ICT [36], FRET [37] and AIEQ/AIEE [38] etc. Apart from these, naphthalimides exhibit remarkable pharmacological properties so they are used as key scaffolds in a number of anti-inflammatory, antiprotozoal, antimicrobial, antitumor and antidepressant agents etc. [39,40]. Based on plethora of advantages offered by 1,8-naphthalimide moiety, large number of derivatives based on this moiety have been synthesized and applied for the sensing of different kinds of analytes.

Literature survey revealed that mainly two techniques are employed for the detection of analytes by using 1,8-naphthalimide based chemosensors which include binding site-signalling subunit approach and chemodosimeter approach. For cations and anions, majority of the chemosensors employ binding site-signalling subunit approach, in which analyte interacts with the binding subunit via electrostatic interactions, hydrogen bonding and van der Waals forces etc. Signaling subunit then converts chemical change occurring at molecular level into signal (color or fluorescence change) (Fig. 2) [41].

In the chemodosimeter approach, after interaction of the probe with an analyte, some bonds are broken and some new bonds are formed leading to the formation of chemically transformed molecule, having different optical properties than the initial probe (Fig. 3) [42].

Encouraged by the remarkable role of 1,8-naphthalimide in the area of supramolecular chemistry, it is no wonder that a number of research articles and further review articles accentuating the role of 1,8-naphthalimide based probes for the detection of a number of analytes in a diverse variety of samples and living organisms

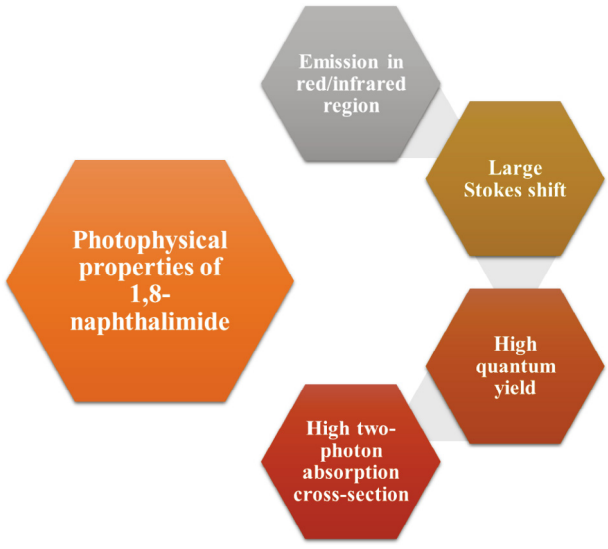

Fig. 1. Photophysical properties of 1,8-naphthalimide.

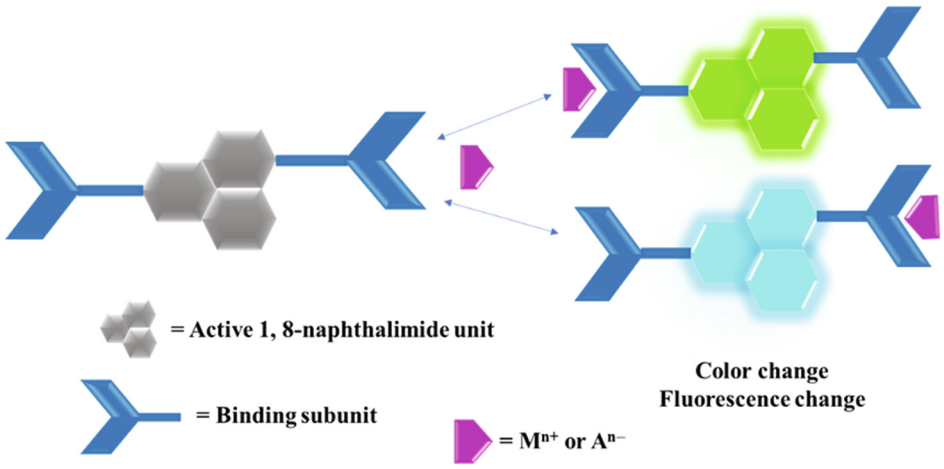

Fig. 2. Pictorial representation of binding of chemosensor with cation and anion (Binding site-signalling subunit approach).

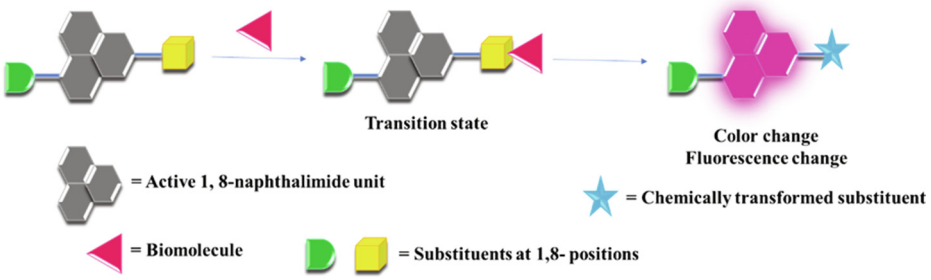

Fig. 3. Diagrammatic representation of binding of probe with biomolecule (Chemodosimeter approach).

have been published [27,43–46]. However, some of these review articles are restricted only to the sensing applications of 1,8-naphthalimide having substitution at a particular position eg. 4-amino-1,8-naphthalimide, 4-hydroxy-1,8-naphthalimide etc. and deal with the sensing of subcellular organelles, enzymes, reactive oxygen species, reactive nitrogen species, reactive sulfur species and neutral molecules etc. [43–45]. Only a limited number of review articles are available in the last three years which deal with the sensing of metal ions, anions and biomolecules and in those too, only a limited number of these analytes are covered [27]. Furthermore, majority of the reviews published till date in this area cover only fluorescent chemosensors based on 1,8-naphthalimide [27,43–46]. The present review deals with all the 1,8-naphthalimide based chemosensors having wide range of structural modifications and covers all the metal ions, anions and biomolecules which have been detected by these in the time period of 2017–2021 covering all kinds of optical changes that involve wide and real-world applications. The review is mainly divided into four categories on the basis of type of analyte sensed (metal ions, anions and biomolecules) (Fig. 4).

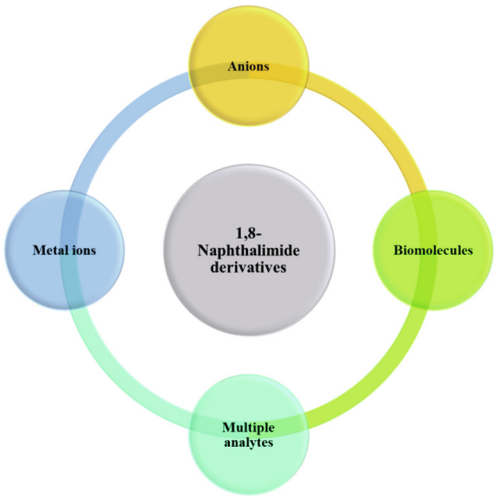

Fig. 4. Different types of analytes analyzed in the present review.

2. Metal ion sensors

Metal ions are widely present in all life forms as they are indispensable for a plethora of biological, chemical and environmental processes [44]. From the physiological point of view, the metal ions are divided into two major categories viz. essential metal ions (Na^+, K^+, Mg^{2+}, Ca^{2+}, Zn^{2+}, $Fe^{2+/3+}$ etc.) and nonessential or toxic metal ions (Hg^{2+}, Cd^{2+}, As^{3+}, Pb^{2+} $Cr^{3+/6+}$, Ni^{2+}, Co^{2+}, etc.) [47]. The natural sources for generation of non-essential metal ions include volcanic activity, metal evaporation from soil and water, soil erosion and geological weathering etc. and other sources include anthropogenic activities such as mining the metal, smelting, foundries, leaching of metals from landfills, waste dumps, livestock and chicken manure, runoffs, automobiles and roadworks etc. [48]. The essential metal ions play crucial role in many biological processes such as regulation of deoxyribonucleic acid (DNA) transcription, intra- and intercellular communication, oxygen transport, proper functioning of nerve cells, photosynthesis and electron

transfer processes etc., however, it has been found that essential metals can be as harmful as non-essential metals if present in excess concentration [49]. Therefore, detection of metal ions has gained considerable attention and has encouraged researchers to synthesize various colorimetric and fluorimetric sensors for their detection at trace levels.

Rapid progress in the supramolecular chemistry over the recent years have befallen incredible improvements in the sensitivity and working medium of the sensors. With continuous structure modifications in naphthalimide moiety, it has been possible to achieve LOD values in the nanomolar range for various metal ions [50–58]. Also, efforts have been carried out in order to impart water solubility to sensing probes and as a result, a number of naphthalimide based probes have been capable to quantify metal ions in pure aqueous medium [59–70]. Furthermore, despite the unpredictability and complexity of environmental and biological samples, several probes have been successful in quantifying the metal ions in real water samples [50,54,57,61,71–87] and living cells [52,54,58–64,67,76,77,82,84,88–96]. Another challenge in the field of chemosensing is the applicability of the chemosensors for on-site detection of metal ions which has limited the sensing field in laboratory only, only a limited number of examples have been found in the last 5 years which have enabled on-site detection of metal ions using paper strips [52,61,65,75–77,97] and smartphone linked sensors [98]. Therefore, attention need to be paid to the development of sensing devices or other strategies for the on-site detection of metal ions.

2.1. Alkaline earth metal (Calcium (Ca^{2+}) and magnesium (Mg^{2+})) ions

Zhang and group reported a fluorescence *turn-on* probe **1** (Fig. 5) for the selective tracking of Ca^{2+} ions with the detection limit down to 0.270 μM [88]. On addition of Ca^{2+} ions to the HEPES:CH_3CN (1:9, v/v, pH = 7.4) solution of **1**, the absorption peak shifted from 375 to 406 nm and in the fluorescence spectrum, 4.5 fold enhancement in fluorescence intensity was observed along with slight blue shift from 537 to 525 nm. These changes were ascribed to the coordination of Ca^{2+} ions with **1** in 1:1 binding ratio with the association constant of 2.05×10^5 M^{-1} (Fig. 6). From the pH dependence studies, it was found that probe **1** worked well in the pH range of 4 to 11. Moreover, the probe **1** was efficiently utilized for the intracellular detection of Ca^{2+} ions in HeLa cells.

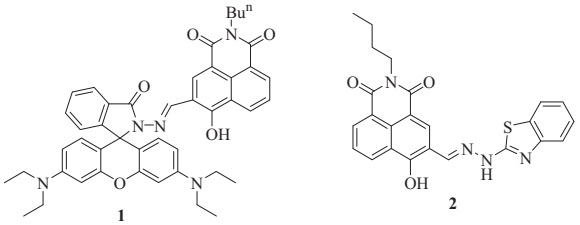

Fig. 5. Structures of chemosensors **1–2.**

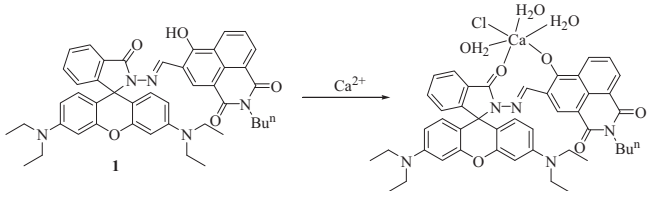

Fig. 6. Proposed mechanism of binding of Ca^{2+} with **1.**

A 1,8-naphthalimide based fluorescent chemosensor **2** (Fig. 5) was synthesized and utilized for the detection of Mg^{2+} ions by Zhang et al. [99]. Addition of Mg^{2+} ions to the ethanolic solution of **2** resulted in 15-fold enhancement in fluorescence intensity at 523 nm along with fluorescence color change from colorless to bright yellow green. These changes were ascribed to the coordination of Mg^{2+} with hydroxyl group and N atom of C = N in 2:1 (**2**.Mg^{2+}) binding ratio (Fig. 7), which was confirmed by proton nuclear magnetic resonance spectroscopy (^{1}H NMR), electrospray ionisation mass spectrometry (ESI-MS) and density functional theory (DFT) calculations. Competition experiments revealed that other competitive ions did not interfere with the detection of Mg^{2+} ions. The detection limit and association constant (K_a) for **2**.Mg^{2+} were measured to be 5.01×10^{-8} M and 6.17×10^5 M^{-1}, respectively. Furthermore, the proposed sensor **2** efficiently detected Mg^{2+} ions in A549 cells based on low cytotoxicity.

2.2. Aluminium (Al^{3+}) ions

Kang et al. synthesized a 1,8-naphthalimide based Schiff base, **3** (Fig. 8), for the selective sensing of Al^{3+} ions in methanol, where

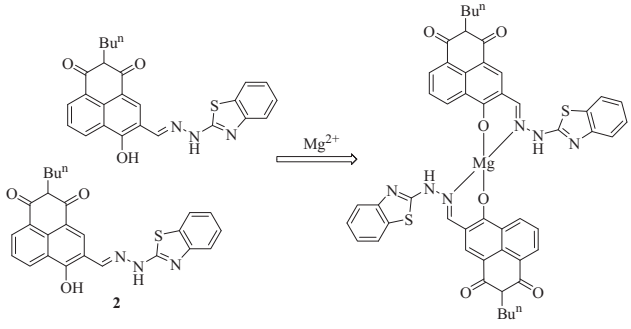

Fig. 7. Proposed mode of binding of Mg^{2+} with **2.**

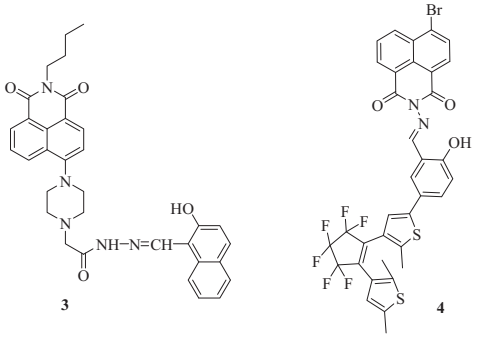

Fig. 8. Structures of chemosensors **3–4.**

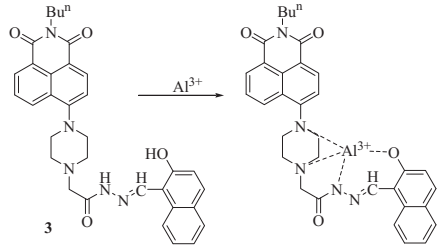

Fig. 9. Mode of interaction of Al^{3+} with **3.**

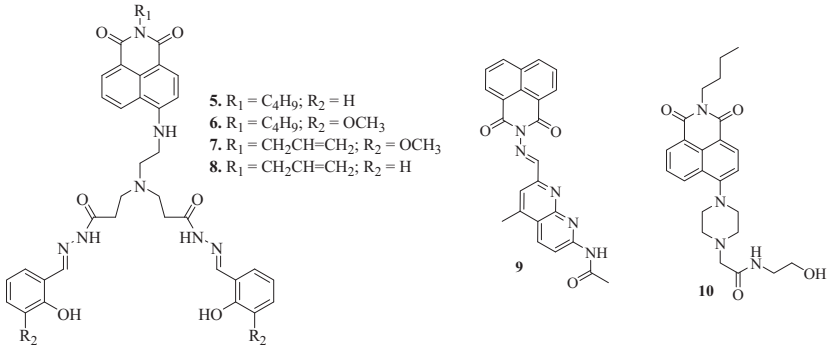

Fig. 10. Structures of chemosensors **5**–**10.**

39-fold enhancement in emission intensity along with blue shift in emission peak from 524 to 508 nm was observed with addition of Al^{3+} ions [50]. These changes were accompanied by fluorescence color change from pale yellow to bright green when observed under 365 nm UV light, which was considered to be due to inhibition of ICT and CHEF processes. The presence of Al^{3+} ions also caused changes in absorption spectrum with visual color change from brown yellow to colorless. ^{1}H NMR and ESI Mass spectra suggested binding of Al^{3+}ions to **3** via oxygen atom of hydroxyl group and nitrogen atoms of amide group and piperazine in 1:1 binding stoichiometry (Fig. 9). Detection limit and association constant were measured to be 7.4 nM and 1.62 $\times$ 10^4 M^{-1}, respectively. To ensure the practical utility of the synthesized chemosensor, it was applied for the detection of Al^{3+} ions in tap water and excellent recoveries in the range of 100.00–100.10 % were observed.

Li et al. reported a fluorescent chemosensor, **4** (Fig. 8), based on a photochromic diarylethene with naphthalimide unit [97]. Irradiation of **4** with 297 nm light led to decrease of emission intensity and fluorescent color change from orange-yellow to dark yellow because of formation of closed-ring isomer. The emission peak in the fluorescence spectrum of **4** at 546 nm was red shifted to 590 nm along with>20-fold increase in emission intensity upon addition of Al^{3+} ions and fluorescence color changed from dark to orange-yellow. These changes were ascribed to the inhibition of isomerization of C = N, internal charge transfer and CHEF processes in the complex **4**.Al^{3+}. ESI–MS and ^{1}H NMR titration experiment indicated the involvement of –OH and N atom of azomethine in complexation with Al^{3+}. The binding stoichiometry, association constant and LOD value were found to be 1:1, 2.55 $\times$ 10^5 M^{-1} and 1.75 $\times$ 10^{-7} M.

The fluorescent *turn-on* sensors, (**5**–**8**) (Fig. 10), containing 1,8-naphthalimide as the fluorophore and Schiff base as the binding site were synthesized for the detection of Al^{3+} ions in aqueous media [71–74]. All the chemosensors, (**5**–**8**), underwent significant changes in their absorption and fluorescence spectrum with addition of Al^{3+} ions (Table 1). These changes were attributed to the $\pi \rightarrow \pi$ transition, inhibition of PET process and CHEF process because of complexation with Al^{3+} ions in 1:1 stoichiometry. Job's plot, ^{1}H NMR titrations and other experimental studies indicated coordinative sites to be N atoms of imine and tertiary amine in the sensors for Al^{3+} binding (Fig. 11).

Schiff base based on 1,8-naphthyridine and naphthalimide **9** (Fig. 10) was synthesized by **Yue** and co-workers and utilized it as a chemosensor for the detection of Al^{3+} ions [100]. Addition of Al^{3+} ions to the solution of **9** resulted in increase in the intensity of absorption peaks at 318, 333 and 356 nm; while the absorption peak at 380 nm decreased in intensity. In the fluorescence spectrum, enhancement in fluorescence was observed at 414 nm in the presence of Al^{3+} ions. These changes were ascribed to the inhibition of PET process due to coordination of Al^{3+} with sensor **9** via nitrogen atoms of 1,8-naphthyridine ring & the CN group and oxygen atom of the carbonyl group (Fig. 12). The association constant and detection limit for **9**.Al^{3+}(1:1) were measured to be 5.64 $\times$ 10^4 M^{-1} and 0.13 μM, respectively.

Li and group reported naphthalimide based naked eye fluorescent *turn-on* sensor, **10** (Fig. 10), that detected Al^{3+} ions over other competitive ions [75]. Addition of Al^{3+} ions to the solution of **10** caused a blue shift in the absorption peak from 400 to 373 nm along with color change from greenish-yellow to colorless. Similarly, blue shift from 520 to 504 nm was observed in fluorescence emission spectrum with significant enhancement in emission intensity after addition of Al^{3+} ions and fluorescence color changed from dark green to bright green. These changes were attributed to the combined effects of ICT and CHEF processes, when coordination of Al^{3+} ions occurred via two nitrogen atoms of piperazine ring, nitrogen atom of amide group and oxygen atom of hydroxyl group (Fig. 13). Detection limit and association constant was measured to be 0.159 μM and 6.37 $\times$ 10^4 M^{-1} respectively.

Another naphthalimide based ratiometric and reversible fluorescent sensor **11** (Fig. 14) was synthesized by **Li** and co-workers and they also detected Al^{3+} ions with the detection limit as low as 0.29 μM [89]. The free sensor exhibited fluorescence emission peak at 518 nm, which was blue shifted to 475 nm along with increase in emission intensity, causing fluorescence color change

Table 1
Solvent system, stability over pH range, fluorescence changes, mechanism, stoichiometry (Ligand:Analyte), K_a* and LOD* values observed in chemosensors (**5**–**8**) upon complexation with Al^{3+} ions.

Sensor	Solvent system	Stability over pH range	Fluorescence changes	Mechanism	Stoichiometry	K_a ($\times$ 10^4 M^{-1})	LOD (μM)	Ref.
5	Methanol-Tris (1:1, v/v, Tris buffer, 5 mM)	5.0–8.0	17-fold enhancement at 534 nm	PET, CHEF	1:1	5.49	0.178	[71]
6	DMF:HEPES (1:1, v/v)	5.0–8.0	Enhancement at 531 with 8 nm blue shift	PET, CHEF	1:1	4.95	0.00865	[72]
7	DMF:HEPES (1:1, v/v)	4.51–10.56	8-fold enhancement at 528 nm	PET, CHEF	1:1	1	0.0034	[73]
8	Tris-HCl buffer (1:1, v/v)	4.51–9.55	Enhancement at 527 nm	PET, CHEF	1:1	2.6	0.34	[74]

*K_a and LOD values have been determined by observing fluorescence changes.

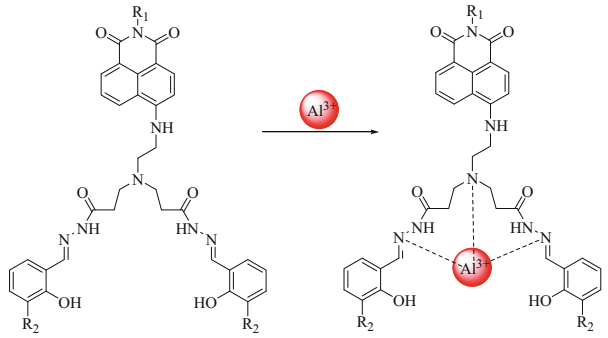

Fig. 11. Schematic representation of Al^{3+} binding with chemosensors **5–8.**

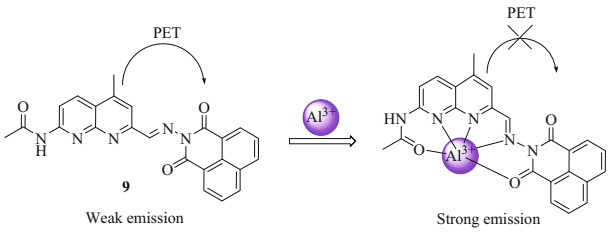

Fig. 12. Possible mechanism of Al^{3+} sensing by chemosensor **9.**

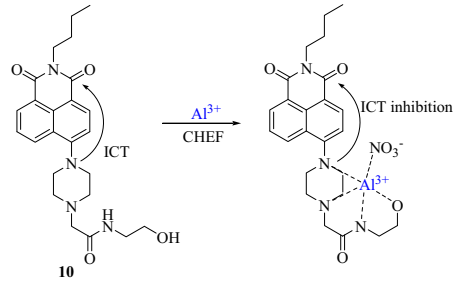

Fig. 13. Possible mode of interaction of Al^{3+} with chemosensor **10.**

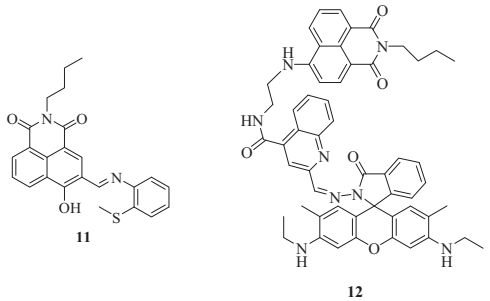

Fig. 14. Structures of chemosensors **11–12.**

from green to blue in UV light upon addition of Al^{3+} ions. Combined results of DFT study and Job's plot indicated 1:1 binding stoichiometry in **11**.Al^{3+} in which binding of **11** to Al^{3+} occurred through N, O and C atoms.

Qin et al. synthesized rhodamine-naphthalene conjugate **12** (Fig. 14), which detected Al^{3+} ions selectively with LOD value of 0.447 μM due to FRET process coupled with ICT process [101]. On addition of Al^{3+} ions to the ethanolic solution of **12**, ratio of fluorescence emission at 524 and 550 nm increased from 0.6 to 4.5 along with fluorescence color change from green to yellow. In addition to this, Al^{3+} ions caused blue shift in fluorescence emission at 524 nm along with enhancement in emission intensity at 550 nm due to ring opening caused by Al^{3+}, which turned the sensor into a donor–acceptor system (Fig. 15).

2.3. Iron (Fe^{3+}/Fe^{2+}) ions

Three 1,8-naphthalimide based sensors **(13a-c)** (Fig. 16) were synthesized by **Liu et al.** based on glycosylation strategy using click chemistry that detected Fe^{3+} ions by observing changes in their fluorescence spectra and order of selectivity towards Fe^{3+} was found to be **13c > 13b > 13a** [59] (Table 2). This was attributed to the fact that **13b** and **13c** had better water solubility as compared to **13a**. Binding stoichiometry in **13c**.Fe^{3+} was found to be 1:2 in which one equivalent of Fe^{3+} was bound to nitrogen atom of piperazine leading to inhibition of PET process and the other equivalent to glycosyl moiety.

Similar sensor **14** (Fig. 16) was synthesized by **Dwivedi** and coworkers for the fluorimetric detection of Fe^{3+} ions (Table 2) [76]. Binding stoichiometry in **14**.Fe^{3+} was found to be 1:1 in which Fe^{3+} was bound to S atom of thiophene and N atoms of most favorable boat conformation of piperazine units. Moreover, cellulose tests trips based on **14** were prepared, which efficiently detected the presence of Fe^{3+} ions. The sensor **14** was also used as a sequential logic circuit as addition of acetate ions regenerated the free sensor leading to *"off–on-off"* switching mechanism.

A *turn-on* fluorescent sensor, **15** (Fig. 16) , based on 1,8-naphthalimide was synthesized by **Tang** and group [51] for the determination of Fe^{3+} ions in DMF/H_2O (3:1, v/v) solution, where N atoms of pyridine and piperazine moieties of **15** acted as binding sites for Fe^{3+} and enhanced the fluorescence by blocking the PET process (Table 2).

Biswas et al. synthesized naphthalimide based sensor **16** (Fig. 16) containing catechol and morpholine for the detection of lysosomal iron [60]. Addition of Fe^{3+} ions led to quenching of fluorescence due to reversed PET process (Table 2). Based on good cell permeability and low cellular toxicity of **16**, it was used for live-cell imaging and efficiently detected lysosomal Fe^{3+} pool.

Yildirim et al. synthesized naphthalimide based probe **17** (Fig. 16) and further developed two cellulose based sensing materials Cel-**17** and PCel-**17** for the detection of Fe^{3+} ions [102]. In the absorption spectrum carried out in ethanol/CH_3CN (1:1, v/v) solution, intensity of the absorption peak at 350 nm increased and new peak appeared at 359 nm upon addition of Fe^{3+} ions to acetonitrile solution of Cel-**17**; while its addition caused significant quenching in fluorescence at 440 nm along with fluorescence color change from bright turquoise to yellow–brown. These changes in the absorption and emission spectrum were ascribed to the binding of paramagnetic Fe^{3+} ions to the donor atoms (O and N) in **17**. In the powder form, upon incorporation of Fe^{3+} ions, the yellow powder turned dark yellow in daylight and bright yellow color turned orange, when observed under UV light. In the presence of Fe^{3+} ions, the gray-white color of PCel-**17** changed to white in daylight and turned from yellow to black under UV light.

Hladysh et al. synthesized 1,8-naphthalimide based simple dye, **18** (Fig. 17), and its poly(3-hexylthiophene) (PHT) based conjugated polymer, **PHT-18** (Fig. 17), which were used for the detection of Fe^{2+} ions [103]. Addition of Fe^{2+} ions to the chloroform/methanol (10:1) solution of **18** slightly blue shifted the absorption band at 396 nm. In the case of **PHT-18**, absorption peak at 405 nm was shifted to 420 nm along with the appearance of two isobestic points at 340 and 415 nm. It was found that quenching of lumines-

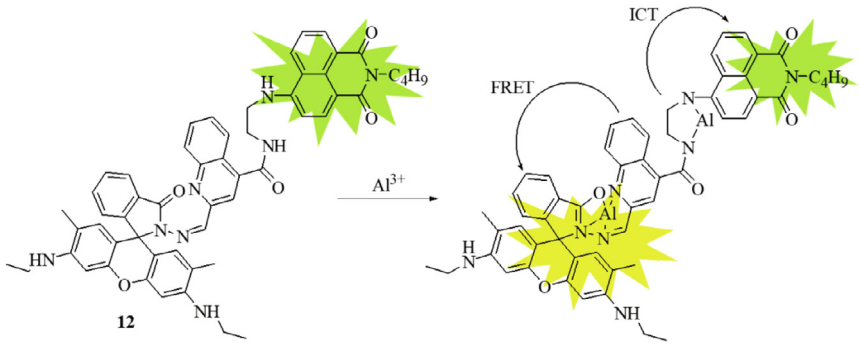

Fig. 15. Ring opening of rhodamine moiety of **12** upon Al^{3+} coordination.

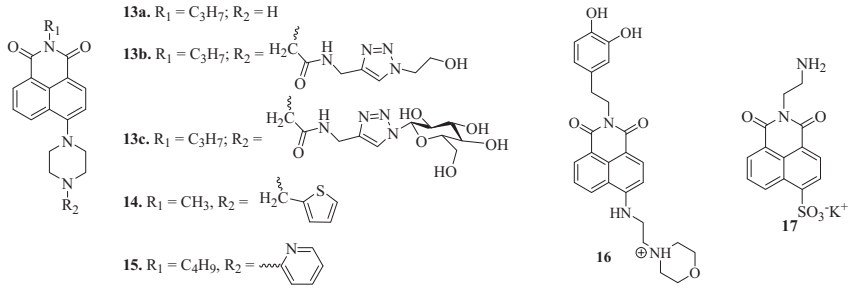

Fig. 16. Structures of chemosensors **13–17.**

Table 2
Solvent system, fluorescence changes, mechanism, stoichiometry (Ligand:Analyte), LOD* and K_a* values observed in chemosensors (**13–16**) upon complexation with Fe^{3+} ions.

Sensor	Solvent system	Fluorescence changes	Mechanism	Stoichiometry	LOD (μM)	K_a ($\times 10^3$ M^{-1})	Ref.
13a	Phosphate buffer	Enhancement at 528 nm	PET	1:2	7.40	–	[59]
13b	Phosphate buffer	–	PET	–	0.273	–	[59]
13c	Phosphate buffer	–	PET	–	0.00427	–	[59]
14	40% H_2O-THF	Enhancement at 528 nm with blue shift of 12–14 nm	PET	1:1	0.373	22	[76]
15	DMF:H_2O (3:1)	15.8 fold enhancement at 530 nm	PET	1:1	0.081	4.41	[51]
16	10 mM MES buffer	Quenching at 542 nm	PET	1:1	0.5	36	[60]

*K_a and LOD values have been determined by observing fluorescence changes.

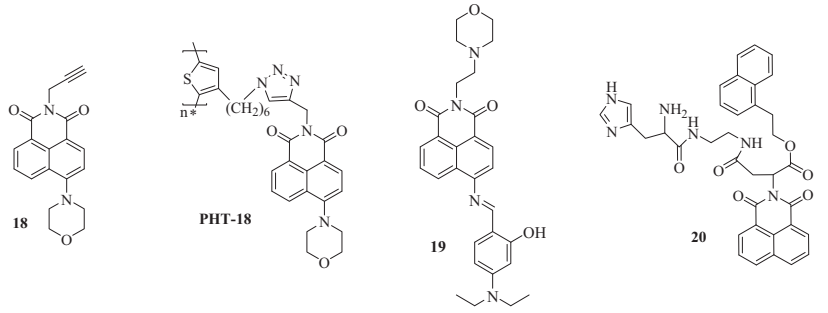

Fig. 17. Structures of chemosensors **18–20.**

cence in **PHT-18** polymer was more efficient than the free luminescent dye **18**. The polymer **PHT-18** exhibited improved sensing ability and extended working range as compared to **18**. Association constant of Fe^{2+} with **PHT-18** was found to be significantly more than that of **18** and detection limit of **PHT-18** was found to be 100 times lower than that of **18**.

A naphthalimide based Schiff base **19** (Fig. 17) was synthesized by **Jothi** and co-workers for the detection of Fe^{3+} ions [77]. Free sensor **19** exhibited absorption peaks at 344 and 430 nm in acetonitrile: water (7:3, v/v) solution. However, after addition of Fe^{3+} ions, new peak appeared at 360 nm along with 30-fold increase in molar absorptivity, attributed to the strong ICT transition and absorption caused by hindered isomerization at C=N due to binding with Fe^{3+}. In the fluorescence spectrum, quenching of fluorescence was observed at 531 nm on adding Fe^{3+} ions. The association constant and LOD for **19**.Fe^{3+} (1:1) stoichiometric

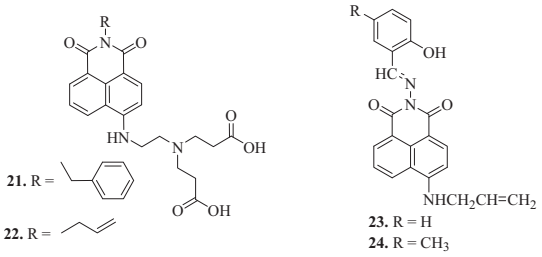

Fig. 18. Structures of chemosensors **21**–**24.**

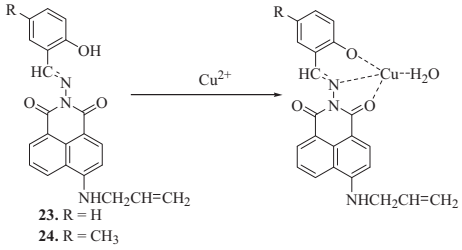

Fig. 19. Mechanism of binding of Cu^{2+} with chemosensors **23**–**24.**

complex were found to be 2.49 × 10^4 M^{-1} and 0.81 μM, respectively. IR spectroscopy and liquid chromatography–mass spectrometry (LC-MS) analysis indicated the binding of Fe^{3+} ions to **19** via coordination with C=N and –OH functional groups. The proposed sensor **19** was successfully used for developing molecular logic function, bioimaging analysis in *Escherichia coli* (*E. coli*) and detection of Fe^{3+} ions in different water bodies, thus highlighting its practical utility.

Sarkar and group synthesized fluorescent organic nanoparticles (FONPs) from naphthalimide based histidine appended amphiphile **20** (Fig. 17) for the selective sensing of Fe^{3+} ions over other competitive ions [90]. The FONPs were formed due to self-assembly of **20** in 99 vol% water in DMSO via J-type aggregation. Due to complex formation between Fe^{3+} and histidine residue of the **20** amphiphile, decrease in emission intensity was observed after addition of 10 μM Fe^{3+} ions to the DMSO-water (fw = 99 vol%) solution of **20**-FONPs. The quenching of bluish-green fluorescence after addition of Fe^{3+} was ascribed to the combined effects of size compatibility and paramagnetic nature of Fe^{3+}, which led to chelation enhanced quenching (CHEQ) effect. Job's plot indicated 1:1 binding stoichiometry between **20**-FONPs and Fe^{3+} ions and morphology of the FONPs changed from spherical to spindle after complex formation. The LOD value of **20**-FONPs for Fe^{3+} was found to be 12.5 ± 1. 2 mM and selectivity study revealed that other ions were not able to quench the fluorescence. Furthermore, it was found that fluorescence was not recovered after addition of several Fe^{3+} chelating agents like 2-aminopyridine, citric acid, L-Dopa, ethylenediamine tetraacetic acid (EDTA), folic acid and glycine, thus indicating strong binding between Fe^{3+} and **20**-FONPs. Further experiments were conducted to evaluate the cytotoxicity of **20**-FONPs against mammalian cells (NIH3T3, B16F10) and due to very low cytotoxicity, these were used for bioimaging of Fe^{3+}. Keeping in consideration the varying oxidative stress inside cells, **20**-FONPs were employed to detect Fe^{2+} to Fe^{3+} redox state transition inside cancer cells (B16F10).

2.4. Copper (Cu^{2+}) ions

Various fluorescence *turn-off* sensors derived from 1,8-naphthalimide employing "fluorophore-spacer-receptor" convention and based on PET mechanism (**21**–**26**) (Figs. 18, 20) were synthesized for the recognition of Cu^{2+} ions with LOD values in the range of μM (Table 3) [104,78,79,105,106,52]. **21** and **22** showed binding with Cu^{2+} through nitrogen atoms of ethane diamine and oxygen atom of carboxyl group to form **21/22**.Cu^{2+} (1:1) complex. Furthermore, reverse-PET mechanism *i.e.* electron transfer from the 1,8-naphthalimide moiety to electron deficient carboxyl group by metal ion complexation was attributed for fluorescence quenching.

The Schiff base possessing sensors **23** and **24** displayed quenching in fluorescence due to complexation of Cu^{2+} with N atom of the C=N group and O atom of the hydroxyl oxygen group (Fig. 19). Sensors **25** (Fig. 21) and **26** (Fig. 22) showed similar type of fluorescence quenching upon addition of Cu^{2+} ions (Table 3).

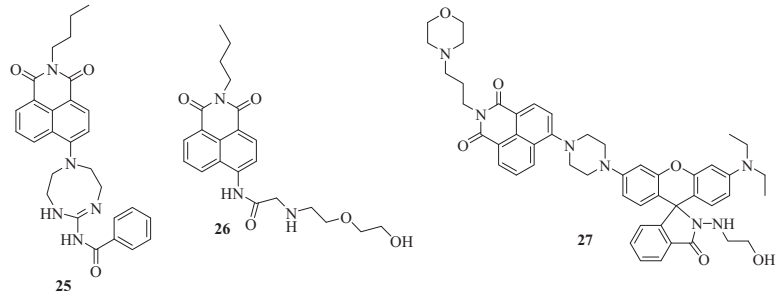

Fig. 20. Structures of chemosensors **25**–**27.**

Table 3
Solvent systems, fluorescence changes, mechanism, stoichiometry (Ligand:Analyte), K_a* and LOD* values of sensors (**21**–**26**) on complexation with Cu^{2+} ions.

Sensor	Solvent	Fluorescence quenching at (nm)	Mechanism	Stoichiometry	K_a (×10^6 M^{-1})	LOD (μM)	Ref.
21	HEPES- DMSO (v/v, 1:1)	529	PET	1:1	1.37	0.0169	[104]
22	HEPES- DMSO (v/v, 1:1)	532	PET	1:1	1.14	0.0467	[78]
23	Tris-HCl /DMF (1:1, v/v)	539	PET	1:1	1.088	0.32	[79]
24	Tris-HCl -DMF (1:1, v/v)	539	PET	1:1	1.328	0.23	[105]
25	EtOH/H_2O (4:1, v/v)	447	PET	1:1	0.0157	–	[106]
26	DMF/HEPES (1/9, v/v)	463	PET	1:1	–	0.00049	[52]

*K_a and LOD values have been determined by observing fluorescence changes.

A FRET based naphthalimide-rhodamine platform **27** (Fig. 20) was synthesized by **Liu** and group for the detection of Cu^{2+} in H_2O-CH_3CN (2:1, v/v) solution by displaying changes in its absorption as well as fluorescence spectrum [53]. The free sensor **27** exhibited absorption and emission peaks at 405 and 519 nm, respectively and on addition of Cu^{2+} ions, a new absorption peak emerged at 548 nm and emission peak shifted from 519 to 580 nm. These changes were ascribed to the hydrolysis of spirolactam to form open ring xanthene as well as FRET process occurring from the donor to the Cu^{2+} triggered ring-opened rhodamine acceptor. The detection limit of **27** was measured to be 1.45 nM. The proposed sensor **27** was also used for the lysosomal imaging of Cu^{2+} ions in living cells.

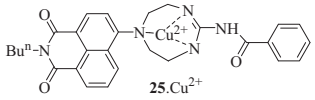

Fig. 21. Representation of binding of Cu^{2+} with **25.**

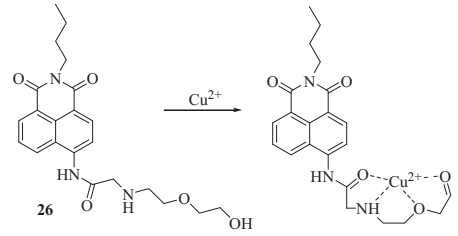

Fig. 22. Possible mode of binding of Cu^{2+} with chemosensor **26.**

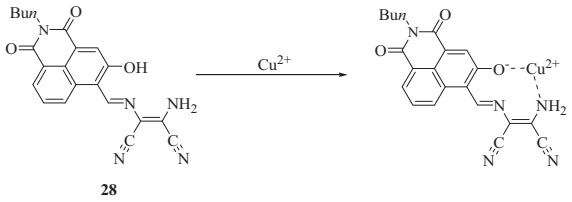

Fig. 23. Binding mode between **28** and Cu^{2+}.

Chang et al. synthesized a naphthalimide based Schiff base, **28**, for the colorimetric detection of Cu^{2+} in simulated semiconductor wastewater [98]. After adding Cu^{2+} ions to the DMSO solution of **28**, the strong absorption band located at 457 nm was red shifted to 565 nm with naked eye color change from yellow to pink. Job's Plot suggested 1:1 binding stoichiometry between **28** and Cu^{2+} (Fig. 23). The detection limit for Cu^{2+} in DMSO was found to be 1.6×10^{-6} M and association constant as calculated from DynaFit curve-fitting program came out to be 5.9×10^4 M^{-1}. Also, selective liquid–liquid extraction of aqueous Cu^{2+} over other metal ions was possible using ethyl acetate. Furthermore, **28** was found to be efficient for extractive signaling of Cu^{2+} in simulated semiconductor wastewater using smartphone as a colorimetric data capture and analysis tool.

Various 1,8-naphthalimide possessing hydrazone derivatives, (**29**–**32**) (Fig. 24), were synthesized for detection of Cu^{2+} ions (Table 4) [91,80,107,54]. Sensor **29** underwent absorption, color and fluorescent changes with addition of Cu^{2+} ions that were ascribed to its hydrolysis via Cu^{2+} promoted electrophilic substitution mechanism, which was confirmed by ESI-MS, Fourier Transform-Infrared spectroscopy (FT-IR) analysis, X-ray diffraction studies and DFT calculations [91]. Also, the probe **29** was successfully used for the fluorescent imaging of Cu^{2+} in HeLa cells.

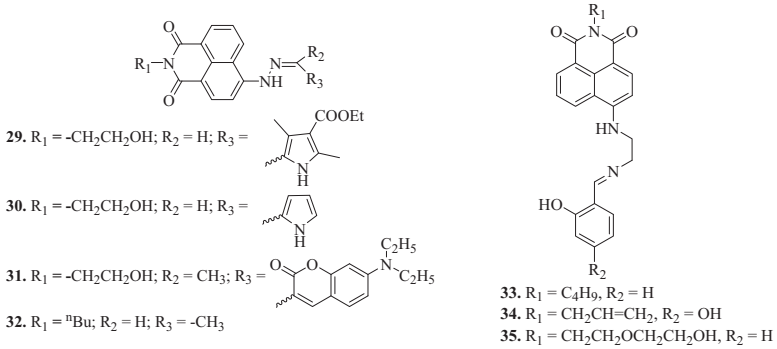

Fig. 24. Structures of chemosensors **29**–**35.**

Table 4
Solvent systems, absorption changes, fluorescence changes, mechanism, stoichiometry (Ligand:Analyte), K_a* and LOD* values of sensors (**29**–**35**) on complexation with Cu^{2+} ions.

Sensor	Solvent	Absorption changes (nm)	Fluorescence changes (nm)	Mechanism	Stoichiometry	K_a ($\times 10^4$ M^{-1})	LOD (μM)	Ref.
29	CH_3CN-H_2O (v/v = 9:1)	480, 335 → 380	620 → 545	–	1:1	–	1.5	[91]
30	CH_3CN - H_2O (v/v = 3:7	485 → 435	550 → 535	PET	1:2	–	0.713	[80]
31	CH_3OH– H_2O (v/v = 9:1)	–	Quenching at 4d41 nm (0–0.5 equivalent) Enhancement at 462 and 570 nm (>0.5 equivalent)	CHQF & PET	–	5.55	0.0390 (0–0.5 equivalent) 0.326 (for > 0.5 equivalent)	[107]
32	CH_3CN-HESPS (4:1, v/v)	437 → 350	Quenching at 550 nm	–	1:1	2.833	0.00032	[54]
33	CH_3CN-HESPS (1:1, v/v)	–	Quenching at 524 nm	Reverse PET	2:1	4.76×10^7	0.033	[108]
34	DMF/Tris-HCl (1:1, v/v)	Decrease at 431 nm	Quenching at 526 nm	Reverse PET	2:1	4×10^8	0.0192	[109]
35	Phosphate buffer	434 → 440 and decrease at 258	Quenching at 532 nm	PET	2:1	–	0.00374	[61]

*K_a and LOD values have been determined by observing fluorescence changes.

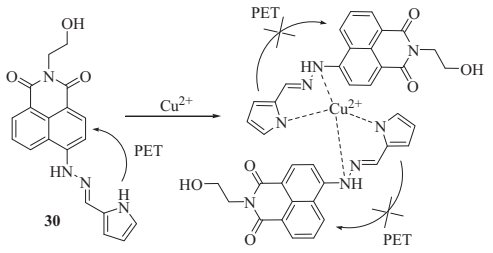

Fig. 25. Possible mechanism of Cu^{2+} sensing by chemosensor **30.**

Another hydrazone 1,8-naphthalimide-based derivative, **30**, synthesized *via* facile condensation and substitution reactions, displayed blue shift in both the absorption and emission bands on addition of Cu^{2+} ions (Table 4) [80]. Upon complexation with Cu^{2+}, electron transfer process (PET) from electron-rich unit (pyrrole group) to the fluorophore (naphthalimide unit) was prohibited, which led to increase in fluorescence. Cu^{2+} was found to bind with **30** in 2:1 stoichiometry, in which Cu^{2+} was coordinated to N atoms of pyrrole and naphthalimide's amine (Fig. 25).

The chemosensor **31** bearing coumarin moiety exhibited different behaviour towards Cu^{2+} ions in different equivalence ranges [107]. The sensor displayed *turn-off* response towards Cu^{2+} in equivalence range of 0 to 0.5 due to complexation of **31** with Cu^{2+} ions, which led to chelation induced quenching of fluorescence (CHQF) mechanism via a photoinduced electron or energy transfer process from metal to fluorophore. In case of equivalence less than 0.5, 2:1 complex was formed between probe and Cu^{2+} in which Cu^{2+} was coordinated to the oxygen atoms of hydroxyl and carbonyl groups. In the equivalence range above 0.5, increase in fluorescence intensity at 462 and 570 nm was observed on addition of Cu^{2+} ions (Table 4) (Fig. 26).

Fu et al. synthesized 1,8-naphthalimide based sensor **32** for the detection of Cu^{2+} ions with the detection limit as low as 320 nM (Table 4) [54]. Addition of Cu^{2+} ions to solution of **32** led to significant quenching of fluorescence due to coordination of Cu^{2+} with N atoms of amino group, leading to the formation of three-membered heterocycles in **32**. Cu^{2+} which was further hydrolyzed to simpler moieties (Fig. 27). Furthermore, it was found that **32** efficiently detected Cu^{2+} in real water samples and lysosomes of 293 T cells.

Three fluorescence *turn-off* sensors, (**33**–**35**) (Fig. 24), for Cu^{2+} ions with 1,8-naphthalimide as the chromophore and a Schiff base as the recognition group were synthesized, in which reverse-PET mechanism (electron transfer from the 1,8-naphthalimide moiety to electron deficient C=N group) was found to be responsible for fluorescence quenching (Table 4) [108,109,61]. The sensor **33** showed binding with Cu^{2+}ions in binding ratio of 2:1, where Cu^{2+} was coordinated to two oxygen atoms and two nitrogen atoms of phenoxy and imine groups, respectively [108] (Fig. 28). The sensor **34** detected Cu^{2+} ions with the detection limit down to 1.92×10^{-7} M due to binding of Cu^{2+} ions with oxygen and nitrogen atoms of **34** (**34**:Cu^{2+} = 2:1) [109].

Another hydrophilic 1,8-naphthalimide based fluorescent chemosensor, **35**, was synthesized by **Liang** and co-workers for Cu^{2+} recognition, in which 2-(2-aminoethoxy)ethanol group improved the hydrophilicity and Schiff base acted as multidentate ligand for Cu^{2+} [61]. Cu^{2+} ions were able to quench the fluorescence which occurred due to PET process from the 1,8-naphthalimide fluorophore to the bound Cu^{2+} (Table 4). The mode of quenching was found to be static quench process. The sensor **35** was successful in Cu^{2+} sensing in real world water samples and living cells, demonstrating its practical utility. Molecular logic gate with IMPLICATION function was also constructed from sensor **35**.

Xu et al. prepared fluorescent ion-imprinted sensor (FIIS) based on **36** (Fig. 29) and used for the detection of Cu^{2+} ions [81]. Addition of Cu^{2+} ions to the solution of FIIS caused quenching in fluorescence with K_a value of 3.98×10^6 M^{-1}, which could be ascribed to the PET mechanism or d-d electron paramagnetic quenching mechanism.

Wenxun and co-workers synthesized high performance hydrophilic tubular fluorescent sensor, **FPM-2**, for the detection of Cu^{2+} ions by immobilizing fluorophore 4-bromo-1,8- naphthalic anhydride **37** (Fig. 29) (later converted to 4-methoxy-1,8-naphthalimide) on poly(*N, N′*-methylene bisacrylamide) (PMBA) microtubes [110]. The tubular fluorescent sensor, **FPM-2**, was typical donor-π-acceptor system based on ICT transition in which naphthalimide group and methoxy group were electron acceptor and electron donor, respectively. Quenching in fluorescence emission peak at 457 nm was observed upon addition of $CuCl_2$. The proposed sensor was found to be reusable many times by using EDTA as the chelating agent for Cu^{2+}. The coordination between Cu^{2+} and the carbonyl group (C=O) of 1,8-naphthalimide group led to change in electron transfer state and caused fluorescence quenching (Fig. 30).

Anbu and co-workers synthesized a naphthalimide-phenanthroimidazole containing fluorescent *turn-off* and reversible sensor **38** (Fig. 29) for the selective sensing of Cu^{2+} ions [92]. In the absorption spectrum, the free sensor **38** exhibited two Soret bands at 240 and 344 nm and three shoulder peaks appeared at 258, 327 and 358 nm in CH_3CN/50 mM:HEPES buffer (pH = 7.2) (0.6:99.4, v/v) medium. On addition of Cu^{2+} ions to the solution of **38**, a new peak appeared at 452 nm after slight red shift along with color change from pale or greenish-yellow to intense yellow under ambient light. In the emission spectrum, the free sensor **38** displayed two peaks at 455 and 578 nm, however, in the presence of Cu^{2+} ions, enhancement in fluorescence emission intensity was observed at 455 nm along with fluorescence color change from blue to green, which was ascribed to the disruption of PET process

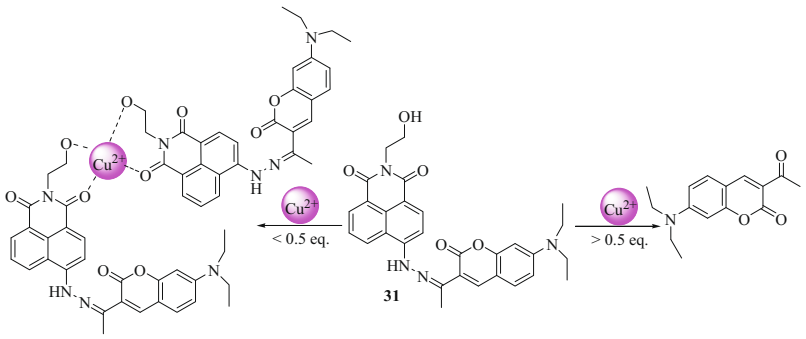

Fig. 26. Two way binding of Cu^{2+} with sensor **31** in its different concentration ranges.

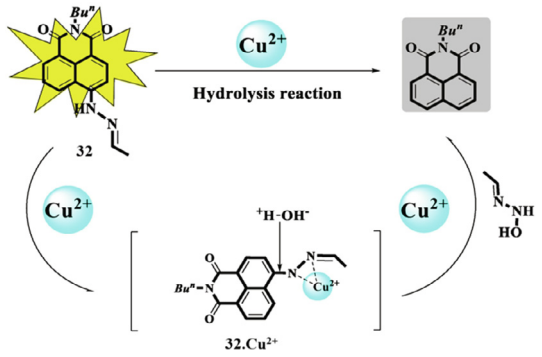

Fig. 27. Cu^{2+} induced hydrolysis reaction of **32**. (Reproduced from Spectrochim. Acta A Mol. Biomol. Spectrosc. 208 (2019) 198–205 [54]).

from phenolic oxygen and piperazinyl aza–nitrogens to the naphthalimide fluorophore due to binding of Cu^{2+} with N_2O group (Fig. 31). The LOD and association constant values were measured to be 0.65 μM and 5.0×10^4 M^{-1} respectively for 1:1 stoichiometric complex of **38.** Cu^{2+}. The practical applications of the synthesized probe **38** include test strip based sensing of Cu^{2+} ions and their imaging in human cervical cancer (HeLa) cell lines.

Wei and group developed a fluorescent *turn-on* 1,8-naphthalimide based Schiff base probe **39** (Fig. 29) for the detection of Cu^{2+} ions with the detection limit as low as 0.48 μM [82]. Upon incorporation of Cu^{2+} ions to the H_2O/THF (v/v: 7/3) solution of **39**, a new emission peak appeared at 490 nm with the fluorescence color change from weak blue to strong cyan. This change was ascribed to the inhibition of PET process due to complexation between **39** and Cu^{2+} ion in 2:1 binding ratio (Fig. 32) with the association constant of 6.045×10^7 M^{-2}. The proposed sensor was found to be stable and exhibited reliable results in the physiological pH range of 5.0 to 9.0. Furthermore, the proposed sensor conveniently detected Cu^{2+} ions in real water samples and Hela cells.

2.5. Zinc (Zn^{2+}) ions

Hamilton et al. synthesized a polymeric fluorescent probe, **40** (Fig. 33), possessing 1,8-naphthalimide as sensing unit and rhodamine as fluorophore attached to common poly(methyl methacrylate) backbone [111]. The polymeric probe then self-assembled in aqueous solution to form nanoparticles, which were used to detect Zn^{2+} ions. Significant enhancement in fluorescence emission at 527 and 580 nm was observed in the presence of Zn^{2+} ions, which was attributed to the inhibition of PET from the dipicolylamine receptor to the fluorophore because of binding with Zn^{2+}. To determine the concentration of Zn^{2+} ions, both the fluorophores (1,8-naphthalimide and rhodamine) in the polymeric probe were excited independently and ratio of their intensities was used to calculate Zn^{2+} concentration.

Liu and co-workers synthesized 1,8-naphthalimide based sensors (**41**–**44**) which displayed selective sensing towards Zn^{2+} ions over other metal ions [62,63,93,64].

The sensor **41** (Fig. 33) possessing iminoethoxyacetic acid and iminopicolinic acid moieties, underwent enhancement in fluorescence with addition of Zn^{2+} ions, which was ascribed to blockage of PET process from coordinated atoms to fluorophore due to change in dipole moment during the process of binding of Zn^{2+} with the aniline [62]. Molecular modelling experiment revealed the binding of Zn^{2+} to N atom of amino aniline and N and O atoms of iminoethoxyacetic acid and iminopicolinic acid arms and to the solvent molecule to form the distorted six-coordination geometry (Fig. 34).

Similar sensors (**42**–**44**) (Fig. 35) synthesized by **Liu et al.** showed significant changes in the fluorescence spectrum with addition of Zn^{2+} ions, whose binding mechanism was confirmed by molecular modelling (Table 5) [63,93,64].

Panchenko et al. synthesized a Zn^{2+} selective fluorescent chemosensor, **45** (Fig. 35), based on 4-methoxy-1,8-naphthalimide derivative containing salicylideneamino as receptor group [112]. Upon addition of Zn^{2+} ions, emission band at 437 nm was shifted to 455 nm with significant increase in fluorescence

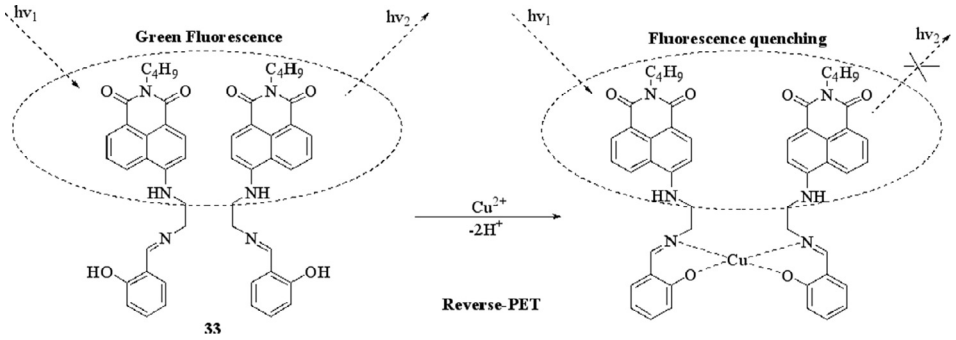

Fig. 28. Binding between **33** and Cu^{2+} ions in 2:1 stoichiometric ratio.

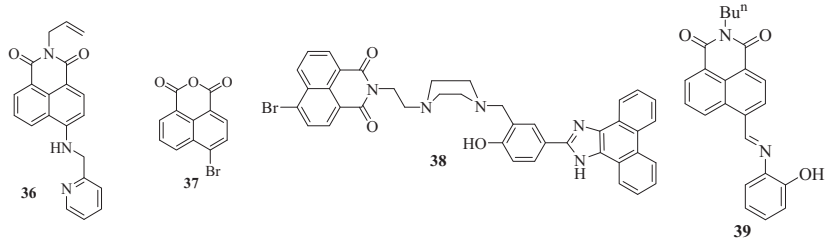

Fig. 29. Structures of chemosensors **36**–**39.**

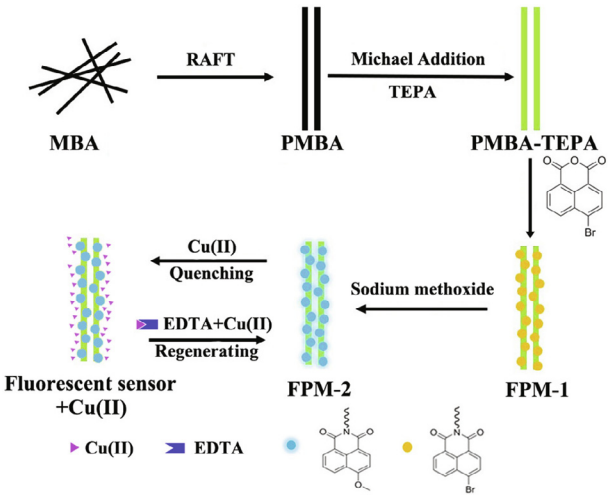

Fig. 30. Pictorial representation of synthesis of **FPM-2** along with quenching and regenerating processes. (Reproduced from React. Funct. Polym. 146 (2020) 104,400 [110]).

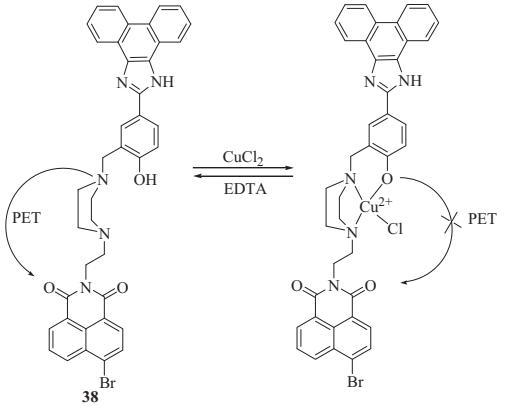

Fig. 31. Proposed mechanism of coordination of Cu^{2+} ions with sensor **38.**

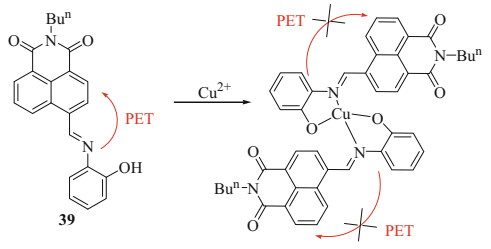

Fig. 32. Possible mode of binding of Cu^{2+} with chemosensor **39.**

intensity (Table 5) due to inhibition of PET process in the free ligand. From Mass spectrometry and ^1H NMR spectroscopy, it was found that on addition of one equivalent of Zn^{2+} ions, Zn^{2+} ions coordinated with receptor moiety and oxygen atom of one of the carbonyl groups of chromophore in 1:1 binding ratio; while on addition of 11 equivalents of Zn^{2+} ions, binding ratio of 2:1 was found between **45** and Zn^{2+} ions.

2.6. Mercury (Hg^{2+}) ions

A rhodamine-naphthalimide conjugated chemosensor **46** (Fig. 36) was synthesized by **Xu et al.** for the ratiometric detection

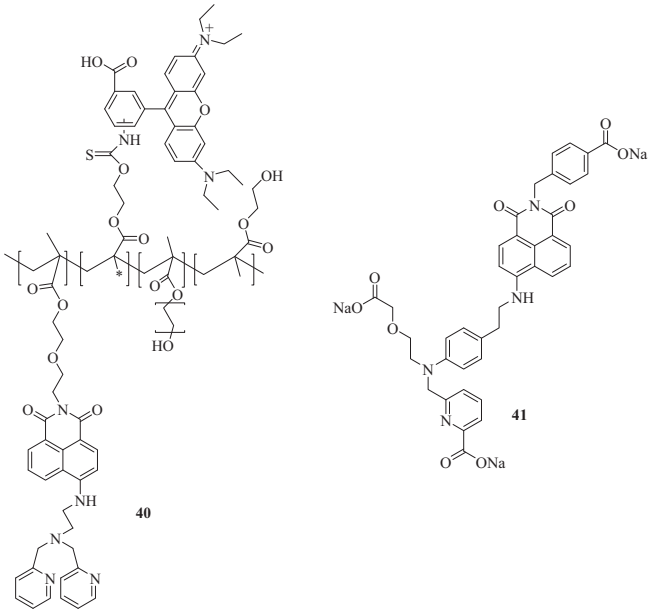

Fig. 33. Structures of chemosensors **40**–**41.**

of Hg^{2+} ions due to generation of FRET signal from 1,8-naphthalimide group to Rhodamine B group on addition of Hg^{2+} ions to **46** [83]. The sensor **46** underwent absorption as well as fluorescence changes with Hg^{2+} ions accompanied by fluorescence color change from light blue to orange (Table 6). Spirolactam ring of **46** opened upon chelation with Hg^{2+} via S atom of the lactam ring, N atoms of imide group and naphthalimide, causing open loop rhodamine B to accept energy of naphthalimide group (Fig. 37). From the pH dependence experiment, it was found that fluorescence intensity of both **46** and **46**.Hg^{2+} remained stable in the wide pH span of 6.0 to 11.0.

Other rhodamine possessing chemosensors **47** and **48** (Fig. 36) showed similar type of spirolactam ring opening with addition of Hg^{2+} ions, where desulfurization reaction occurred (Table 6) (Figs. 38, 39) [65,84]. Further, addition of I^- to **47**.Hg^{2+} complex regenerated the free sensor indicating the reversibility of the sensor.

Lv and co-workers synthesized 1,8-naphthalimide based chemosensor, **49** (Fig. 36), with a reactive aliphatic hydroxyl group for the detection of Hg^{2+} ions, which was stable in the pH range of 4.3–9.0 [85]. Addition of Hg^{2+} ions to the CH_3CN/H_2O (15/85, v/v) solution of **49** caused enhancement in fluorescence accompanied by emergence of green color fluorescence, however, the ultraviolet–visible (UV–Vis) spectrum of **49** remained unperturbed with addition of metal ion (Table 6). According to the proposed sensing mechanism, one of the Hg^{2+} was bound to the sulfur atom of thiourea unit and got removed as HgS via an irreversible reaction. Another Hg^{2+} ion showed binding with hydroxyl and carbonyl oxygen atoms of imide side of **49** in a reversible manner (Fig. 40).

Liu and co-workers synthesized naphthalimide-piperazine-pyridine-based polystyrene sensors (**50a** and **50b**) (Fig. 41) with different linker lengths for the detection of Hg^{2+} ions [86]. Enhancement in fluorescence intensity at 520 and 525 nm was observed on addition of Hg^{2+} ions to the CH_3CN/HEPES buffer (1:1, v/v, pH = 7.2) solution of **50a** and **50b**, respectively. Sensor **50a** exhibited higher fluorescence response towards Hg^{2+} ions as compared to **50b** with the lower detection limit of 1.01 μM as compared to LOD value of 1.98 mM for **50b**. The DFT calculations pointed to chelation-induced PET process for Hg^{2+} detection by the sensors **50a** and **50b**.

Another switchable fluorescence solid polymer, **51** (Fig. 41), based on a photo-crosslinked membrane functionalized with 1,8-

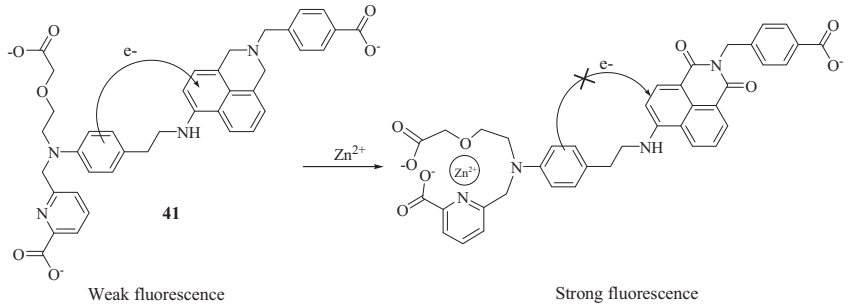

Fig. 34. Proposed mechanism of coordination of Zn^{2+} ions with sensor **41**.

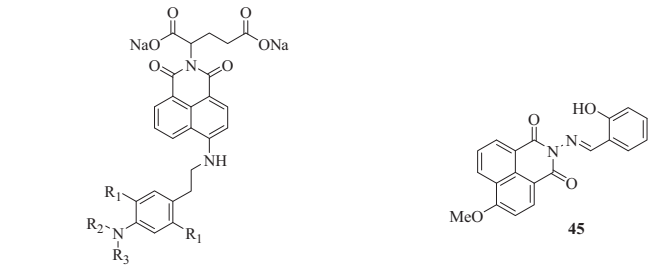

42. R_1 = OMe; R_2 = R_3 = -CH_2COONa
43. R_1 = OMe; R_2 = H; R_3 = -$CH_2CH_2OCH_2COONa$
44. R_1 = H; R_2 = -CH_2COONa; = R_3 = -$CH_2CH_2OCH_2COONa$

Fig. 35. Structures of chemosensors **42**–**45.**

naphthalimide derivative, synthesized by **Fernández-Alonso et al.** displayed about 3-fold increase in fluorescence intensity with addition of Hg^{2+} in pure water as it promoted enhancement due to PET inhibition process from the piperazine to the naphthalimide moiety [66]. The LOD and K_a values for 1:1 stoichiometric complex of **51**.Hg^{2+} were measured to be 2.5 × 10^{-6} μM and 3627 M^{-1}, respectively.

The fluorescence of isocyano-functionalized, 1,8-naphthalimide-based sensor, **52** (Fig. 42), changed from ultraviolet (∼389 nm) region to visible (∼560 nm) light region with addition of Hg^{2+} ions to its high-water-fraction medium [THF/water = 3/7 (v/V), pH = 7.4]) [87]. FT-IR and ^{1}H NMR spectral studies confirmed the hydrolysis of isocyano group of **52** into amino group, causing the change in fluorescence (Fig. 43). The detection limit of proposed sensor **52** towards Hg^{2+} ions was measured to be 9.1 × 10^{-8} M. Furthermore, **52** efficiently detected Hg^{2+} ions in tap water samples and **52**-doped agarose gels were prepared for the detection of Hg^{2+} in solid state.

Liu and group synthesized 4-amino-1,8-naphthalimide-based fluorescent sensor **53** (Fig. 42) possessing iminodiacetic acid and picolinic acid as metal chelating groups for the detection of Hg^{2+} ions in aqueous medium and living cells [67]. Addition of Hg^{2+} ions to the HEPES buffer solution of **53** caused 25-fold enhancement in fluorescence intensity of the emission peak centered at 550 nm, however, other ions did not show any effect on the spectrum, indicating highly selective nature of **53** towards Hg^{2+} ions. Binding of Hg^{2+} ions lowered the energy level of the iminodiacetic acid and picolinic acid moieties than highest occupied molecular orbital (HOMO) of the excited 4-amino-1,8-naphthalimide, making electron transfer difficult and switching on the fluorescence. The asso-

Table 5
Fluorescence changes, LOD* values, mechanism and stoichiometry of sensors (**42**–**45**) on complexation with Zn^{2+} ions in HEPES buffer solution (20 mM, pH = 7.4).

Sensor	Observed fluorescence enhancement at 550 nm	LOD (ppb)	Mechanism	Stoichiometry	Ref.
42	30-fold	65.41	PET	–	[63]
43	41-fold	112.45	PET	1:1	[93]
44	20-fold	–	PET	–	[64]
45	5-fold	50.5	PET	1:1 (1 equivalent of Zn^{2+}) 2:1 (for **45**:Zn^{2+} in the presence of 11 equivalents of Zn^{2+})	[112]

* LOD values have been determined by observing fluorescence changes.

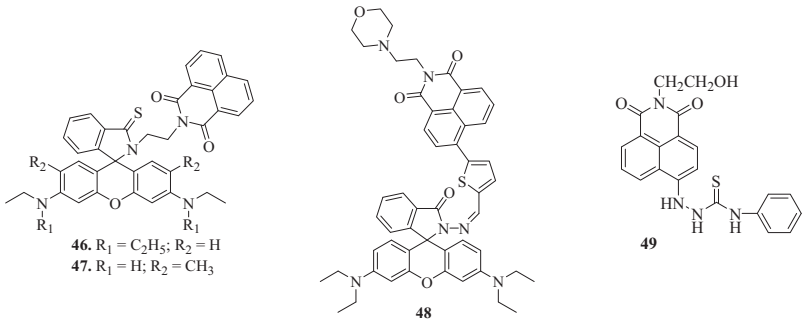

Fig. 36. Structures of chemosensors **46**–**49.**

Table 6
Solvent systems, absorption and fluorescence changes, naked eye color changes, mechanism, stoichiometry (Ligand:Analyte), K_a* and LOD* values of sensors (**46**–**49**) on binding with F^- ions.

Sensor	Solvent	Absorption changes (nm)	Fluorescence changes (nm)	Color changes	Mechanism	Stoichiometry	K_a ($\times 10^3$ M^{-1})	LOD (μM)	Ref.
46	EtOH/HEPES (v/v, 9:1, pH = 7.0)	450–650 → 558	381 → 385	Colorless → pink	FRET	1:1	2.75	0.059	[83]
47	HEPES/CH_3CN (40:60, V/V)	New peak at 533	New peak at 560	Colorless → yellow	–	–	–	0.49	[65]
48	EtOH/HEPES (5:1, V/V)	275, 324, 347, 395 → 560	Enhancement at 469 (11 nm red shift) and 585	Pale yellow → pink	FRET & PET	1:1	0.00893	0.052	[84]
49	CH_3CN/H_2O (15/85, v/v)	–	Enhancement at 527 nm	–	–	1:2	1.78×10^5 **	0.138	[85]

*K_a and LOD values have been determined by observing fluorescence changes.
K_a value is in the units M^{-2} and has been determined for **49:Hg^{2+} (1:2) by observing fluorescence changes.

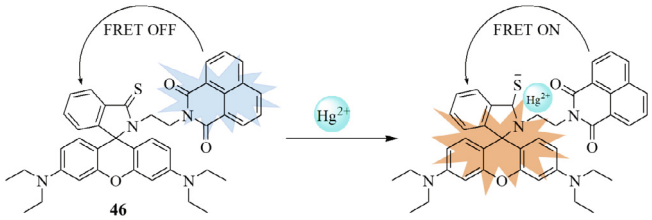

Fig. 37. Spirolactam ring opening of **46** upon coordination with Hg^{2+} ions.

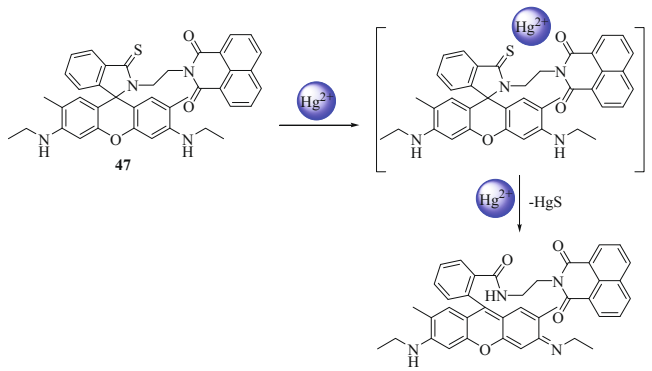

Fig. 38. Hg^{2+} mediated desulfurization reaction of chemosensor **47.**

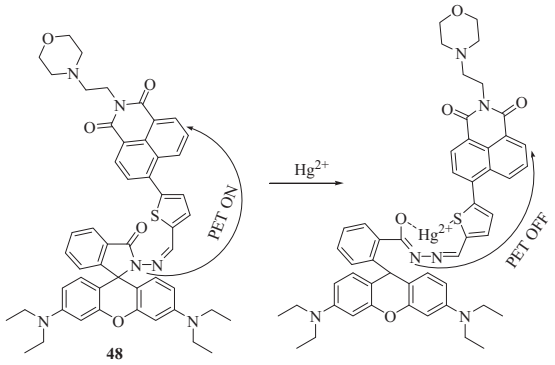

Fig. 39. Possible mechanism of sensing of Hg^{2+} by chemosensor **48.**

ciation constant and LOD of **53**. Hg^{2+} was measured to be 1.46×10^8 M^{-1} and 20.66 ppb, respectively. Moreover, the sensor **53** was efficiently used for imaging of intracellular Hg^{2+} levels in living cells (HeLa cells).

A histidine functionalized 1,8-naphthalimide based sensor, **54** (Fig. 42), having excellent water solubility resulted in quenching of blue fluorescence at 384 nm upon addition of Hg^{2+} ions [68]. ^1H NMR-titration, IR and mass spectrometry (MS) spectra indicated that Hg^{2+} was complexed to **54** via O–Hg^{2+}–N (O of carboxyl group and N of imidazole group) coordination bond, which led to shielding effect of the electrons on the naphthalene ring (Fig. 44). The association constant and detection limit were measured to be 1.14×10^5 M^{-2} and 0.1785 μM, respectively. The sensor was found to be stable in the pH range of 3.0–7.0 and the sensor was reusable as addition of I^- to the **54**. Hg^{2+} regenerated the free sensor.

Bahta et al. synthesized 1,8–naphthalimide-amino acid conjugates **(55a** and **55b)** (Fig. 45) for the selective sensing of Hg^{2+} ions, where **55a** and **55b** existed as nano-aggregates [55]. On addition of Hg^{2+} ions to the MeOH/H_2O (1:99, v/v) solution of **55a** and **55b**, significant changes in the absorption and fluorescence spectrum were observed. The absorption spectrum of **55a** and **55b** showed decrease in absorption intensity of bands located at 343 and 341 nm, respectively. In the fluorescence spectrum, 20- and 21-fold enhancement was observed at 395 and 386 nm for **55a** and **55b**, respectively. Coordination of **55a/55b** with Hg^{2+} via acidic oxygen and sulphur atoms of thio groups increased the rigidity of the molecule, which restricted the free rotations in **51a** and **55b**, resulting in enhancement of fluorescence intensity via CHEF effect and increase in concentration resulted in AIEE. Association constant and LOD between metal and ligand (2:1 complex) was measured to be 3.4×10^9 (22 nM) and 4.6×10^9 M^{-2} (5.6 nM) for **55a** and **55b**, respectively.

Panchenko and co-workers synthesized two 1,8-naphthalimide based chemosensors, (**56a** and **56b**) (Fig. 45) and tested their ability to detect Hg^{2+} ions [56]. Among these, no changes were observed in the fluorescence spectra of **56b** on addition of any of the metal ions, however, on addition of Hg^{2+} ions to the methanol–water (40 vol% MeOH) solution of **56a**, significant increase in the emission intensity of band centered at 531 nm was observed because of inhibition of PET process. The detection limit and binding ratio in **56a**. Hg^{2+} came out to be 25 nM and 1:1 respectively. Other competitive ions did cause any interference in the detection of Hg^{2+} ions except Cu^{2+} and Pb^{2+} ions, which showed a little effect.

1,8-naphthalimide-sulfamethizole probe, **57** (Fig. 45), existed in the form of nano-aggregates in DMSO/water (1:99 v/v) solution as indicated by its absorption spectrum [57]. Addition of Hg^{2+} ions to solution of **57** resulted in increase in absorption intensity of peak located at 267 nm; while the band at 343 nm decreased in intensity. In the fluorescence spectrum, emission peak at 390 nm was shifted to 483 and 478 nm upon addition of Hg^{2+} and Ag^+ ions, respectively. AIE was caused by **57** in aqueous medium due to hydrophobic nature of naphthalimide moiety, leading to excimer emission upon intramolecular excimer formation via metal ion-induced assembly (Fig. 46). No other ion showed any change in

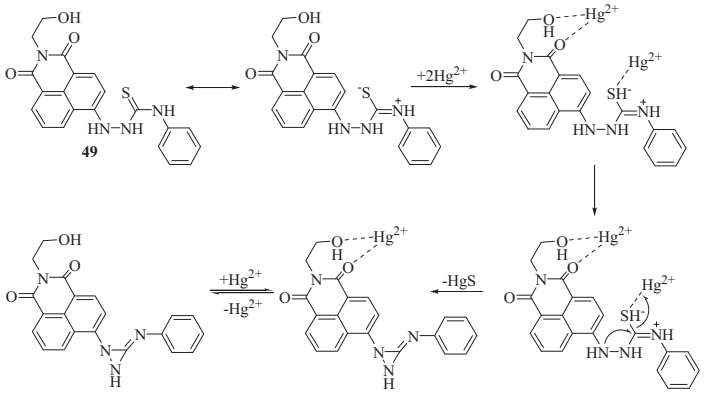

Fig. 40. Proposed mechanism of binding of Hg^{2+} with sensor **49** in 2:1 stoichiometric ratio.

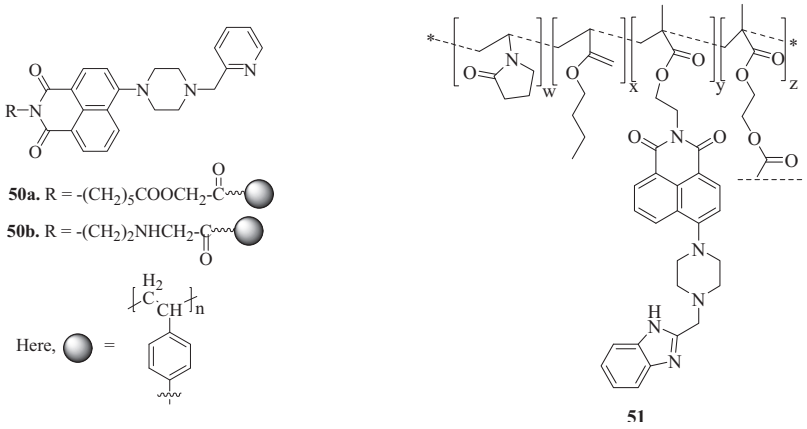

Fig. 41. Structures of chemosensors **50–51.**

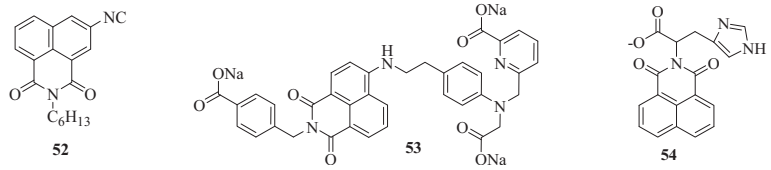

Fig. 42. Structures of chemosensors **52–54.**

the fluorescence spectrum except Ag^+ but the change exhibited by Ag^+ ion was different from that exhibited by Hg^{2+} ion. IR, NMR and stoichiometric calculation data revealed that Hg^{2+} was coordinated to **57** via –NH, $-SO_2$ and thiadiazole ring of sulfamethizole moiety in 1:2 ratio, giving LOD value of 14.7 nM.

Chen and co-workers synthesized a two-photon fluorescent probe **58** (Fig. 45) based on 1,8-naphthalimide for the selective sensing of Hg^{2+} ions with the detection limit as low as 43 nM [58]. Absorption band centered at 370 nm was shifted to 450 nm on addition of Hg^{2+} ions to the HEPES buffer (1.0 mM, pH = 7.4) solution of **58** along with naked eye color change from colorless

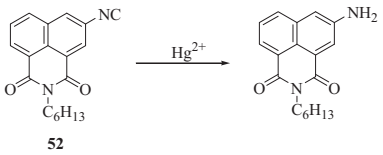

Fig. 43. Representation of mechanism of sensing of Hg^{2+} by **52.**

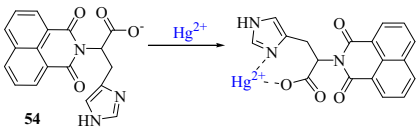

Fig. 44. Possible mode of interaction of Hg^{2+} with chemosensor **54.**

to yellow. In the fluorescence spectrum, intensity of the emission peak at 450 nm decreased and increase was observed in the intensity of peak at 560 nm. This process was accompanied by fluorescence color change from blue to green. These changes were ascribed to Hg^{2+} induced cleavage of thiophosphinate ester P–O bond in **58** to generate anionic species, which behaved as ICT system and exhibited spectral changes (Fig. 47). Furthermore, the proposed sensor **58** also detected Hg^{2+} ions in solid state as it caused both naked eye and fluorescence color changes upon grinding with the salts of mercury ion. Moreover, **58** efficiently detected Hg^{2+} ions in live HeLa cells as well as liver tissues.

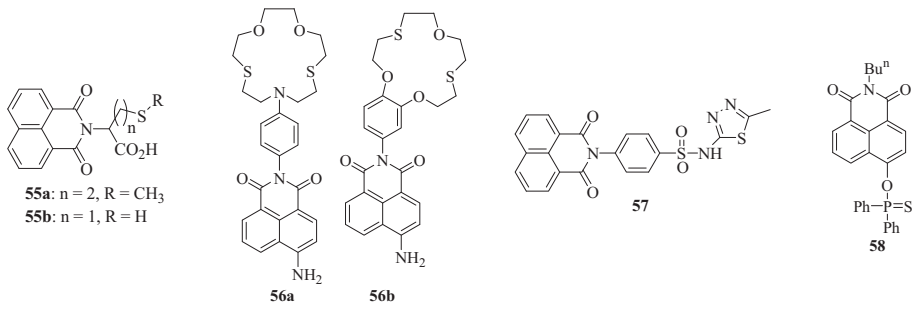

Fig. 45. Structures of chemosensors **55–58.**

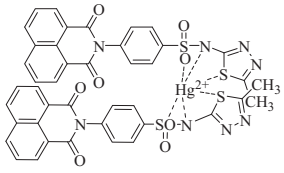

Fig. 46. Representation of binding of Hg^{2+} with **57.**

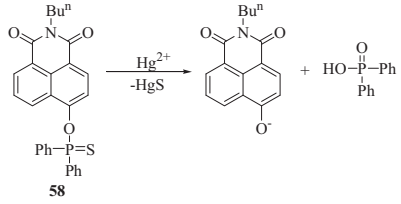

Fig. 47. Mechanism of sensing of Hg^{2+} by **58.**

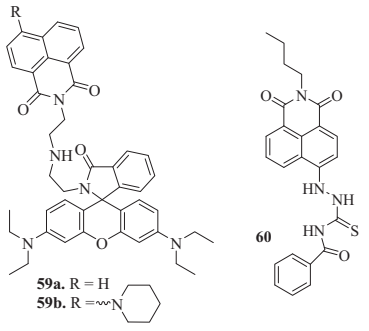

Fig. 48. Structures of chemosensors **59–60.**

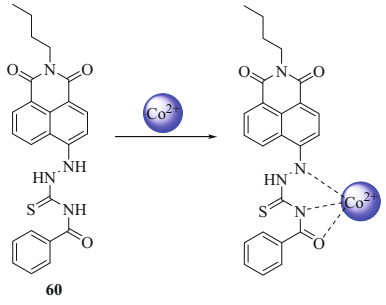

Fig. 49. Schematic representation of sensing mechanism for Hg^{2+} by **60.**

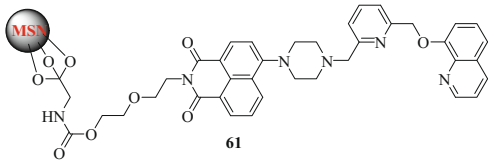

Fig. 50. Structure of chemosensor **61.**

2.7. Other metal ions [Chromium (Cr^{3+}), Cobalt (Co^{2+}), Silver (Ag^{+}), Lead (Pb^{2+}), Holmium (Ho^{3+}) ions]

Two 1,8-naphthalimide anchored rhodamine B based sensors (**59a** and **59b**) (Fig. 48) were synthesized by **Adhikari et al.** [94] which offered the ratiometric detection of Cr^{3+} ions ascribed to the CHEF process due to binding of secondary nitrogen and oxygen with Cr^{3+}, which further led to FRET process due to spirolactam ring opening of rhodamine. Addition of Cr^{3+} ions to the aqueous CH_3CN (7:3, v:v) solution of **59a/59b** resulted in appearance of a new absorption peak at 555/556 nm; while new emission peak was observed at 575/582 nm, respectively. Furthermore, it was found that **59b** exhibited good cell permeability and efficiently detected Cr^{3+} ions in Hep3B, SiHa, HeLa, MCF-7 and HEK293T cells.

Liu et al. synthesized a thiourea appended naphthalimide based chemosensor, **60** (Fig. 48), for Co^{2+} detection with K_a of 1.2×10^4 M^{-1} and LOD of 0.26 μM [95]. The absorption peak of the free sensor in CH_3CN/HEPES (4/1, v/v) at 510 nm disappeared upon addition of Co^{2+} ions along with visible color change from pink to colorless. This was attributed to decreased ICT transition due to extremely decreased electron-donating ability of the nitrogen atoms of **60** because of their coordination with Co^{2+} (Fig. 49). In the fluorescence emission spectrum, 33-fold enhancement in fluorescence intensity was observed along with slight blue shift due to suppression of ICT and PET processes. Furthermore, the sensor **60** was found to be non-toxic, exhibited significant cell permeability and efficiently detected Co^{2+} in HepG2 cells.

Wu et al. synthesized a reusable bifunctional fluorescent sensor, **61** (Fig. 50), by grafting naphthalimide based fluorescent probe on the surface of the mesoporous silica nanoparticles, which was capable of removal of Ag^{+} ions (maximum adsorption capacity = 14.8 mg g^{-1}) and its selective detection in aqueous medium with detection limit as low as 7.2 μM [69]. On addition of Ag^{+} ions to the solution of **61** in the deionized water, 2.5-fold increase in fluorescence intensity and minor blue shift in emission from 535 to 530 nm was observed. The practical utility of the proposed sensor **61** was indicated by the successful detection (recoveries = 104–106 %) and adsorption (adsorption efficiency = 77–91 %) of Ag^{+} ions in tap water and waste water.

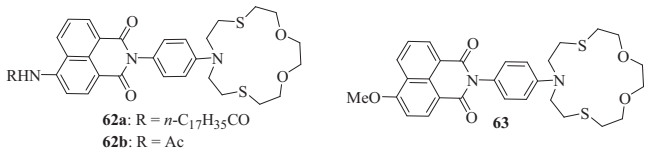

Fig. 51. Structures of chemosensors **62–63.**

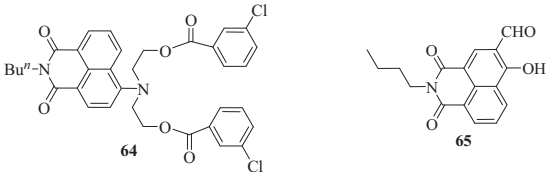

Fig. 52. Structures of chemosensors **64–65.**

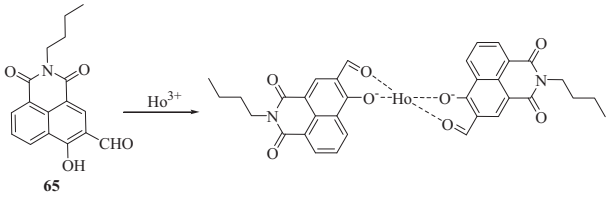

Fig. 53. Possible mode of interaction of Hg^{2+} with **65.**

Panchenko and co-workers synthesized 1,8-naphthalimide based sensors, **62a** and **62b** (Fig. 51), containing an azadithia-15-crown-5 ether receptor and then developed composite material based on **62a** using polyvinyl chloride as **62b** was insoluble in the polymeric sensor membrane [113]. Significant enhancement in fluorescence was observed after keeping sensor based on **62a** in the aqueous solution of Ag^+ ions. The optimum conditions for the analysis of Ag^+ using the composite material based on **62a** were found to be pH of 6.0 and exposure time of 14 min. The LOD of this material towards Ag^+ came out to be 2.1 μM, when exposure time was 14 min.

Similar fluorescent PET chemosensor, **63** (Fig. 51), based on 4-methoxy-1,8-naphthalimide bearing *N*-phenylazadithia-15-crown-5 ether as the receptor was synthesized by **Panchenko** and co-workers [70]. Addition of Ag^+ ions to the solution of **63** enhanced the emission peak at 460 nm, however, only minor changes in the absorption spectrum were observed. Binding stoichiometry in **63**.Ag^+ complex was found to be 1:1 and detection limit came out to be 0.38 μM. Possible cause for the enhancement in fluorescence was considered to be retardation of PET process.

1,8-naphthalimide based sensor, **64** (Fig. 52), was synthesized by **Fu** and co-workers and used for the sensing of Pb^{2+} ions in EtOH/H_2O (v/v = 4:1) solution [114]. The free sensor **64** exhibited strong fluorescence intensity at 528 nm, which decreased in intensity upon addition of Pb^{2+} ions due to its coordination with N, carbonyl O and OH of the **64**.

Zhang et al. synthesized a 1,8-naphthalimide based sensor **65** (Fig. 52) for the ratiometric detection of Ho^{3+} ions with the detection limit down to 6×10^{-8} M [96]. Incorporation of Ho^{3+} ions to the HEPES:DMSO = 1:1 (v/v, pH = 7.4) solution of **65** blue shifted the absorption peak from 425 to 370 nm along with visual color change from light yellow to nearly colorless. In the fluorescence spectrum, intensity of the emission peak at 512 nm decreased and a new peak appeared at 480 nm accompanied by fluorescence color change from yellow-green to cyan. These changes were attributed to the coordination of Ho^{3+} with **65** via hydroxyl and aldehyde groups (Fig. 53). Interference studies revealed that the proposed sensor **65** was highly selective towards Ho^{3+} ions over other ions. The binding stoichiometry and association constant in **65**.Ho^{3+} came out to be 1:2 and 6.37×10^{11} M^{-1}, respectively. The proposed sensor **65** also detected Ho^{3+} ions in A549 cells efficiently (Fig. 54).

3. Anion sensors

Anions play a number of crucial roles in biological, environmental, chemical and industrial processes [115]. For an instance, fluoride ion is added in toothpaste as it is beneficial for good dental health and treatment of osteoporosis; cyanide ion has applications in metallurgy, gold mining, electroplating and in industrial production of organic chemicals and pyrophosphate ion helps in metabolism and energy transduction etc. [116–118]. Despite the various benefits offered by anions, their excess intake may result in numerous disorders and interminable toxicity [115]. Thus, the detection of anions is fundamental for the monitoring of controlled uptake of anions by living beings and for this purpose, a number of 1,8-naphthalmide based sensors have been synthesized by the researchers working in this area.

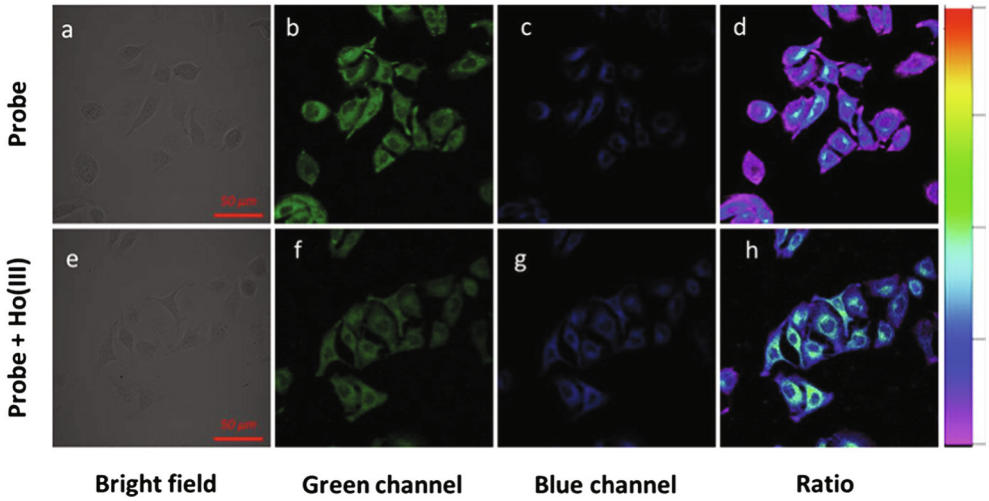

Fig. 54. Fluorescence images of A549 cells incubated with probe **65**. (Reproduced from Spectrochim. Acta A Mol. Biomol. Spectrosc. 174 (2017) 230–235 [96]).

Advancements made in sensing of anions over the last few years include enhanced sensitivity with LOD values in nanomolar range [119–122], competence to detect anions in pure aqueous medium [123–126], applicability of the chemosensors for the detection of anions in real world samples viz. real water [119,123,124,127–129], toothpaste [129,130], mouthwash [129] etc. and visualization of anions in living cells and living organisms [120,121,131–133]. Furthermore, for the rapid, convenient and on-site detection of various anions, some of sensors have been linked to smartphone [127,129], enabling the detection of anions via digital colorimetry; while use of paper strips for the quantification of anions [123,127,129] eliminated the need of experienced personnel, expensive instrument and tedious sample preparation. Although, there has been improvement in sensitivity, selectivity and practical utilization of chemosensors for the detection of anions but the number of sensors possessing these attributes are still very less and efforts need to be made in these directions.

3.1. Fluoride (F^-) ions

Yuan et al. synthesized 1,8-naphthalimide based sensors, **66–67** (Fig. 55), which selectively detected F^- ions over other competitive ions (Table 7) [130,134]. Upon addition of F^- ions to the DMSO solution of **66**, significant changes in the absorption spectrum were observed, which might be ascribed to the amide tautomerization triggered by F^- that extended the conjugated structure of the whole molecule (Fig. 56) [130]. In the fluorescence spectrum, decrease in fluorescence intensity was observed on addition of F^- ions (Table 7).

Significant changes were observed in the absorption and emission spectrum of **67** in the presence of F^- ions (Table 7) which were attributed to combined effects of excited state intramolecular proton transfer (ESIPT) and PET processes [134]. ^{1}H NMR titration studies indicated deprotonation of hydroxyl group of **67** due to hydrogen bond interaction between O–H and F^- ions (Fig. 57).

Li and group synthesized a 1,8-naphthalimide based probe, **68** (Fig. 55), that underwent significant changes in the absorption and emission spectrum due to its deprotonation caused by F^- ions (Fig. 58) and detected F^- ions with LOD value of 107 nM (Table 8) [119]. Furthermore, the proposed sensor efficiently detected F^- ions in real water samples.

Xiao et al. synthesized a naphthalimide based chemosensor **69** (Fig. 55) for naked eye detection of fluoride ion [135]. In the absorption spectrum, red shift in the absorption peak and emergence of new peak was observed along with visual color change from yellow to blue upon incorporation of F^- ions. In the fluorescence spectrum, intensity of emission band reduced to 1/14 and color changed from orange to non-fluorescent blue observable under UV light (Table 8). ^{1}H NMR titration studies indicated that F^- induced deprotonation of N–H of **69** occurred due to hydrogen bond interaction between naphthyl hydrazine and fluoride ions (Fig. 59).

A chemosensor, **70** (Fig. 55), based on 1,8-naphthalimide and benzothizazole was synthesized by **Chen et al.** for the naked eye and fluorescent detection of F^- ions due to hydrogen-bond interaction between F^- and amino proton of **70** followed by deprotonation of amino group (Table 8) [136].

1,8-naphthalimide based Schiff base, **71** (Fig. 55), acted as the dual mode chromofluorogenic sensor for F^- ions detection with binding stoichiometry between **71** and F^- ions to be 1:3, indicating that binding of F^- occurred with one N–H and two O–H groups of **71**, followed by deprotonation resulting into enhanced electron density, which directed to augment ICT and PET processes as confirmed by ^{1}H NMR titration experiments (Table 8) [127]. The colorimetric response of **71** towards F^- was combined with smartphone, which eliminated the need of skilled personnel for operating sophisticated instruments. In addition to this, test strips were developed for the easy and cost-effective sensing of F^- ions. The sensor **71** was also applied for the sensing of fluoride ions in real water samples and exhibited good response.

A 1,8-naphthalimide linked pyridoxal Schiff base, **72** (Fig. 60), was synthesized by **Pati et al.** and utilized for the detection of F^- ions by observing changes in its UV–Vis and fluorescence spectrum [137]. Further, **72** was conveniently modified to gel because of the presence of pyridine ring and other hydrogen bond donors and acceptors present in it. Addition of F^- ions to the gel form of **72**

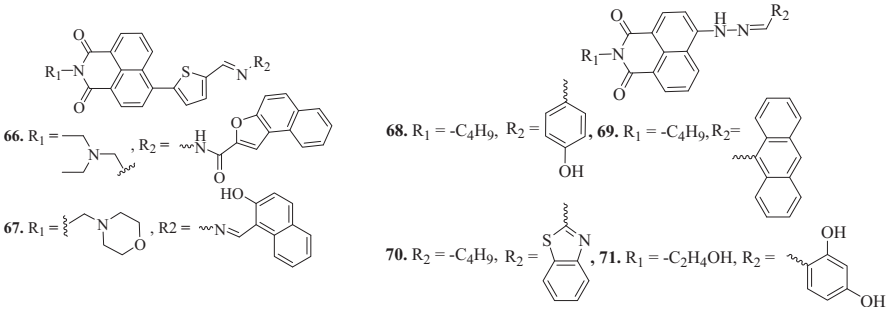

Fig. 55. Structures of chemosensors **66–71.**

Table 7
Solvent systems, absorption and fluorescence changes, naked eye color changes, mechanism, stoichiometry (Ligand:Analyte), K_a* and LOD* values of sensors (**66–67**) on binding with F^- ions.

Sensor	Solvent	Absorption changes (nm)	Observed fluorescence quenching at (nm)	Color changes	Mechanism	Stoichiometry	K_a (x × 10^3 M^{-1})	LOD (μM)	Ref.
66	DMSO	Decrease at 350, 404 and new band at 515	554	Yellow → red	PET	1:1	5.91	0.55	[130]
67	THF	350 → 490 420 → 572	593	Yellow → light purple	PET & ESIPT	1:1	22.9	0.015	[134]

*K_a and LOD values have been determined by observing fluorescence changes.

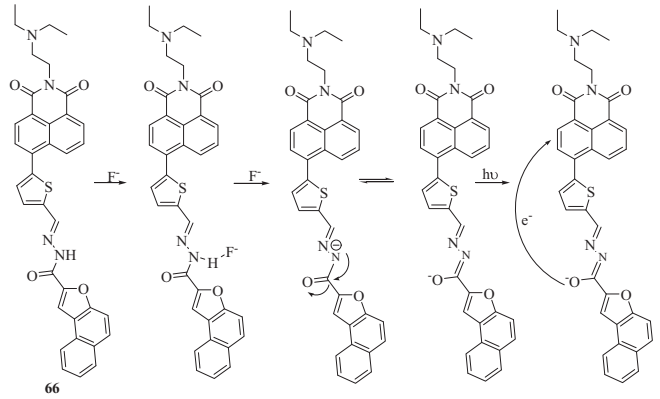

Fig. 56. Tautomerization of amide group in **66** by F^-.

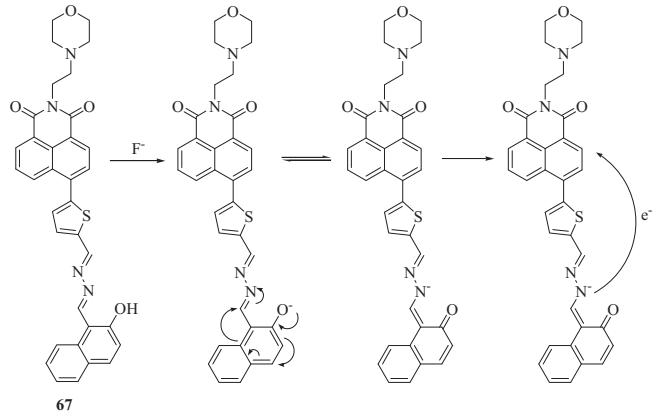

Fig. 57. Plausible mechanism of sensing of F^- ions by **67.**

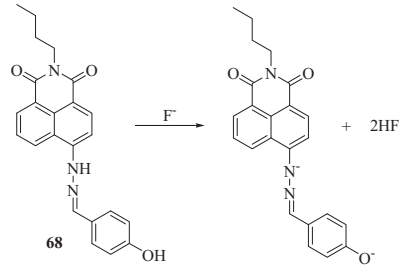

Fig. 58. F^- mediated deprotonation reaction of **68.**

ruptured the gel and converted it into sol form with color change from greenish yellow to blue and the gel form was revived on addition of Ca^{2+} ions. Thus, the proposed sensor efficiently detected F^- ions in both gel and solution states. Furthermore, compound **72** was attached to a solid Merrifield resin to form polymeric beads (**72a-b**) and their sensing properties towards F^- ions were examined. Both the beads conveniently detected F^- by showing color change and the action of F^- was reversed by addition of calcium perchlorate for upto 3 times. The color change shown by **72a** (orange to greenish blue) was found to be sharper than that of **72b**. AcO^- and $H_2PO_4^-$ also exhibited minor effects on the spectra of all the three states, but more sensitive behaviour was displayed towards F^- ions only.

A fluorescent sensor, **73** (Fig. 60), based on naphthalimide and imidazolium moieties was synthesized by **Kongwutthivech et al.** for colorimetric and fluorimetric detection of F^- ions because of electrostatic and hydrogen bonding interactions between acidic proton of **73** and F^- ion [138]. The proposed sensor **73** offered naked eye detection of fluoride ion by changing the color of solution from green to purple. In the fluorescence spectrum, large quenching was observed at 530 nm on addition of fluoride ions. The binding ratio in **73**.F^- was found to 1:1 and LOD and limit of quantification (LOQ) of **73** towards F^- was measured to 0.18 mM and 0.60 mM.

Yang and co-workers synthesized a 1,8-naphthalimide based colorimetric chemosensor **74** (Fig. 61) for the ratiometric detection of F^- ions [128]. On addition of fluoride ions to the DMSO solution of **74**, the absorption peak was red shifted from 422 to 583 nm along with naked eye color change from yellow to purple. From the pH dependence studies, it was found that pH hardly influenced the functioning of sensor **74** and it was stable in the wide pH span. The proposed sensor was found to be highly selective towards F^- ions over other ions and displayed excellent sensitivity with the detection limit down to 0.61 μM. From the DFT study, the plausible sensing mechanism at low concentration was revealed to be hydrogen bonding between **74** and F^-, whereas at high concentration, deprotonation of O–H group took place.

A 1,8-naphthalimide based chemosensor, **75** (Fig. 61), was synthesized by **Yadav** and co-workers for the selective and reversible detection of F^- ions with the detection limit down to 0.7413 μM [129]. On addition of F^- ions to the DMSO/H_2O (9:1, v/v) solution of **75**, the absorption peak underwent large red shift of 217 nm from 450 to 667 nm causing color change from yellow to green, possibly due to augmented ICT from amino proton of NC to conjugated and electron withdrawing 1,8-naphthalimide moiety. The proposed sensor exhibited efficient colorimetric sensing of F^- ions in pH range 6.5 to 7.0. From the absorption studies, binding stoichiometry and association constant for **75**.F^- came out to be 1:1 and 0.67 × 10^5 M^{-1}, respectively. In the emission spectrum, quenching in fluorescence was observed at 536 nm along with slight blue shift, which was ascribed to enhancement in PET and ICT processes as a consequence of increased electron density on N atom due to deprotonation of –NH group. For the practical utility, test strips based on **75** were prepared and colorimetric response of **75** towards F^- ions was integrated with smartphone leading to the development low cost, portable and user friendly analytical technique for the determination of fluoride ions. Furthermore, the proposed sensor efficiently quantified F^- ions in real life samples such as toothpaste, mouthwash and real water samples.

Table 8
Solvent systems, absorption and fluorescence changes, naked eye color changes, stoichiometry (Ligand:Analyte), K_a* and LOD* values of sensors (**68–71**) on binding with F^- ions.

Sensor	Solvent	Absorption changes (nm)	Fluorescence changes (nm)	Color changes	Stoichiometry	K_a (× 10^4) (M^{-1})	LOD (μM)	Ref.
68	DMSO	476 → 596	Quenching at 571	Orange → purple	–	–	0.107	[119]
69	DMSO-H_2O (v/v, 7:1)	460 → 630, 364	Quenching at 556	Yellow → blue	1:1	–	0.806	[135]
70	CH_3CN	Decrease at 445 → 620	505 → 660	yellow → blue	1:1	1.46	0.41	[136]
71	DMSO-H_2O (v/v, 9:1)	480 → 587, 625	Quenching at 584	Orange → blue	1:3	0.817 × 10^9 **	0.00134	[127]

*K_a and LOD values have been determined by observing fluorescence changes.
K_a value is in the units M^{-3} and has been determined for **71:F^- (1:3) by observing fluorescence changes.

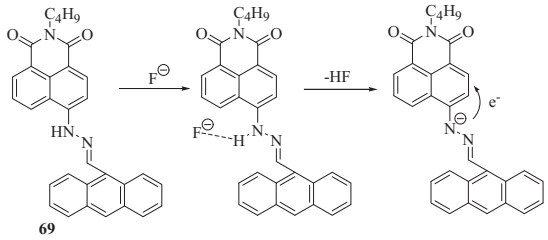

Fig. 59. Mechanism of sensing of F^- by **69.**

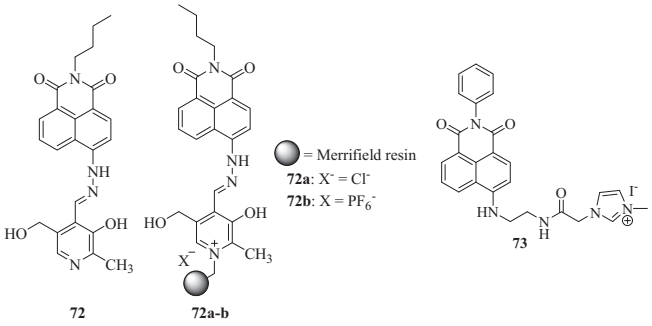

Fig. 60. Structures of chemosensors **72–73.**

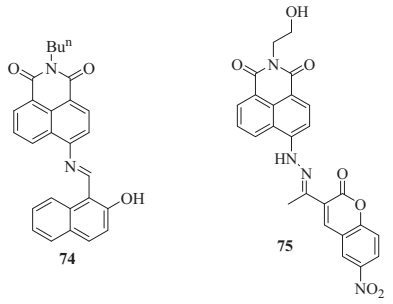

Fig. 61. Structures of chemosensors **74–75.**

3.2. Cyanide (CN^-) ions

A fluorescent turn-on sensor based on naphthalimide–benzo thiazole conjugate **76** (Fig. 62) was synthesized by **Reddy et al.** and utilized for the detection of CN^- ions with detection limit down to 3.55×10^{-8} M [139]. Upon incorporation of CN^- to the THF solution of **76**, absorption peak at 367 nm decreased along with red shift to 353 nm accompanied by appearance of a new peak at 506 nm with simultaneous appearance of two isobestic points at 302 and 436 nm. In the fluorescence spectrum, 21-fold enhancement in the intensity of emission peak at 411 nm was observed. The reason for these spectral changes as analyzed by ^1H, ^{13}C, DEPT, and mass spectroscopy came out to be disruption in the conjugation between benzothiazole and naphthalimide units of **76**.

Aromatic carboxyl functionalized 1,8-naphthalimide based chemosensor **77** (Fig. 62) was synthesized by **Wang et al.**, which displayed changes in its fluorescence spectrum along with color change from bright blue to colorless under UV lamp with addition of CN^- ions (Table 9) [123]. Free sensor **77** was regenerated when H^+ ions were added to the solution of **77**.CN^- and it was found that this "*on–off–on*" process could be repeated at least three times with a little loss of fluorescence intensity. The hydrogen bond in the free sensor was destroyed on addition of CN^- ions, making intramolecular rotation possible and the state changed from ICT to twisted ICT (TICT) state, which was confirmed to be the mechanism of detection of CN^- ions by **77** by ^1H NMR titration experiments.

3.3. Hypochlorite (ClO^-) ions

Lee and co-workers synthesized a naphthol-naphthalimide based *turn-on* fluorescent sensor, **78** (Fig. 62), that underwent significant absorption and fluorescence changes with addition of ClO^- ions in aqueous media, attributed to deprotonation of –OH proton by ClO^- ions (Table 9) [140].

Another similar naphthalimide based fluorescent probe **79** (Fig. 62), synthesized by **Lee** and group displayed quenching of fluorescence due to deprotonation of –NH proton by ClO^-, which was demonstrated by ESI-MS, ^1H NMR studies, fluorescence and UV–Vis spectroscopy and time-dependent DFT (TD-DFT) calculations (Table 9) [124].

3.4. Sulfide (S^{2-}), bisulfite (HSO_3^-) ions

Lohar et al. synthesized a naphthalimide based chemosensor, **80** (Fig. 63), for the fluorimetric detection of sulfide ions based on ICT process via nucleophilic addition of monoanion (HS^-) of H_2S (Table 10) [131]. Nucleophilic addition of HS^- to the C = N unit produced an intermediate, in which electron supply to the naphthalimide moiety through benzene ring was facilitated, leading to enhancement of fluorescence based on ICT process (Fig. 64). Moreover, being non-toxic, the sensor **80** was successfully used for imaging of the intercellular distribution of the sulfide ions in *Bacillus subtilis* and *Candida* sp. cells.

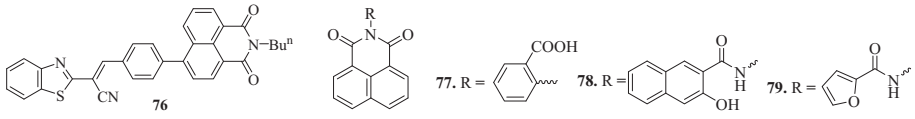

Fig. 62. Structures of chemosensors **76–79.**

Table 9
Solvent systems, absorption and fluorescence changes, mechanism, K_a* and LOD* values of sensors (**77–79**) in the presence of various analytes.

Sensor (Analyte)	Solvent	Absorption changes (nm)	Fluorescence changes (nm)	Mechanism	K_a (M^{-1})	LOD (μM)	Ref.
77 (CN^-)	Pure water (pH = 7.2)	–	Quenching at 390	ICT-TICT	6.08×10^5	0.0138	[123]
78 (ClO^-)	Bis-tris buffer/MeOH (9:1, pH 7.0)	Decrease at 250 and 350	Enhancement at 395	–	–	10.67	[140]
79 (ClO^-)	PBS buffer (0.01 M PBS, pH 7.4)	Increase at 290 and decrease at 260	Quenching at 395	ICT	–	0.60	[124]

*K_a and LOD values have been determined by observing fluorescence changes.

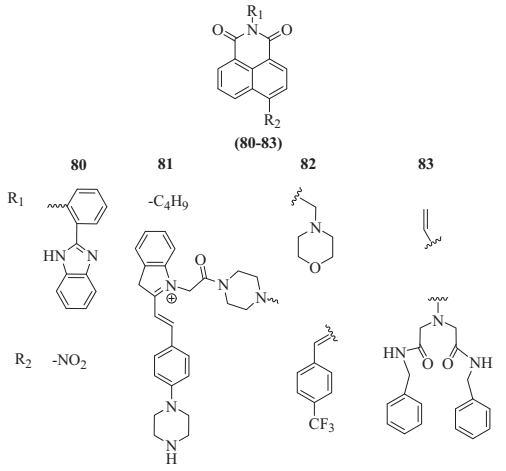

Fig. 63. Structures of chemosensors **80**–**83.**

A FRET based chemosensor **81** (Fig. 63) derived from naphthalimide and hemicyanine was synthesized by **Shen et al.**, whose red fluorescence was quenched; while green fluorescence was recovered in the presence of HSO_3^- ions (Table 10) [120]. The quenching in red fluorescence was ascribed to the destruction of D–π–A system of hemicyanine because of Michael addition reaction between HSO_3^- and C=C double bonds conjugated with indole (Fig. 65). Destruction of FRET structure caused by the broken hemicyanine was responsible for the recovery of green fluorescence. In the absorption spectrum, peak at 545 nm disappeared completely due to Michael addition between bisulfite and C=C double bonds of **81**, while only a slight change was observed in the absorption peak at 375 nm. The probe **81** conveniently detected F^- ions in MCF-7 cells and mitochondria.

Everitt and co-workers synthesized 1,8-naphthalimide based sensor **82** (Fig. 63) containing a strong electron-withdrawing group ($-CF_3$) for the quantitative detection of HSO_3^- ions in the aqueous media by displaying significant absorption and emission changes (Table 10) [121]. These changes were attributed to nucleophilic addition based mechanism, where HSO_3^- ion, being a good nucleophile, underwent nucleophilic addition reaction with **82**, which was facilitated by electron-withdrawing group ($-CF_3$) on it

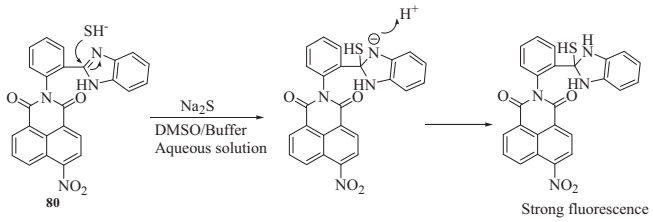

Fig. 64. Possible mechanism of nucleophilic addition of HS^- on sensor **80.**

(Fig. 66). Furthermore, **82** successfully detected HSO_3^- ions in RK13 epithelial cells.

3.5. Picrate ions

The chemosensor **83** (Fig. 63) based on 1,8-naphthalimide detected picrate anions in the DMF solution by quenching of fluorescence along with disappearance of yellow-green fluorescence (Table 10) [141]. This change was attributed to the hydrogen bonding of picrate ion with amide group of **83** and subsequent deprotonation, leading to inhibition of PET. Comparative studies revealed that other competitive ions had no effect on the sensing of picrate ions.

3.6. Pyrophosphate and phosphonate ions

Naphthalimide-based polyammonium chemosensors (**84a-84d**) (Fig. 67) were synthesized and their binding properties towards anions were studied by **Oshchepkov et al.** [125] Among the synthesized compounds, **84a**, **84b** and **84d** detected pyrophosphate in basic pH (8.0–9.0); while sensor **84c** was able to sense pyrophosphate at pH = 5.6. Due to binding with pyrophosphate, enhancement in fluorescence was observed in all the cases. This change was ascribed to inhibition of PET because of deprotonation of (**84a-84d**). Furthermore, it was found that **84a** and **84d** exhibited both *turn-on* and *turn-off* response depending on the pH of the medium. *Turn-off* response in case of **84a** and **84d** was observed at pH less than 7.0 and 8.6, respectively. From UV–Vis and NMR studies, it was found that **84a** and **84d** underwent aggregation in the presence of pyrophosphate, which led to quenching in fluorescence.

Table 10
Solvent systems, absorption and fluorescence changes, naked eye color changes, mechanism and LOD* values of sensors (**80**–**83**) in the presence of various analytes.

Sensor (Analyte)	Solvent	Absorption changes (nm)	Fluorescence changes (nm)	Color changes	Mechanism	LOD (μM)	Ref.
80 (S^{2-})	water/DMSO (3:1, v/v)	New peak appeared at 472	Enhancement at 502	Colorless → quiet yellow	ICT	2.4	[131]
81 (HSO_3^-)	PBS (containing 40% DMF)	Disappeared at 545, slight change at 375	590 → 527	Red → yellow	FRET	0.0612	[120]
82 (HSO_3^-)	PBS buffer /DMSO (4:6)	398 to 360	Quenching at 491	–	–	0.0032	[121]
83 (Picrate ions)	DMF	–	Quenching at 516	–	PET	0.66	[141]

*LOD values have been determined by observing fluorescence changes.

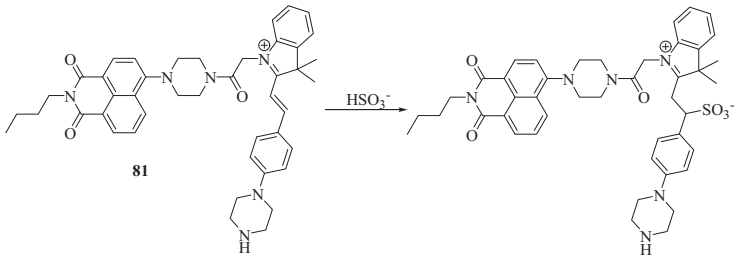

Fig. 65. Proposed mode of sensing of HSO_3^- ions by **81.**

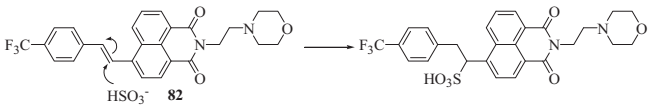

Fig. 66. Nucleophilic addition reaction of HSO_3^- with sensor **82.**

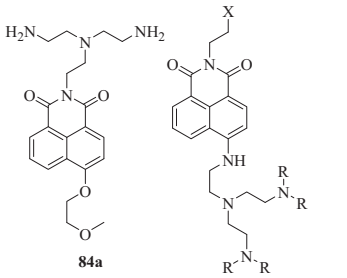

Fig. 67. Structures of chemosensors **84a-d.**

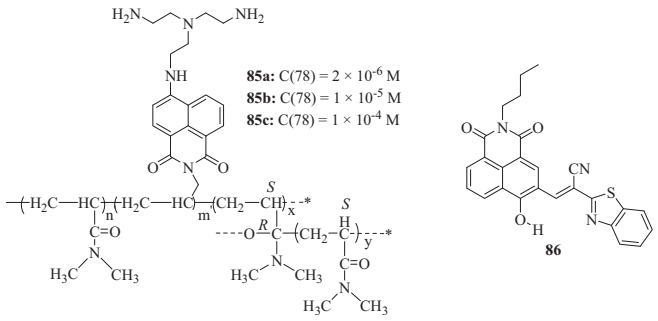

Fig. 68. Structures of chemosensors **85–86.**

Oshchepkov and group synthesized chemosensor, **85** (Fig. 68), containing a triamine subunit and 1,8-naphthalimide with an allyl group and utilized it for the detection of industrial phosphonates viz. ATMP (amino*tris*(methylenephosphonate) and HEDPA (1-hydroxyethane 1,1-diphosphonate) [126]. The proposed sensor selectively detected phosphonates over other anions and exhibited significant fluorescence enhancement at 545 nm in the presence of phosphonates (ATMP and HEDPA). This change was ascribed to hindrance caused in PET process due to protonation of free amine groups in **85**. ATMP caused more enhancement in fluorescence than HEDPA as binding in **85**-ATMP (K_a = 17700 M^{-1}) was found to be stronger than that of **85-**HEDPA. Further, cryopolymers (**85a-85c)** based on **85** were synthesized for the sensing of phosphonates. Quenching in fluorescence of (**85a-85c)** was observed due to self-aggregation of dye molecules in the presence of phosphonates. Detection limits of **85** and (**85b-85c**) towards ATMP detection were measured to be 0.02, 0.1 and 0.15 mmol L^{-1}, respectively.

3.7. Peroxynitrite ($ONOO^-$) anions

A 1,8-naphthalimide based chemosensor **86** (Fig. 68) was synthesized by **Fu et al.** for the visualization of endogenous $ONOO^-$ in living cells [122]. With addition of $ONOO^-$ to the PBS and ethanol solution of **86**, absorption intensity at 336 and 490 nm decreased; while increased at 356 and 442 nm. These changes were accompanied by naked eye solution color change from orange to pale yellow. In the fluorescence spectrum, 34-fold enhancement in fluorescence intensity was observed in the presence of $ONOO^-$ at 518 nm and detection limit of **86** towards peroxynitrite detection was measured to be 37 nM. These changes were ascribed to the nucleophilic attack of $ONOO^-$ on cyano substituted electron-withdrawing C = C bond, leading to release of N–CHO (Fig. 69). Furthermore, the proposed sensor **86** efficiently visualized endogenous and exogenous peroxynitrite in living cells.

3.8. Superoxide anions

Zhang et al. synthesized a two-photon naphthalimide based probe, **87** (Fig. 70), for the ratiometric detection of superoxide anion ($O_2^{\cdot-}$) with the detection limit down to 0.370 μM [132]. On addition of superoxide anion to the HEPES-DMSO (1:1, pH 7.4) solution of **87**, the absorption peak was shifted from 375 to 431 nm and in the fluorescence spectrum, emission peak shifted from 475 to 540 nm with 18-fold enhancement in fluorescence. These spectral changes were ascribed to the superoxide anion mediated deprotection of diphenylphosphinate group and consequent self-immolation to expose amidogen (Fig. 71). The proposed sensor was found to be highly selective towards superoxide anions

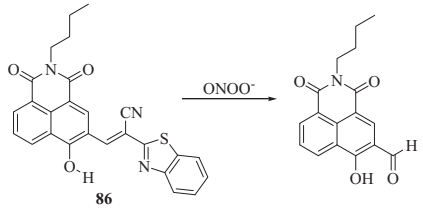

Fig. 69. Mechanism of $ONOO^-$ sensing by **86.**

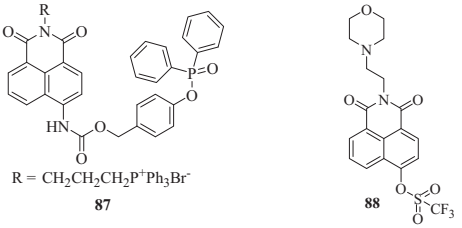

Fig. 70. Structures of chemosensors **87–88.**

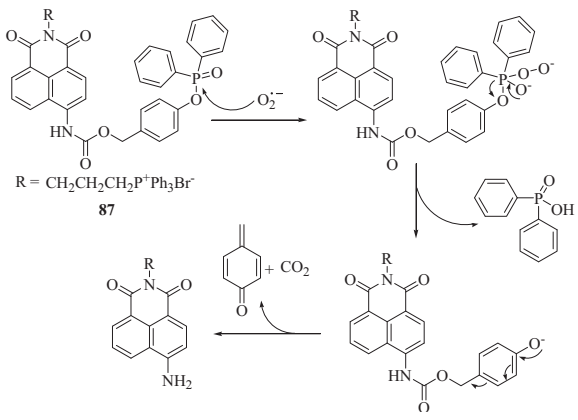

Fig. 71. Proposed mechanism of sensing of superoxide anion by **87** by nucleophilic substitution.

for other competitive analytes. Furthermore, the probe **87** was utilized for the imaging of superoxide anions in Daphnia magna and mitochondria of living cells.

A 1,8-naphthalimide based two-photon probe **88** (Fig. 70) was synthesized by **Ma** and co-workers for the tracking of superoxide anions by observing changes in its absorption and emission spectrum [133]. In the presence of superoxide anions, increase was observed in the absorption and emission intensity, which was ascribed to the removal of hydroxyl group from triflate (Fig. 72). The detection limit of **88** towards superoxide anions were measured to be 0.047 nM. Furthermore, based on low cytotoxicity and high tissue penetration ability, it was used for the imaging of superoxide anions in lysosome of HeLa cells, zebrafish and pneumonia tissue of living mice.

4. Sensors for biomolecules

Biomolecules play very important role in a number of fields including biology, environment, food, public health, and medicine etc. [142]. Various amino acids are responsible for normal functioning of biological processes in the human body as they regulate various cellular processes, however, even a slight change in their concentration may lead to various diseases [143]. For example, abnormal level of cysteine may result in Parkinson's disease, liver damage and skin lesions etc. and deficiency of glutathione is associated with neurodegeneration, inflammation and so forth [144].

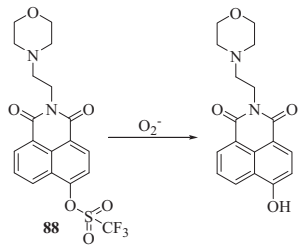

Fig. 72. Possible mechanism of sensing of superoxide anions by **88.**

Thus, monitoring the levels of various biomolecules in living organisms is vital for the early diagnosis of many diseases. In this respect, a number of 1,8-naphthalimide based probes have been reported for the convenient detection of various biomolecules.

Key features of the naphthalimide based chemosensors targeted for the detection of biomolecules over the recent years include high sensitivity (nanomolar LOD) [145–151], application in pure aqueous medium [143–145,150,152,153] and imaging of biomolecules in living cells, tissues and organisms [143–149,154–159]. Despite various advantages offered by these naphthalimide based sensors, modifications need to be made in order to make portable and cost-effective devices to increase their utilization.

4.1. Biothiols (glutathione, cysteine and homocysteine)

A naphthalimide-indole fused sensor **89** (Fig. 73) was synthesized by **Rong et al.**, which detected biothiols glutathione (GSH), cysteine (Cys) and homocysteine (Hcy) by displaying changes in the absorption spectrum and enhancement in fluorescence in PBS buffer solution (Table 11) [145]. The detection was possible due to blockage of PET process, when recognition group got separated from the fluorophore due to nucleophilic reaction between **89** and GSH (Fig. 74). Selectivity and anti-interference studies revealed that other biological amino acids did not interfere with the detection of biothiols. Furthermore, the proposed sensor **89** efficiently detected biothiols in MCF-7 cells.

Zhu et al. synthesized a fluorescent probe, **90** (Fig. 73), by combination of 4-hydroxy-1,8-naphthalimide and 4-chloro-7-nitrobenzofurazan and utilized it for the detection of biothiols (GSH, Cys, Hcy) [152]. The free sensor **90** exhibited no fluorescence because of enhancement of PET effect and suppression of ICT process, however, on addition of biothiols, substantial enhancement in fluorescence was observed (Table 11). In the absorption spectrum, significant absorption changes (Table 11) were observed along with visual color change from colorless to light yellow. On reaction of **90** with biothiols, ether bond had been broken to yield smaller products leading to multiple enhancements (Fig. 75). The proposed sensor efficiently detected biothiols in living cells, zebrafish and distinguished cancer cells from normal cells.

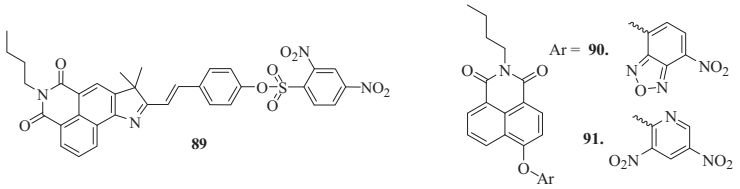

Fig. 73. Structures of chemosensors **89–91.**

Table 11
Solvent systems, absorption and fluorescence changes, naked eye color changes and LOD* values of sensors (**89–91**) in the presence of biothiols (GSH, Cys, Hcy).

Sensor (Analyte)	Solvent	Absorption changes (nm)	Fluorescence enhancement at (nm)	Color changes	LOD (μM)	Ref.
89 (GSH)	PBS buffer (10 mM, 1 mM CTAB, pH = 7.4)	421 → 447	590	–	0.00897	[145]
89 (Cys)	PBS buffer (10 mM, 1 mM CTAB, pH = 7.4)	421 → 447	590	–	0.00987	[145]
89 (Hcy)	PBS buffer (10 mM, 1 mM CTAB, pH = 7.4)	421 → 447	590	–	0.0102	[145]
90 (GSH)	PBS solution (10 mM, pH = 7.4)	375 → 475	550	colorless → light yellow	0.058	[152]
90 (Cys)	PBS solution (10 mM, pH = 7.4)	375 → 475	550	colorless → light yellow	0.031	[152]
90 (Hcy)	PBS solution (10 mM, pH = 7.4)	375 → 430	550	colorless → light yellow	0.066	[152]
91 (GSH)	tris buffer solution (20 mM, pH 7.4, containing 10% DMSO, v/v)	Increase at 450	550 (3.4-fold)	colorless → pale yellow	0.46	[144]
91 (Cys)	tris buffer solution (20 mM, pH 7.4, containing 10% DMSO, v/v)	Increase at 450	550 (7.0-fold)	colorless → pale yellow	0.32	[144]
91 (Hcy)	tris buffer solution (20 mM, pH 7.4, containing 10% DMSO, v/v)	Increase at 450	550 (2.8-fold)	colorless → pale yellow	0.88	[144]

* LOD values have been determined by observing fluorescence changes.

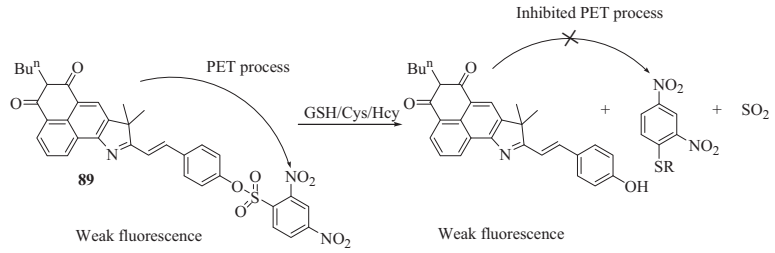

Fig. 74. Proposed nucleophilic reaction between **89** and GSH.

Zhuo et al. synthesized 3,5-dinitropyridin-2-yl substituted naphthalimide based fluorescent probe **91** (Fig. 73), which underwent color change from colorless to pale yellow and emittance of lemon-yellow fluorescence observable under UV lamp with addition of biothiols (GSH, Cys, Hcy) (Table 11) [144]. These biothiols were detected by **91** on the basis of biothiol triggered nucleophilic aromatic substitution mechanism to yield 4-hydroxy-1,8-naphthylimide fluorescent dyes (Fig. 76).

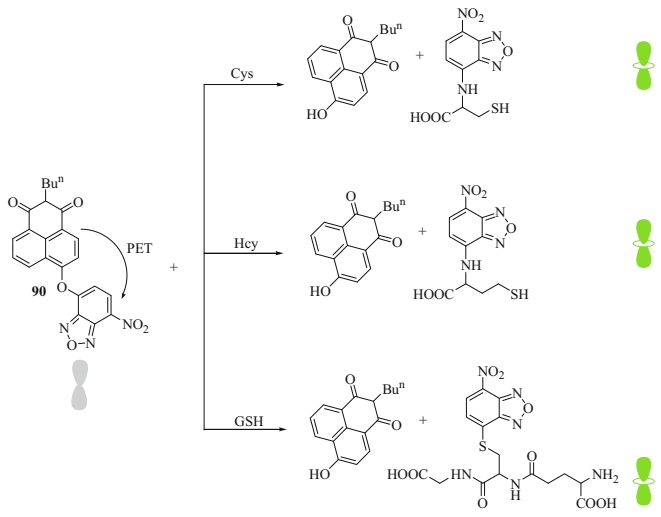

Fig. 75. Proposed mechanism of binding of **90** with biothiols.

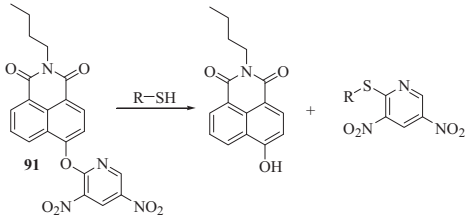

Fig. 76. Sensing of biothiols by **91.**

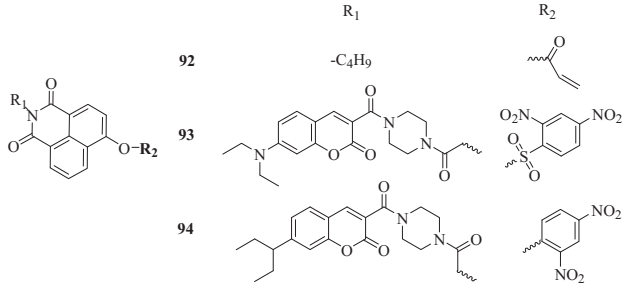

Fig. 77. Structures of chemosensors **92–94.**

4.2. Selenocysteine

An ICT based 1,8-naphthalimide possessing chemosensor **92** (Fig. 77), synthesized by **Tian et al.**, detected selenocysteine by showing changes in absorption as well as fluorescence spectrum along with naked eye color change from colorless to faint yellow and fluorescence color change from blue to yellow (Table 12) [146]. These changes were ascribed to the selenocysteine triggered hydrolysis of **92** to from an electron rich acrylate (4-hydroxynaphthalimide), which was responsible for distinct fluorescence signal. Selectivity studies revealed that other biothiols, amino acids, reactive oxygen species and seleno compounds did not show any interference to the sensing of selenocysteine in biological conditions. The proposed sensor also detected selenocysteine in HeLa cells.

A FRET-ICT dual modulated fluorescent probe, **93** (Fig. 77), based on 1,8-naphthalimide was synthesized by **Wang** and co-workers for the detection of cellular selenocysteine [147]. The free sensor **93** exhibited one emission peak with blue fluorescence, however, on addition of selenocysteine, it displayed two distinct emission bands with blue and green fluorescence (Table 12). These changes were ascribed to the cleavage of ester group by selenocysteine leading to blockage of ICT effect and restoration of FRET effect (Fig. 78).

A two-photon-FRET-based 1,8-naphthalimide derived fluorescent sensor **94** (Fig. 77) displayed absorption and emission changes with fluorescence color change from blue to yellow with addition of selenocysteine (Table 12) [148]. Recovery of FRET process due to release of naphthalimide fluorophore was responsible for these fluorescence changes (Fig. 79). The proposed sensor **94** efficiently detected selenocysteine in the HeLa cells, living tissues and zebrafish.

4.3. Cysteine

Aydin and co-workers synthesized a 1,8-naphthalimide based fluorescent probe **95** (Fig. 80) for the selective sensing of cysteine over other biologically important amino acids with the detection limit as low as 9.06 nM [149]. Upon incorporation of cysteine to the EtOH: H_2O (90: 10, v/v, 0.0670 M PBS buffer pH = 7.0) solution of **95**, 7.2-fold decrease in emission intensity was observed at 416 nm. From the Matrix-assisted laser desorption/ionization-time of flight mass spectrometry (MALDI-TOF-MS) spectra and DFT studies, the proposed sensing mechanism was found to be addition-cyclization-elimination strategy and ICT recognition mechanism (Fig. 81). Furthermore, the probe **95** was utilized for the imaging of cysteine in the healthy hepatocytes (THLE2) and hepatocellular carcinoma cells (HepG2).

Yu and co-workers synthesized 1,8-naphthalimide based chemosensor, **96** (Fig. 80), on the basis of "receptor$_1$-fluorophore-

Table 12
Solvent systems, absorption changes, fluorescence changes, mechanism and LOD* values of sensors (**92**–**94**) on addition of selenocysteine.

Sensor	Solvent	Absorption changes (nm)	Fluorescence changes (nm)	Mechanism	LOD (nM)	Ref.
92	20 mM PBS with 5% DMSO co-solvent, pH 7.4	345 → 449	Decrease at 420 and increase in new band range from 500 to 650	ICT	12.0	[146]
93	DMSO/PBS (1:99, v/v, pH 7.4)	–	Decrease at 482 and increase at 550	FRET-ICT	6.9	[147]
94	DMSO/PBS (1:99, v/v, pH 7.4)	406 → 419	463 → 545	TP-FRET	7.88	[148]

* LOD values have been determined by observing fluorescence changes.

spacer-receptor$_2$" model, which underwent emission and absorption changes with visual color change from colorless to pale yellow with incorporation of cysteine (Table 13) [154]. This change was attributed to the formation of phenolic hydroxyl group via Michael addition and intramolecular cyclization reactions in **96** on reaction with cysteine that eliminated the PET quenching process of **96** and resulted in strong fluorescence (Fig. 82). Based on the low cytotoxicity and biocompatibility of **96**, it was used for cellular imaging of cysteine and exhibited satisfactory results.

Similar Michael addition and intramolecular cyclization reactions (Fig. 83) between another 1,8-naphthalimide based chemosensor, **97** (Fig. 80) and cysteine were responsible for significant changes in naked eye color change from pale yellow to blue-violet and absorption as well as fluorescence spectrum (Table 13) [143].

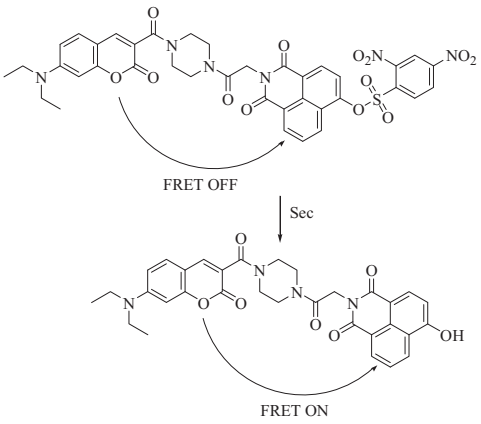

Fig. 78. Mechanism of sensing of selenocysteine by **93.**

4.4. Tyrosinase

Sidhu et al. synthesized two naphthalimide based sensors, **98**–**99**, that detected tyrosinase by showing changes in the emission spectrum with low detection limit (Table 13) [155,156]. The fluorescence change observed in sensor **98** (Fig. 80) was ascribed to the oxidation of 3-hydroxyphenyl moiety to the *o*-dihydroxy derivative, which led to the release of 4-aminonaphthalimide unit from **98** (Fig. 84). The sensor **98** was able to do cellular imaging efficiently, when applied to A375 cells.

Similar type of formation of *o*-dihydroxy derivative by the oxidation of 4-hydroxyphenethylamine moiety was observed, when fluorescent probe **99** (Fig. 85) was covalently linked to carbon dots via naphthalimide fluorophore. The probe **99** was also used for imaging of endogenous tyrosinase and satisfactory results were obtained.

4.5. Nicotinamide adenine dinucleotide-hydrogen (NADH)

A 1,8-naphthalimide based sensor **100** (Fig. 85) synthesized by **Podder** and co-workers, detected NADH levels in living cells, where enhancement in fluorescence was observed upon addition of NADH and nicotinamide adenine dinucleotide phosphate (NAD(P)H) due to *turning on* of the ICT process (Table 13) [157]. Further-

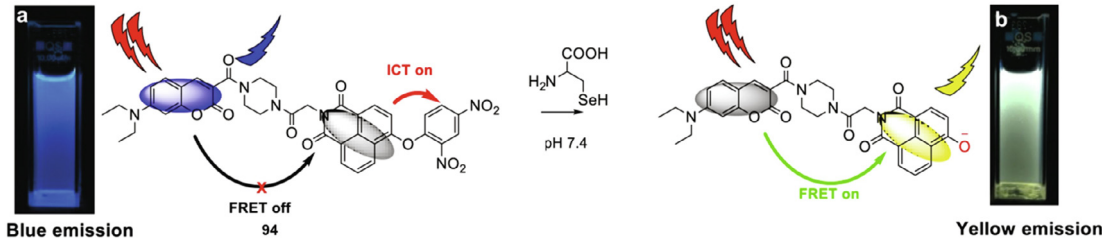

Fig. 79. Pictorial representation of mechanism of interaction of selenocysteine with **94**. (Reproduced from J. Hazard. Mater. 381 (2020) 120,918 [148]).

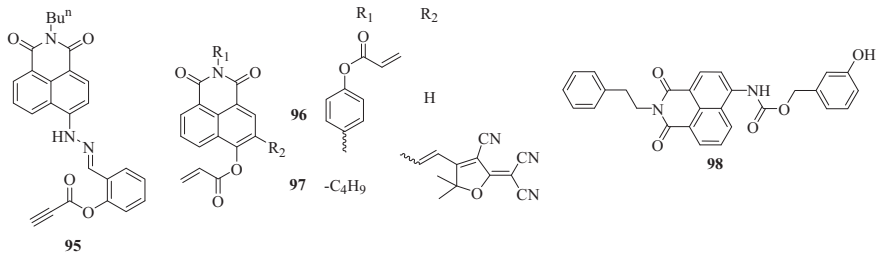

Fig. 80. Structures of chemosensors **95**–**98.**

more, the probe **100** accurately determined the NADH levels in normal cells as well as cancer cells.

4.6. Dipicolinic acid (DPA)

An ICT based hybrid assembly consisting of naphthalimide-histidine receptor, **101** (Fig. 85), coupled with DNA was synthesized by **Verma** and group for the sensing of DPA, which acted as a biomarker for *Bacillus anthracis* spores [150]. On addition of dipicolinic acid to the aqueous solution of **101**, negligible changes in absorption and fluorescence spectrum were observed due to hindrance of amide bond formation between the receptor **101** and DPA, which could be modulated in the presence of DNA. The addition of salmon sperm DNA to the solution of **101** resulted in hypochromic shift in the absorption spectrum and fluorescence quenching of emission peak located at 545 nm, proposing intercalation of DNA with **101**. Moreover, the Circular dichroism (CD) spectrum showed increase in intensities of both the positive and negative bands, again pointing to binding of **101** with DNA via intercalating mode. The DNA-**101** hybrid assembly displayed significant changes in the absorption as well as emission spectrum with addition of dipicolinic acid due to CT interactions between the donor and the acceptor moieties of DNA-**101** hybrid (Table 13). Here, the electron-donating amino group of **101** affected both ICT within the DNA-**101** and the emission maxima, which was responsible for fluorescence detection of DPA (Fig. 86).

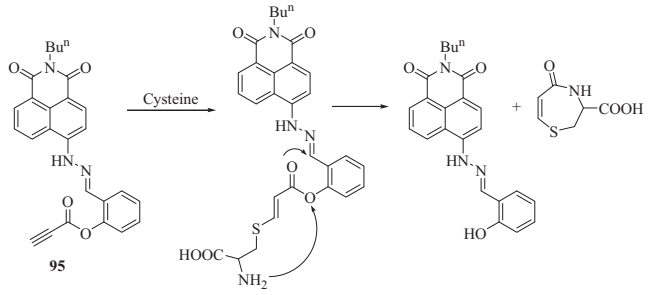

Fig. 81. Possible mechanism of detection of cysteine by **95.**

4.7. Thioredoxin reductase and cancer cells

A carbon dot (energy donor) based naphthalimide (energy acceptor) coupled pair, **102** (Fig. 87), was developed by **Sidhu et al.** for the detection of thioredoxin reductase and cancer cells [158]. Enhancement in fluorescence of **102** was observed in the presence of thioredoxin reductase along with fluorescence color change from orange-yellow to blue (Table 13). This change was ascribed to breakage of disulfide bonds in linker units leading to

Table 13
Solvent systems, absorption and fluorescence changes, naked eye color changes, mechanism and LOD* values of sensors (**96–102**) in the presence of various analytes.

Sensor (Analyte)	Solvent	Absorption changes (nm)	Fluorescence changes (nm)	Color changes	Mechanism	LOD (μM)	Ref.
96 (Cysteine)	DMSO/H_2O (9:1, v/v)	340 → 374, isobestic point at 360	Enhancement at 559	colorless → pale yellow	–	0.12	[154]
97 (Cysteine)	PBS buffer solution	350, 450 → 556, 475	Enhancement at 665	pale yellow → blue-violet	ICT	0.093	[143]
98 (Tyrosinase)	10:90 v/v CH_3CN: PBS	–	467 to 535	–	–	0.2[a]	[155]
99 (Tyrosinase)	PBS solution	–	Decrease at 540 nm	–	FRET & PET	1.2[a]	[156]
100 (NADH)	PBS buffer with 1% DMSO	–	Enhancement at 460 and 550	–	–	1.075[b] 1.114[c]	[157]
101 (Dipicolinic acid)	HEPES buffer	430 → 451	Enhancement at 520	–	ICT	0.012	[150]
102 (Thioredoxin reductase)	HEPES buffer	–	Enhancement at 450 and quenching at 565	–	FRET	0.072	[158]

*LOD values have been determined by observing fluorescence changes.
[a] LOD values are in the units U mL^{-1}.
[b] for emission at 460 and [c] for emission at 550.

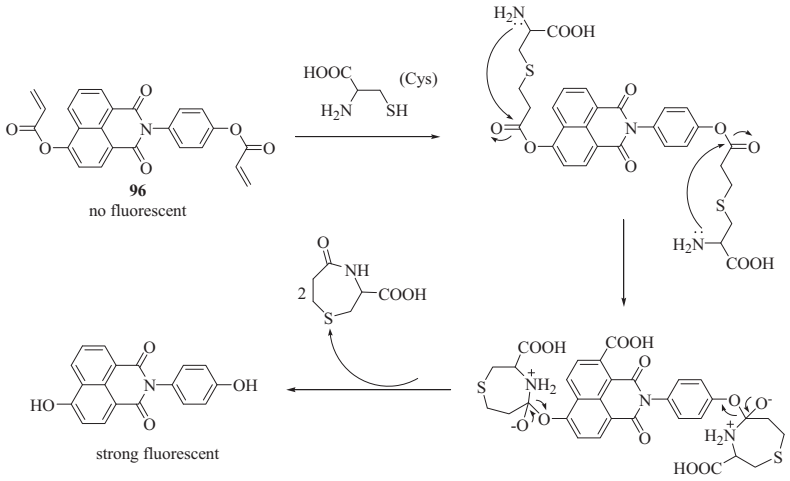

Fig. 82. Possible sensing mechanism of cysteine using sensor **96.**

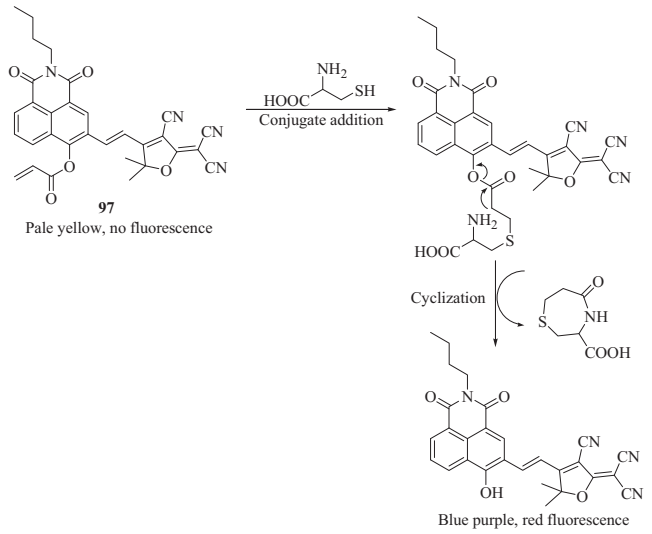

Fig. 83. Possible sensing mechanism of cysteine using sensor **97.**

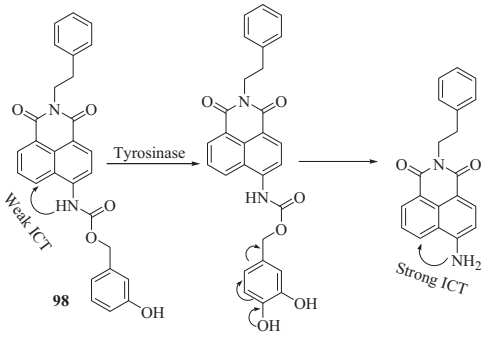

Fig. 84. Possible mechanism of sensing of tyrosinase using sensor **98.**

separation of two fluorophore units by which energy transfer process got eliminated. The proposed sensor was also utilized for the detection of cancer cells.

4.8. Triphosphate (TPP) and TPP based biomolecules

1,8-Naphthalimide based charged sensors **(103a** and **103b)** (Fig. 88) were synthesized for the sensing of TPP and TPP based biomolecules by **Mondal et al.** [160]. Addition of $P_3O_{10}^{5-}$ (PPPi) to the CH_3CN-H_2O (1:1, v/v, pH = 6.8, 10 mM HEPES buffer) solution of **103a** and **103b** quenched the fluorescence emission at 451 nm. $HP_2O_7^{3-}$ and $P_2O_7^{4-}$ also perturbed the emission but to a lesser extent than PPPi. Similarly, adenosine triphosphate (ATP) produced more spectral changes as compared to adenosine diphosphate (ADP) and adenosine mono phosphate (AMP). The association constant (LOD) values for **103a**.PPPi and **103b**.PPPi were found to be 3.62 × 10^4 M^{-1} (0.672 μM) and 7.04 × 10^3 M^{-1} (6.82 μM), respectively, displaying more sensitivity of **103a** towards the detection of PPPi. In the UV–Vis spectrum of **103a**, decrease in absorption intensity at 362 nm and quenching in fluorescence at 451 nm was observed and maximum decrease was observed in case of PPPi amongst all tested anions. Furthermore, it was found that guanosine triphosphate (GTP), cytidine triphosphate (CTP) and thymidine triphosphate (TTP) also exhibited significant spectral changes, making the proposed sensors non-selective for ATP detection over these triphosphate based biomolecules. The sensors **103a**.PPPi and **103b**.PPPi were also able to detect Ca^{2+} and Mg^{2+} ions in aqueous solution.

4.9. Acetylcholine

Mangalath et al. 2017 synthesized pH sensitive graphene oxide-naphthalimide nanoconjugates **(GO-104** and **rGO-104)** (Fig. 89), among which **GO-104** was used for the detection of acetylcholine (ACh) [161]. The nanoconjugates exhibited highly quenched fluorescence in aqueous solutions due to π-π interaction of the chromophores with the graphene oxide surface and internal PET processes (Fig. 89). However, lowering the pH resulted in enhancement of the fluorescence. This was due to protonation of the N atoms of **104** and all oxygen containing functional groups of **GO/rGO** surface at lower pH, which perturbed the strong interaction of **104** with GO surface. Also, protonation of N-atoms enhanced the hydrophilicity and solubility of **104** in aqueous media, resulting in the dynamic dislocation of the molecules of **104** from the **GO** surface. The ability of **GO-104** for the detection of pH change was further employed for its use towards enzymatic hydrolysis of ACh to choline and acetic acid by lowering the pH, which was detected by *turn-on* response of **GO-104**.

4.10. Glucosyltransferases

Feng et al. synthesized a two-photon ratiometric fluorescent probe *N*-(n-butyl)-4-hydroxy-1,8-naphthalimide **105** (Fig. 90) for the detection of glucosyltransferases in fungal samples [159]. The product formed upon reaction of **105** with glycosyltransferase exhibited blue fluorescence under UV light, which was helpful in the isolation of fungal strains having over-expression of glucosyltransferases from complex soil samples. The emergence of blue fluorescence was ascribed to the acceptance of glucosyl group by phenolic hydroxyl group because of its capacity as good electron donor. Since 4-OH led to strong ICT effect upon excitation, its glucolysation to yield 4-*O*-*β*-D-glucopyranosyl-*N*-butyl-1,8-naphthalimide imparted significant changes in the emission spectrum (Fig. 91). Using the strategy proposed, two fungal strains were isolated, which were identified to be *Rhizopus oryzae* and *Mucor circinelloides*.

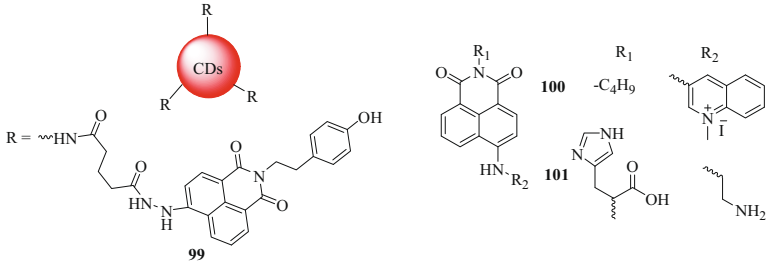

Fig. 85. Structures of chemosensors **99**–**101.**

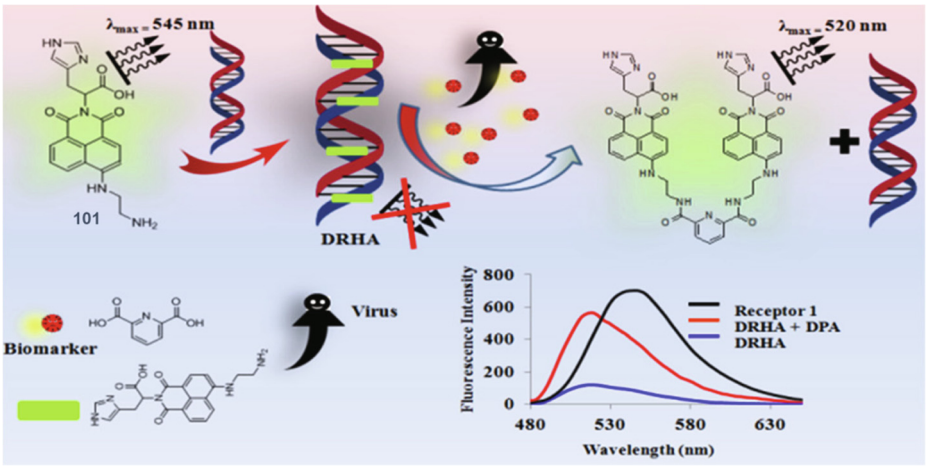

Fig. 86. Pictorial representation of DPA sensing by **101** (Reproduced from Langmuir 34 (2018) 6591–6600 [150]).

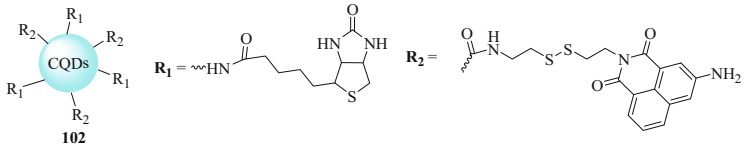

Fig. 87. Structure of chemosensor **102.**

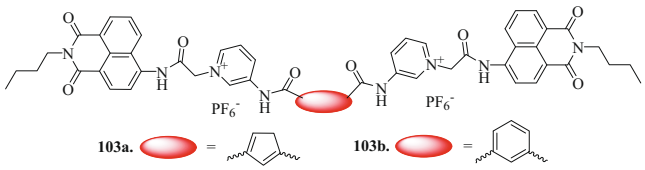

Fig. 88. Structures of chemosensors **103a-b.**

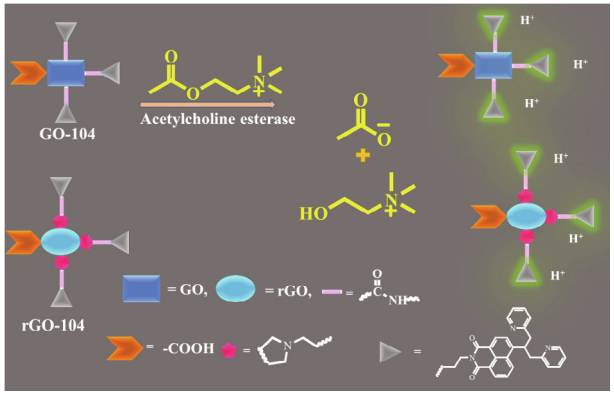

Fig. 89. Sensing of Ach. by **GO-104** and **rGO-104.**

4.11. Heparin

Ghosh and co-workers synthesized 1,8-naphthalimide based derivative, **106** (Fig. 90), having naphthyl residue and 3-aminopyridyl units at both ends that detected heparin by forming its FONPs in DMSO-H_2O binary solvent mixture [151]. **106** possessing FONPs exhibited orange fluorescence as naphthyl residue promoted ICT process. Further, positively charged protamine (Pro) interacted with negatively charged aminopyridine residues of FONPs to yield **106** based FONP-Pro conjugates with diminished fluorescence intensity. Addition of heparin to the **106** based FONP-Pro conjugates, *turned on* the fluorescence, as protamine was removed from the surface of conjugates because of very strong interaction between heparin and protamine (Fig. 92). LOD of **106** based FONP-Pro conjugates towards heparin was measured to be as low as 12 nm.

Another heparin detecting naphthalimide based sensor, **107** (Fig. 90), was synthesized by **Zheng et al.** due to their AIE as **107** had both positive and negative charges in the molecule, making the electrostatic interaction possible, leading to aggregation of **107** [153]. Incorporation of heparin to the Tris-HCl (10 mM, pH 6.0) buffer solution of **107** caused enhancement in fluorescence at 365 nm with solution color change from light yellow to bright green. LOD value of the proposed sensor **107** towards heparin was measured to be 7.56 ng/mL. Further, **107**.heparin complex was utilized for the detection of protamine (a drug used to treat bleeding caused by excessive heparin injection). On addition of protamine to the solution of **107**.heparin, its fluorescence intensity decreased by a factor of 5.1 because protamine weakened the electrostatic interaction between **107** and heparin.

5. Sensors for multiple analytes:

A symmetrical tripod, **108** (Fig. 93), having three 4-(*N*-methylpiperazine)-1,8-naphthalimide was synthesized by **Staneva et al.** and was evaluated for antimicrobial activity along with its use as metal ion sensor [162]. When Zn^{2+}, Ni^{2+}, Pb^{2+} and Cu^{2+} metal ions were added to the acetonitrile solution of **108**, enhancement in fluorescence was observed, but highest enhancement was shown by Zn^{2+} ions.

A 1,8-naphthalimide based sensor, **109** (Fig. 93), was synthesized by **Jang** and co-workers for the detection of trivalent cations

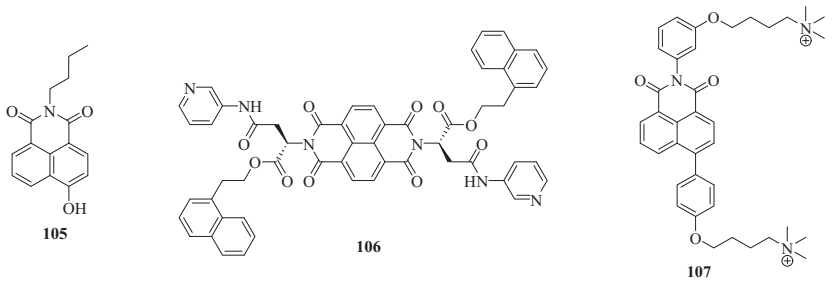

Fig. 90. Structures of chemosensors **105–107.**

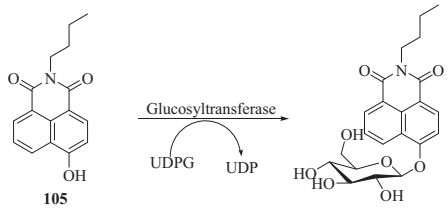

Fig. 91. Sensing of glucosyltransferase by **105.**

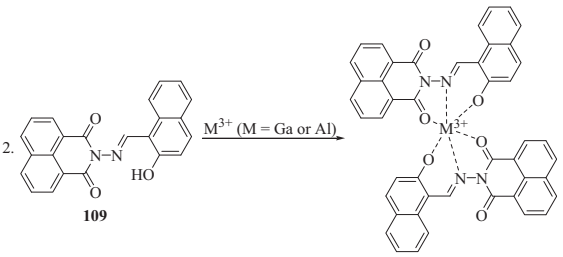

Fig. 94a. Proposed binding mode between **109** and M^{3+} (M = Ga or Al).

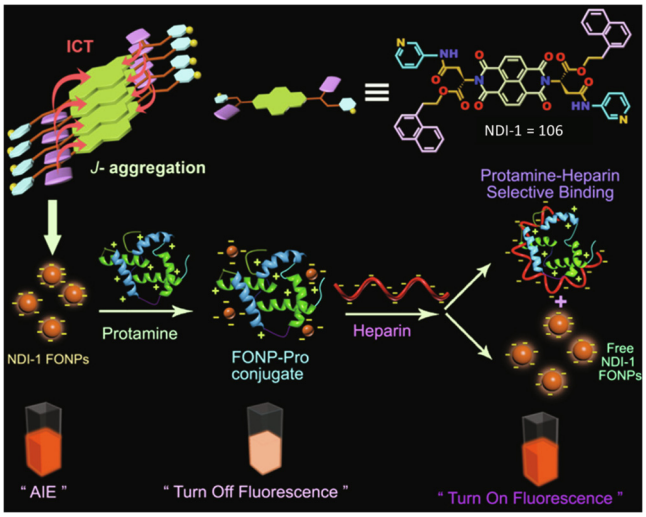

Fig. 92. Proposed mechanism of detection of heparin using **106** based FONP-Pro conjugates (Reproduced from Langmuir 35 (2019) 15180–15191 [151]).

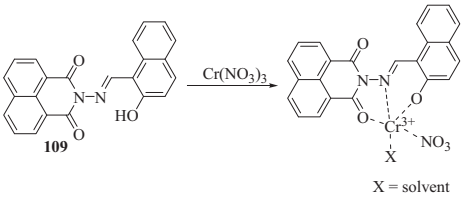

Fig. 94b. Proposed binding mode between **109** and Cr^{3+}.

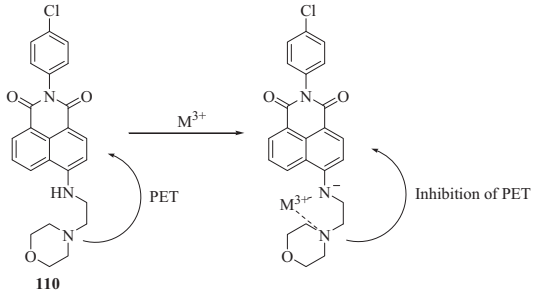

Fig. 95. Proposed mode of interaction between **109** and M^{3+}.

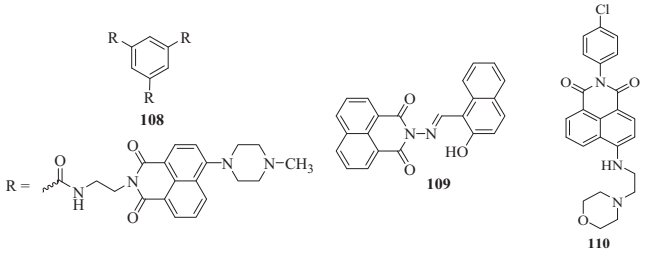

Fig. 93. Structures of chemosensors **108–110.**

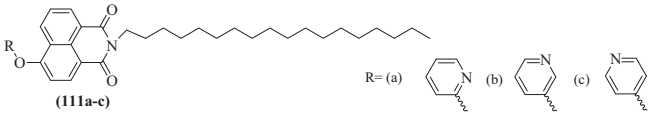

Fig. 96. Structures of chemosensors **111a-c.**

viz. Ga^{3+}, Al^{3+} and Cr^{3+} [163]. The free sensor **109** exhibited very little fluorescence, however, on addition of Ga^{3+}, Al^{3+} and Cr^{3+} ions, significant enhancement in fluorescence was observed at 550, 535 and 356 nm, respectively. This process was accompanied by appearance of blue-green and yellow fluorescence in the presence of Ga^{3+} and Al^{3+}ions, respectively. Binding stoichiometry in both **109**.Ga^{3+} and **109**.$Al^{3+}$was measured to be 2:1, in which metal cations were bound to oxygen atoms of the naphthalene groups and nitrogen of the imine moiety (Fig. 94a). On the contrary, Cr^{3+} showed binding with **109** in 1:1 stoichiometric ratio (Fig. 94b). The association constant values for **109**.M^{3+} were found to be 9.0×10^7 M^{-2} (for **109**.Ga^{3+} 2:1), 9.0×10^7 M^{-2} (for **109**.Al^{3+} 2:1) and 1.1×10^3 M^{-1} (for **109**.Cr^{3+} 1:1).

A PET based morpholine-type naphthalimide chemosensor **110** (Fig. 93) was synthesized by **Ye** and co-workers and utilized for the detection of Fe^{3+}, Al^{3+} and Cr^{3+} ions [164]. On addition of Fe^{3+}, Al^{3+} and Cr^{3+} ions to the methanolic solution of **110**, respective blue shift of 23, 18 and 18 nm was observed in the absorption maxima located at 438 nm and pale-yellow color of the solution deepened. In the fluorescence spectrum, significant enhancement in fluorescence at 509 nm was observed in the presence of these three trivalent metal ions. The changes in the fluorescence spectrum were ascribed to the prohibition of electron transfer between lone pair of electrons on nitrogen atom of morpholine and naphthalimide fluorophore due to coordination of nitrogen atoms of **110** with trivalent metal cations (Fig. 95). The association constant values for **110**:M^{3+} (1:1) stoichiometric complexes were calculated to be 5.34×10^4, 3.32×10^4 and 4.99×10^4 M^{-1} for Fe^{3+}, Al^{3+} and Cr^{3+} ions, respectively; while LOD values were found as 0.65, 0.69 and 0.68 μM, respectively. On addition of EDTA to **110**.M^{3+} solutions, fluorescence spectra were regained, indicating the reversible nature of probe and on the basis of this reversibility, INHIBIT logic gate was developed. Furthermore, the proposed sensor efficiently detected these trivalent cations in C2C12 (Mouse myoblast) cells.

Cao et al. synthesized a series of gelators based on naphthalimide derivatives **(111a-111c)** (Fig. 96) with different molecular isomers viz. 2-hydroxypyridine, 3-hydroxypyridine and 4-hydroxypyridine as terminal groups [165]. Among these, **111b** and **111c** formed stable organogels; while for **111a**, only precipitates, solution or partial gel was obtained. Upon studying the photophysical properties, **111a** did not show any detection ability towards any metal ion; while **111b** and **111c** efficiently detected Fe^{3+} and Hg^{2+}ions in CH_3CN solution as well as in the gel form as indicated by the changes caused by these ions in the absorption and fluorescence spectrum (Table 14).

Two chemosensors (**112a** and **112b**) (Fig. 97) were synthesized by **Georgiev** and co-workers on the basis of "fluorophore-receptor$_1$-spacer-receptor$_2$" model and their sensing properties towards pH and various cations were evaluated in 100% aqueous medium, where fluorescence spectrum of **112a** and **112b** got perturbed in the presence of H^+, OH^-, Cu^{2+} and Hg^{2+} ions [166]. In the acidic medium, sensors **112a** and **112b** exhibited blue fluorescence as PET quenching process was not feasible due to the protonation of the tertiary amine ("receptor$_2$"). The blue fluorescence kept on decreasing as the pH of the medium was changed from neutral to alkaline as "push–pull" character of the ICT transition got reduced due to deprotonation of N-imide unit (Fig. 98). In the presence of Cu^{2+} and Hg^{2+} ions also, large fluorescence quenching was observed at 396 nm. Binding ratio in **112a**/**112b**.Cu^{2+} was found to be 1:1 in which metal ions were bound to amido carbonyls and tertiary alkylamino nitrogen of **112a** and **112b**. The association constant values for Cu^{2+} and Hg^{2+} were measured to be 5.7×10^5 and 1.8×10^5 M^{-1} for **112a** and 2.5×10^5 and 2.1×10^5 M^{-1} for **112b**, respectively. The LOD values of Cu^{2+} and Hg^{2+} were calculated to be 1.5×10^{-6} and 1.9×10^{-6} M for **112a** and 1.8×10^{-6} and 2.3×10^{-6} M for **112b**, respectively. Furthermore, INH and doubly disabled INH logic gates were developed from the proposed sensors.

Table 14
Absorption and fluorescence changes, K_a* and LOD* values of sensors (111a-**111c**) in CH_3CN solution as well as in gel forms.

Sensor (Analyte)	Absorption changes	Fluorescence changes (nm)	K_a (x $\times 10^5$ M^{-1})	LOD (μM)	Ref.
111a solution (Fe^{3+}, Hg^{2+})	No change	No change	–	–	[165]
111b solution (Fe^{3+})	Increase at 239 and 355 nm with 4–5 nm blue shift	80 % decrease at 420	0.164	47.6	[165]
111b solution (Hg^{2+})	Increase at 239 with slight blue shift and blue shift of 355	420 (88.7 % decrease) → 409	0.379	7.01	[165]
111c solution (Fe^{3+})	273 → 330 350 → 344 Increase at 231 and 237	Decrease at 492 & Increase at 383	1.44	32.6	[165]
111c solution (Hg^{2+})	–	Decrease at 492 & Increase at 383	0.199	1.77	[165]
111b gel (Fe^{3+})	–	92 % quenching with 27 nm blue shift	–	–	[165]
111b gel (Hg^{2+})	–	48.9 % quenching with 12 nm blue shift	–	–	[165]
111c gel (Fe^{3+})	–	96 % quenching with 14 nm blue shift	–	–	[165]
111c gel (Hg^{2+})	–	39.2 % quenching with 30 nm blue shift	–	–	[165]

*K_a and LOD values have been determined by observing fluorescence changes.

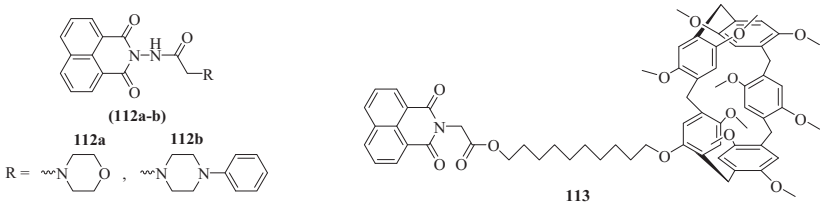

Fig. 97. Structures of chemosensors **112–113.**

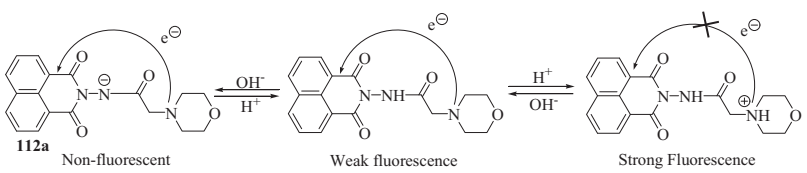

Fig. 98. Photophysical behaviour of **112a** with change in pH.

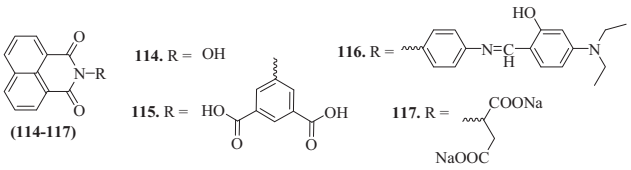

Fig. 99. Structures of chemosensors **114**–**117.**

Lin et al. synthesized supramolecular polymer based on naphthalimide-functionalized pillar [5] arene **113** (Fig. 97) and developed an efficient method for providing controllable multi-stimuli responsive properties to it by introducing donor–acceptor and redox effect of iodine into the system [167]. Addition of CN^- ions to the gel **113**.I_2, *turned on* the fluorescence of the gel by enhancing the fluorescence at 540 nm due to redox reaction between CN^- and I_2, which removed I_2 from the gel and free form of gel was regenerated. Other anions had no impact on the fluorescence spectrum of the gel. LOD of I_2 controlled gel towards CN^- ion detection was measured to be 4.1×10^{-8} M. The gel **113**.I_2 also detected Hg^{2+} ions and cysteine by showing fluorescence *turn-on* response at 540 nm with LOD values 1.0×10^{-7} and 3.3×10^{-8} M, respectively. Further, it was found that **113**.I_2 efficiently detected all the three analytes not only in gel form but also in DMSO-H_2O binary solution and in living cells.

Kavitha and group synthesized a naphthalimide based sensor, **114** (Fig. 99), for the detection of Bi^{3+} with the detection limit as low as 0.58 μg mL^{-1} [168]. In the absence of metal ion, fluorescence of **114** was quenched in neutral aqueous solution due to PET process occurring by electron transfer from the lone pair on nitrogen (donor) of the central chain to the naphthalimide (acceptor). Addition of Bi^{3+} caused enhancement in fluorescence as PET was blocked due to strong coordination between **114** and Bi^{3+}. Significant changes were observed in the UV–Vis spectrum (Table 15) in the presence of Bi^{3+} but with no visual color change. Binding ratio in **114**.Bi^{3+} was found to be1:1, in which Bi^{3+} was coordinated to N atom, C=O and OH groups of **114** (Fig. 100) as confirmed by UV–Vis, fluorescence, FT-IR and ^1H NMR spectra. Furthermore, the sensor **114** exhibited *turn-off* response at 383 nm with increase in pH from 5.0 to 12.0 due to pH dependent ionization of the hydroxyl group of **114**.

Wang et al. synthesized a fluorescence "*on–off–on*" 1,8-naphthalimide based sensor, **115** (Fig. 99), for the detection of Fe^{3+} ions in pure water and complex **115**.Fe^{3+} was further utilized for the sensing of cyanide (CN^-) ions [169]. Significant changes were observed in the absorption and fluorescence spectrum (Table 15) with drastic fluorescence color change form blue to colorless observable under UV lamp. The proposed mechanism of binding of **115** with Fe^{3+} was through carbonyl oxygen atoms adopting Fe–O–C–O–Fe modes (Fig. 101). Further, on addition of CN^- ions, the completely quenched fluorescence due to **115**.Fe^{3+} was regained and other competitive ions did not show any interference with the detection of Fe^{3+} and CN^- ions. To check the practical utility of **115** and **115**.Fe^{3+}, test strips based on these were prepared, which conveniently detected Fe^{3+} and CN^- ions.

A fluorescent naphthalimide based sensor **116** (Fig. 99) possessing Schiff base functionality was synthesized by **Zhang** and group for the detection of Fe^{3+} and CN^- ions [170]. The proposed sensor efficiently detected both the ions as indicated by the changes in absorption and fluorescence spectrum (Table 15). The test strips based on **116** were fabricated, which efficiently detected Fe^{3+} and CN^- ions (in bitter almonds). The imine and hydroxyl groups of **116** acted as good ion binding sites involving hydrogen bond interactions and **116** detected Fe^{3+} via coordination mechanism through "O" and "N" heteroatoms in "O-Fe^{3+}-N" manner and CN^- ions through deprotonation mechanism (Fig. 102).

Zhang and co-workers synthesized a water soluble fluorescent "*off–on–off*" chemosensor **117** (Fig. 99) based on aspartic acid functionalized 1,8-naphthalimide derivative, which efficiently detected Fe^{3+} and further **117**.Fe^{3+} detected $H_2PO_4^-$ in aqueous media (Table 15) [171]. The Fe^{3+} concentration sensed by sensor **117** was in close agreement with results obtained by ICP (inductively coupled plasma) experiments.

Liu and co-workers synthesized a naphthalimide based *turn-on* fluorescent sensor **118** (Fig. 103) for the sensing of Fe^{2+} and $H_2PO_4^-$ ions [172]. The addition of Fe^{2+} ions to the DMSO solution of **118**

Table 15
Solvent systems, absorption and fluorescence changes, color changes, K_a* and LOD* values of sensors (**114**–**118**) in the presence of various analytes.

Sensor	Solvent	Absorption changes (nm)	Fluorescence changes (nm)	Color changes	K_a ($\times 10^4$ M^{-1})	LOD (μM)	Ref.
114 (Bi^{3+})	Pure water	Increase at 342.5	Enhancement at 383	–	0.0332	2.72	[168]
115 (Fe^{3+})	Pure water	Enhancement at 348 and broad shoulder peak emerged in the region of 350–420	Disappearance at 396	Blue → colorless	4.57	0.197	[169]
115.Fe^{3+} (CN^-)	Pure water	Decrease at 348 and disappearance of shoulder peak in the region of 350–420	Increase at 396	–	–	2.6×10^{-4}	[169]
116 (CN^-)	DMSO/ H_2O (8:2, v/v)	–	Enhancement at 467	–	–	0.063	[170]
116 (Fe^{3+})	DMSO	346 to 338	Quenching at 467	yellow → dark	–	0.23	[170]
117 (Fe^{3+})	Pure water	–	Quenching at 385	–	2.9	0.497	[171]
117.Fe^{3+} ($H_2PO_4^-$)	Pure water	–	Enhancement at 385	–	–	5.27	[171]
118 (Fe^{2+})	DMSO	–	Quenching at 531	–	–	–	[172]
118.Fe^{2+} ($H_2PO_4^-$)	DMSO	–	Enhancement at 531	–	–	0.1897	[172]

*K_a and LOD values have been determined by observing fluorescence changes.

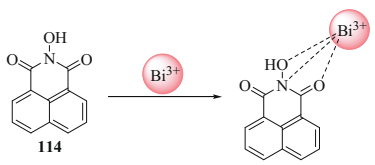

Fig. 100. Schematic representation of interaction of Bi^{3+} with **114.**

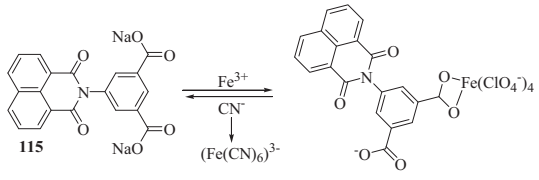

Fig. 101. Possible mechanism of sensing of Fe^{3+} by **115** and sensing of CN^- by **115**. Fe^{3+}.

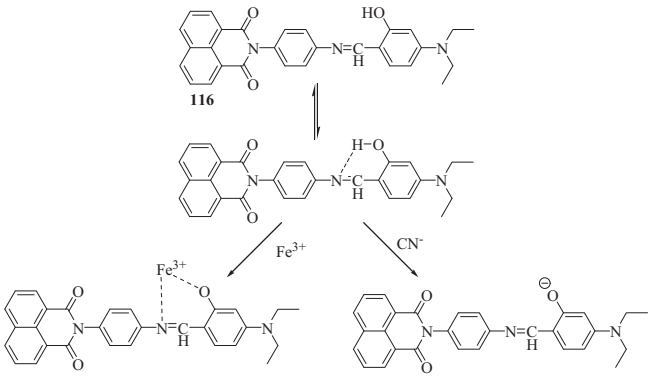

Fig. 102. Possible mechanism of sensing of Fe^{3+} and CN^- by **116.**

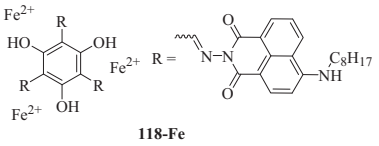

Fig. 103. Structure of chemosensor **118.**

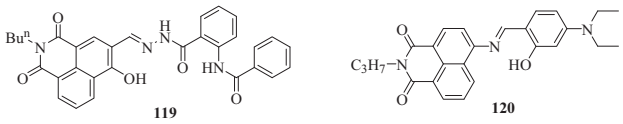

Fig. 104. Structures of chemosensors **119–120.**

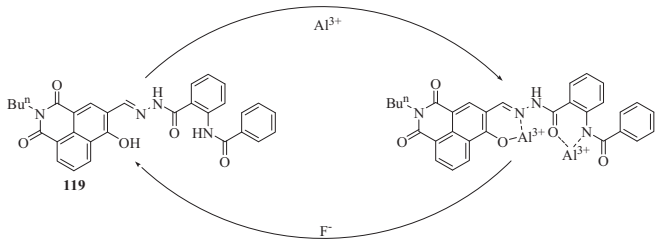

Fig. 105. Representation of sequential binding of Al^{3+} with **119** and F^- with **119**. Al^{3+}.

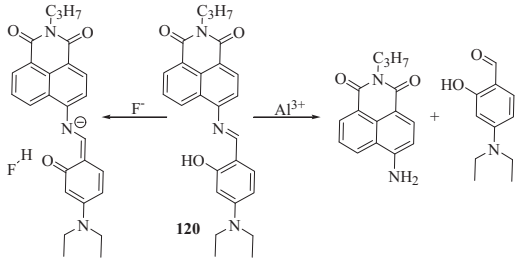

Fig. 106. Proposed mechanism of sensing of Al^{3+} and F^- by **120.**

caused quenching of yellow green fluorescence (Table 15) which was regained on addition of $H_2PO_4^-$ ions to **118**. Fe^{2+} due to $H_2PO_4^-$ mediated displacement of Fe^{2+}.

Zhang et al. synthesized a naphthalimide based fluorescent *off–on-off* chemosensor, **119** (Fig. 104), for the quantification of Al^{3+} and F^- ions [173]. Upon incorporation of Al^{3+} ions to the DMSO/H_2O (9/1, v/v, pH 7.4, HEPES buffer, 0.2 mM) solution of **119**, significant enhancement in fluorescence emission intensity was observed at 513 nm along with slight blue shift and fluorescence color changed from colorless to bright green. In the absorption spectrum, absorption peak at 350 nm was shifted to 470 nm with clear isobestic point at 416 nm accompanied by color change from yellow to bluish green under UV light. The probe **119** coordinated to Al^{3+} in 1:2 manner and detection limit and association constant values were measured to be 80 nM and 4.22×10^{10} $M^{-1/2}$ respectively. From the IR spectrum and DFT study, the possible mechanism for detection of Al^{3+} came out to be inhibition in ESIPT process as a consequence of supressed C=N isomerization due to coordination Al^{3+} with phenolic-O, imine-N, carbonyl-O and amine-N atoms in **119** (Fig. 105). Further, the *in-situ* formed **119**. Al^{3+} was employed for the detection of F^- ions with the detection limit down to 44 nm. In the presence of F^- ions, the emission intensity at 513 nm was quenched, which was again enhanced upon addition of Al^{3+} ions indicating the reversible nature of probe **119** upto 3 cycles. Furthermore, the proposed sensor efficiently determined Al^{3+} ions in HeLa cells and in the form of test strips.

An ESIPT-ESICT based dual-channel ratiometric probe **120** (Fig. 104) derived from naphthalimide was synthesized by **Kumar** and co-workers for the detection of Al^{3+} and F^- ions [174]. Addition of Al^{3+} ions to the H_2O/CH_3CN (1:9; v/ v, pH = 7.2) solution of **120** led to increase in absorption intensity at 460 nm and decrease at 340 nm along with color change from orange to yellow. In the emission spectrum, new emission peak appeared at 540 nm and color of the fluorescence changed from reddish-orange to yellow. In the presence of fluoride ions, emission peak appeared at 570 nm with fluorescence color change from orange to purple. These changes were ascribed to the Al^{3+} mediated hydrolysis of **120** and deprotonation of **120** in the presence of F^- ions (Fig. 106). The LOD values of **120** towards Al^{3+} and F^- ions were measured to be 3.2×10^{-8} M and 4.6×10^{-7} M, respectively.

A PET based chemosensor **121** (Fig. 107) was synthesized by **Dwivedi et al.** in which naphthalimide and anthracene chromophores were joined through a molecular bridge of piperazine and triazole units [175]. On addition of Cr^{3+} ions to the solution of **121**, changes were observed in the absorption and fluorescence spectrum (Table 16) and bright green color fluorescence appeared in the solution, which was ascribed to the suppression of PET process. In **121**. Cr^{3+}complex, Cr^{3+} was bound to **121** via N atoms of a piperazine-triazole molecular bridge. Incorporation of PO_4^{3-} to the solution of **121**. Cr^{3+} diminished the fluorescence intensity and produced *turn-off* state. Further, based on "*off–on-off*" switching process, INHIBIT logic gate was constructed. Based on good permeability and cytocompatibility of the proposed sensor, it was used for the imaging of Cr^{3+} and PO_4^{3-} in HeLa cells and satisfactory results were obtained. Moreover, the probe **121** was used to print secret letters using ink containing Cr^{3+}, which were readable only under UV light.

Another naphthalimide based chemosensor **122** (Fig. 107) detected Al^{3+} and ClO^- ions in methanol, wherein addition of Al^{3+} ions blue shifted the absorption peak of the free sensor because of decreased conjugation due to reduction in electron donating ability of piperazine ring to naphthalimide after complexation with Al^{3+} (Table 16) [176]. In the fluorescence spectrum, enhancement in fluorescence was observed in the presence of Al^{3+} ions due to the CHEF effect because of formation of a rigid system after binding with Al^{3+}. Binding ratio in **122**.Al^{3+} was found to be 1:1 in which Al^{3+} ion was coordinated to **122** via two nitrogen atoms of piperazine ring and amide nitrogen atom (Fig. 108). Addi-

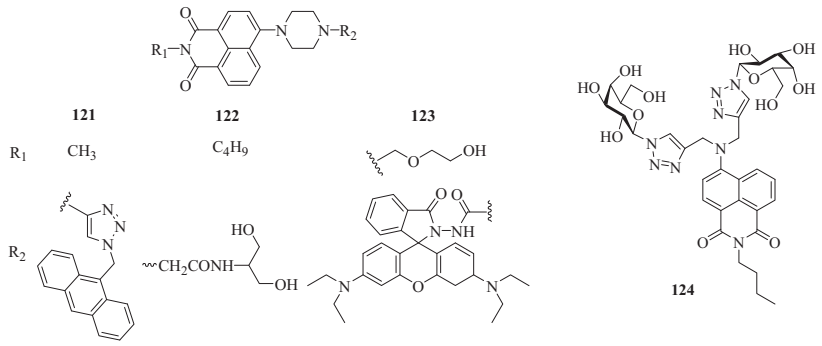

Fig. 107. Structures of chemosensors **121**–**124.**

Table 16
Solvent systems, absorption and fluorescence changes, color changes, mechanism, stoichiometry (Ligand:Analyte), and LOD* values of sensors (**121**–**124**) in the presence of various analytes.

Sensor	Solvent	Absorption changes (nm)	Fluorescence changes (nm)	Color changes	Mechanism	Stoichiometry	LOD (μM)	Ref.
121 (Cr^{3+})	THF/Tris-HCl buffer (v/v 4:6)	Disappearance at 410	Enhancement at 529 with 14 nm blue shift	–	PET	1:1	0.05567	[175]
121.Cr^{3+} (PO_4^{3-})	THF/Tris-HCl buffer (v/v 4:6)	–	Quenching at 529	–	PET	–	0.39	[175]
122 (Al^{3+})	MeOH	399 to 378 nm	Enhancement at 505	yellow → colorless	CHEF	1:1	0.0203	[176]
122.Al^{3+}(ClO^-)	MeOH	378 to 399	Quenching at 505	–	–	–	0.0234	[176]
123 (Cu^{2+})	CH_3CN-H_2O (v/v, 9/1)	Appearance at 564	Appearance at 528 and 610	Light yellow → pink	PET	1:1	0.17	[177]
123.Cu^{2+} (H_2S)	CH_3CN-H_2O (v/v, 7/3)	Disappearance at 564	Quenching at 528 and 610	pink → light yellow	–	–	0.23	[177]
124 (Cu^{2+})	Pure water	–	10-fold quenching at 535	–	–	1:1	0.0123	[178]
124.Cu^{2+} (S^{2-})	Pure water	–	Increase at 535	–	–	–	0.0032	[178]

*LOD values have been determined by observing fluorescence changes.

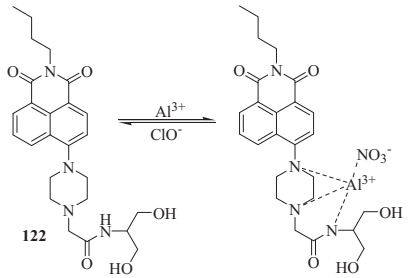

Fig. 108. Proposed mechanism of sensing of Al^{3+} by **122** and ClO^- by **122**.Al^{3+}.

tion of ClO^- ions to the methanolic solution of **122**. Al^{3+} quenched the fluorescence, thus acting as *turn-off* sensor for ClO^- ions as free sensor **122** was regenerated. Moreover, INHIBIT molecular logic gate was constructed based on behaviour of **122** towards Al^{3+} ions and **122**. Al^{3+} towards ClO^- ions.

A chemosensor, **123** (Fig. 107), based on naphthalimide-rhodamine B derivative was synthesized by **Wang** and group for the sequential detection of Cu^{2+} and H_2S [177]. Incorporation of Cu^{2+} ions to the solution of **123** caused significant changes in the absorption and fluorescence spectrum with fluorescence color change from green to light yellow (Table 16). These changes were ascribed to 1:1 binding stoichiometry of **123**. Cu^{2+}, in which spiro-

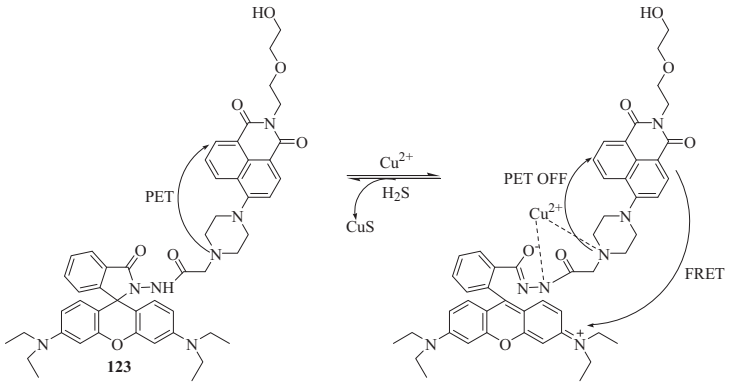

Fig. 109. Plausible mechanism of detection Cu^{2+} by **122** and H_2S by **122**.Cu^{2+}.

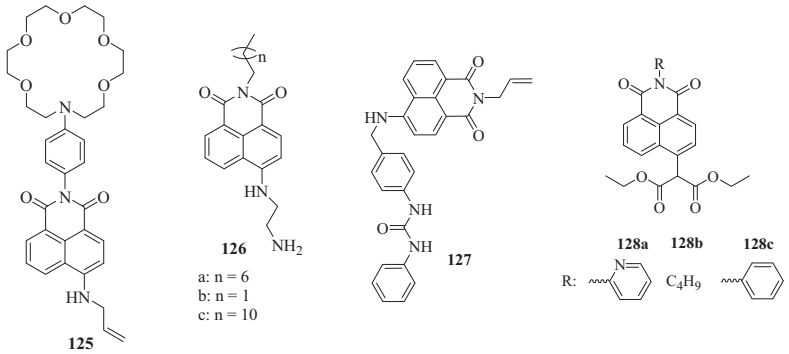

Fig. 110. Structures of chemosensors **125–128.**

lactam rhodamine B structure was changed to open ring amide structure due to binding of Cu^{2+} with amino group on the piperazine of **123**, which disturbed the PET process (Fig. 109). Further, **123**. Cu^{2+} complex was employed for the detection of H_2S as it caused significant changes in its absorption and fluorescence spectrum due to decomplexation reaction (Table 16).

A chemosensor **124** (Fig. 107) based on 1,8-naphtahlimde was employed for the detection of $Cu^{2+}$and S^{2-} ions by observing the changes in fluorescence spectrum (Table 16) [178]. Addition of Cu^{2+} ions to the aqueous solution of **124** resulted in decrease in fluorescence intensity due to coordination of probe with the paramagnetic Cu^{2+} center. Further, the fluorescence emission of **124**. Cu^{2+} was recovered on addition of S^{2-} ions due to displacement mechanism.

Oshchepkova et al. synthesized copolymer gel based on a crown-containing allyl derivative of 1,8-naphthalimide **125** (Fig. 110) as it contained double bond essential for copolymerization with *N,N*-dimethylacrylamide (DMA) and *N,N'*-methylene bis (acrylamide) (MBA) and investigated metal detection properties of both the monomer and polymer gel forms [179]. Addition of Mg^{2+}, Ca^{2+} and Ba^{2+} ions to the acetonitrile solution of **125** caused increase in fluorescence intensity by factors of 1.1, 3.0 and 9.4, respectively. Further the response of gels prepared from **125** was analyzed towards metal ion sensing, among which only Ca^{2+} and Ba^{2+} ions caused significant enhancement in the fluorescence intensity by factors of 2.3 and 4.8. The difference in the sensing ability of monomer **125** and its polymer was ascribed to the fact that once the critical positive charge in polymer was reached, it became unable to bind cations and a portion of ionophoric groups did not participate in complexation.

N–alkyl naphthalimide fluorophore conjugates (**126a-126c**) (Fig. 110) possessing an ethylenediamine moiety were synthesized by **Narula et al.** and used them for the differential detection of Zn^{2+} and Al^{3+} [180]. On addition of analytes to **126a** in sodium dodecyl sulfate (SDS) surfactant medium at critical micellar concentration, it was not able to detect any ion, however, when the sensing was carried out at half of critical micellar concentration, Zn^{2+} and Al^{3+} ions increased the fluorescence intensity by 12–14 fold along with blue shift of 6–8 nm. LOD values of **126a** towards Zn^{2+} and Al^{3+} ions were measured to be 85 and 57 nM, respectively. Among the synthesized conjugates, **126a** exhibited best results for the detection of Zn^{2+} and Al^{3+}. Further, **126**.Zn^{2+} complex was used for the detection of DPA. On addition of aqueous solutions of DPA to the solution of **126a**.Zn^{2+}, decrease in emission band at 515 nm was observed. The order of sensing ability of **126**.Zn^{2+} complexes towards DPA came out to be **126a**.Zn^{2+} > **126b**.Zn^{2+} > **126c**.Zn^{2+}.

4-amino-1,8-naphthalimide based sensor **127** (Fig. 110) possessing urea functionality showed 73%, 70% and 15% fluorescence quenching by acetate, dihydrogen phosphate and bromide ions, respectively, in DMSO with 0.5% v/v water [181]. It was found that anion upon binding with urea causes a positive allosteric effect due to which secondary binding event occurred to further form 1:2 and 2:1 complexes after initial formation of 1:1 complexes between **127** and corresponding anions.

1,8-naphthalimide based sensors **(128a-128c)** (Fig. 110) were synthesized by **Yan** and co-workers for the determination of F^- ions and trace water [182]**.** All the three probes exhibited similar response towards F^- ions with naked eye color change from colorless to violet due to keto-enol tautomerism. The free sensors (**128a-128c**) exhibited absorption band in the visible region (250–400 nm). Addition of F^- ions to the DMSO solution of (**128a-128c**) caused the appearance of new absorption peak at 560 nm; while absorption peak at 265 nm underwent hyperchromic effect with minor change at 350 nm. Although the response of probes (**128a-128c**) towards F^- was similar, their sensitivity was different. Detection limits (association constant) of the (**128a-128c**) towards F^- ions were measured to be 7.6×10^{-8} (3.629×10^3 M^{-1}), 9.4×10^{-8} (1.879×10^3 M^{-1}) and 1.1×10^{-7}(5.946×10^3 M^{-1}) M, respectively. The different types of hydrogen bonding in (**128a-128c**) were held responsible for their different sensitivity as **128c** was not assisted by intramolecular hydrogen bonding, in **128b** there was hydrogen bond between hydroxyl group and the benzene ring and in case of **128a**, hydrogen bonding occurred between the hydroxyl group and pyridinium nitrogen. The F^- complexes of (**128a-128c**) were employed for the detection of trace water as addition of trace water to these complexes regenerated the free sensors.

Ghosh et al. synthesized a 1,8-naphthalimide based sensor with imino-phenol functionality **129** (Fig. 111), which was employed for the sensing of Fe^{3+} and Cu^{2+} in a sol–gel medium [183]. The compound **129** formed stable red gels in DMF-H_2O (1:1, v/v) and DMSO-H_2O (1:1, v/v) with minimum gelation concentrations of 8 and 10 mg ml^{-1}, respectively. On addition of Cu^{2+} ions to the CH_3-CN and CH_3CN-H_2O (4:1, v/v) solution of **129**, changes in absorption and fluorescence spectrum were observed due to the interaction of metal ions with the imino-phenol binding site in **129** (Table 17). The proposed sensor **129** exhibited reversible nat-

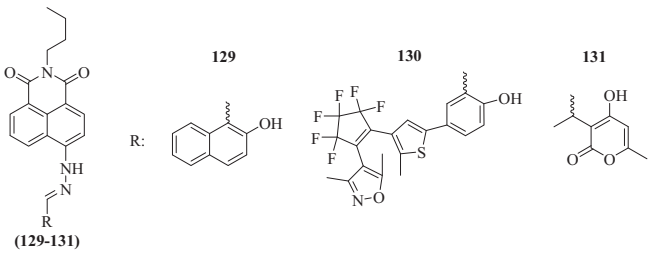

Fig. 111. Structures of chemosensors **129–131.**

Table 17
Solvent systems, absorption and fluorescence changes, color changes, mechanism, stoichiometry (Ligand:Analyte), LOD* values and K_a* values of sensors, (**129**–**131**) in the presence of various analytes.

Sensor	Solvent	Absorption changes (nm)	Fluorescence changes (nm)	Color changes	Mechanism	Stoichiometry	LOD (μM)	K_a ($\times 10^5$)	Ref.
129 (Cu^{2+})	CH_3CN	Decrease at 455	Quenching at 545 with 35 nm blue shift	Yellow → colorless	MLCT	–	0.497	0.140	[183]
129 (Cu^{2+})	CH_3CN-H_2O (4:1, v/v)	Decrease at 455	Quenching at 560 with 37 nm blue shift	Yellow → pale orange	–	–	0.413	0.014	[183]
130 (Cu^{2+})	CH_3CN	Decrease at 441	Decrease at 542	Greenish yellow → colorless	–	1:1	2.4	0.313	[184]
130 (F^-)	CH_3CN	–	441 to 579	Greenish yellow → blue	ICT	–	–	–	[184]
131 (Cu^{2+})	THF/H_2O (2:1)	Disappeared at 412	Sharp decrease at 520	Yellow → colorless	CHQF, PET	2:1	0.962×10^{-6}	1.26	[185]
131 (F^-)	THF/H_2O (2:1)	Decrease at 412 and splitted into 408 and 428, appearance at 580 and 620	Quenched at 520 with 5 nm blue shift	Yellow → blue	ICT, PET	2:1	1.2	1.5	[185]
131 (CN^-)	THF/H_2O (2:1)	Disappeared at 412 and appeared at 581 and 622	Quenched at 520 with 5 nm blue shift	Yellow → violet	ICT, PET	1:1	2.79	0.62	[185]

*K_a and LOD values have been determined by observing fluorescence changes.

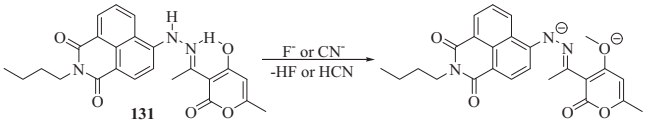

Fig. 112. F^- or CN^- mediated deprotonation of **131.**

ure on addition of S^{2-} ions in the solution phase due to formation of CuS. The gel formed in DMSO-H_2O (1: 1, v/v) solution was not able to detect any ion. However, addition of Fe^{3+} ions to the gel formed in DMF-H_2O (1:1, v/v) disrupted the gel to sol due to the coordination of Fe^{3+} with the imino-phenol segment of gel. This gel to sol conversion helped in the detection of Fe^{3+} ions and Fe^{3+} induced broken gel was regenerated after addition of KF. Further, it was found that this gel could also be used for the detection of *in situ* oxidation of Fe^{2+} to Fe^{3+} in the presence of a suitable oxidizing agent. However, the proposed sensor **129** was not able to detect Fe^{3+} ions in the solution form.

Fu and co-workers synthesized a sensor based on diarylethene with a 1,8-naphthalimide Schiff base unit **130** (Fig. 111), which showed specific detection ability for Cu^{2+} and F^- ions [184]. Incorporation of Cu^{2+} and F^- ions to the solution of **130** caused significant changes in the absorption and fluorescence spectrum (Table 17). On addition of EDTA to the solution of **130**. Cu^{2+}, fluorescence of the solution was not regained indicating the irreversible nature of **130**. The change due to F^- ions was ascribed to enhancement in ICT process due to increased electron density on nitrogen atom caused by deprotonation of N–H and O–H.

Saini et al. synthesized a chemosensor derived from 1,8-naphthalimide and dehydroacetic acid **131** (Fig. 111) and utilized it for the detection of Cu^{2+}, F^- and CN^- ions [185]. Addition of Cu^{2+}, F^- and CN^- ions to the solution of **131** caused significant changes in the absorption and emission spectrum (Table 17). Possible cause of spectral change due to Cu^{2+} ions was reduction in ICT process with CHQF because of reduced electron density upon coordination with Cu^{2+}. The absorption changes due to F^- and CN^- ions were attributed to the deprotonation and subsequent ameliorated electron donor propensity of N-/O- moiety facilitating the ICT process (Fig. 112). Emission intensity of the proposed sensor was quenched in the presence of both cations and anions due to inherent paramagnetism and enhanced PET process. Binding ratio of 2:1 was found for **131**.Cu^{2+} and **131**.F^- while it was 1:1 for **131**.CN^-.

Two similar 1,8-naphthalimide based chemosensors (**132** and **133**) (Fig. 113) detected F^- ions and oxyfluorfen by displaying changes in its absorption as well as emission spectrum (Table 18) [186,187]. Absorption and fluorescence changes were ascribed to the deprotonation of –NH of **132/133** due to hydrogen bonding interaction with F^-. Further, the proposed sensors **132/133** were also employed for the detection of oxyfluorfen as it caused significant reduction in fluorescence.

Goel et al. synthesized a 1,8-naphthalimide based Schiff base **134** (Fig. 113) and on addition of Hg^{2+} and HSO_4^- ions, significant absorption and emission changes were observed due to hydrolysis of probe **134** (Table 18) [188]. The sensor **134** also exhibited strong intercalation properties with DNA.

A 1,8-naphthalimide based chemosensor **135** (Fig. 114) was synthesized by **Dwivedi et al.**, where addition of Fe^{3+} ions resulted in enhancement of fluorescence which was ascribed to PET-off process because upon binding with Fe^{3+}, charge transfer from electron rich ionophore site to chromophore got restricted due to more confinement of electron density towards the metal center (Table 19)

Table 18
Solvent systems, absorption and fluorescence changes, color changes, LOD* values and K_a* values of sensors, (**132**–**134**), in the presence of various analytes.

Sensor	Solvent	Absorption changes (nm)	Fluorescence changes (nm)	Color changes	LOD (μM)	K_a ($\times 10^6$)	Ref.
132 (F^-)	CH_3CN	289, 354 → 443	Quenching at 443	Colorless → yellow	0.52	0.0187	[186]
132 (Oxyfluorfen)	CH_3CN	–	Quenching at 443	–	0.83	–	[186]
133 (F^-)	DMSO	367 → 501	Quenching at 472	Colorless → light pink	0.848	–	[187]
133 (Oxyfluorfen)	DMSO	–	Quenching at 472	–	1.21	–	[187]
134 (Hg^{2+})	CH_3OH	380 → 430	Enhancement at 580	pale yellow → bright yellow	0.0005	6.89	[188]
134 (HSO_4^-)	CH_3OH	380 → 430	Enhancement at 530	–	0.05	0.0563	[188]

*K_a and LOD values have been determined by observing fluorescence changes.

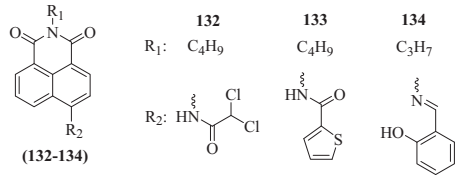

Fig. 113. Structures of chemosensors **132–134.**

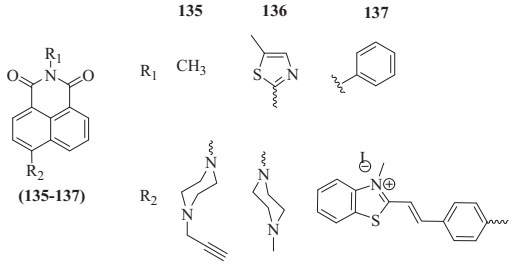

Fig. 114. Structures of chemosensors **135–137.**

[189]. Further, upon incorporation of PPi to the solution of **135**. Fe^{3+}, quenching in fluorescence was observed and bright green color turned to colorless. The sensor **135** was also employed for imaging of Fe^{3+} and PPi ions in living cells, polymerase chain reaction (PCR) product and Zebra fish. The optical properties exhibited by **135** in the presence of tested ions mimicked "write-read-erase-read" function through an INHIBIT logic gate.

Li and group synthesized a naphthalimide based sensor **136** (Fig. 114) for the detection of Fe^{3+} ions and acidic lysosomes by observing changes in the absorption and emission spectrum (Table 19) [190]. The spectral changes in the presence of Fe^{3+} ions were ascribed to the fact that addition of Fe^{3+} ions caused protonation of methyl piperazine unit, which led to enhancement in fluorescence.

Naphthalimide-benzothiazole hybrid chemosensor **137** (Fig. 114) detected cyanide and tryptophan in aqueous media, where the changes in absorption and emission spectrum were ascribed to the blockage of ICT process due to nucleophilic addition of cyanide and tryptophan on the carbon of imine group leading to formation of carbon–nitrogen single bond (amine) and consequently disrupting the conjugation (Fig. 115) (Table 19) [191]. Furthermore, for the practical applicability of **137**, its alginate beads were prepared which efficiently detected both the analytes.

Pang et al. synthesized naphthalimide based sensor **138** (Fig. 116) possessing amide functionalities that was able to detect F^- and AcO^- ions in benzene [192]. In the UV–Vis spectrum, absorption peak of the free sensor located at 414 nm was shifted to two new peaks at 350 and 464 nm on addition of F^- ions. However, in the presence of AcO^- ions, absorbance peak at 414 nm was

Table 19
Solvent systems, absorption and fluorescence changes, color changes, mechanism, stoichiometry (Ligand:Analyte), LOD* values and K_a* values of sensors (**135–137**) in the presence of various analytes.

Sensor	Solvent	Absorption changes (nm)	Fluorescence changes (nm)	Color changes	Mechanism	Stoichiometry	LOD (nM)	K_a (x 10^5)	Ref.
135 (Fe^{3+})	Phosphate buffer (THF:H_2O; 1:99, v/v)	398 → 380	Enhancement at 529 with 4 nm blue shift	–	PET	1:1	1.05	0.565	[189]
135.Fe^{3+} (PPi)	Phosphate buffer (THF:H_2O; 1:99, v/v)	–	Decrease at 525	–	–	–	420	–	[189]
136 (Fe^{3+})	Ethanol-HEPES buffer (80:20, v/v)	410 → 381	Enhancement at 515	–	PET	–	–	3.75	[190]
137 (CN^-)	EtOH-H_2O; 1–1, v/v	394 → 346	520 → 453	Yellow → red	ICT	1:1	4.5	–	[191]
137 (Tryptophan)	EtOH-H_2O; 1–1, v/v	394 → 355	520 → 444	Yellow → red	ICT	1:1	15.2	–	[191]

*K_a and LOD values have been determined by observing fluorescence changes.

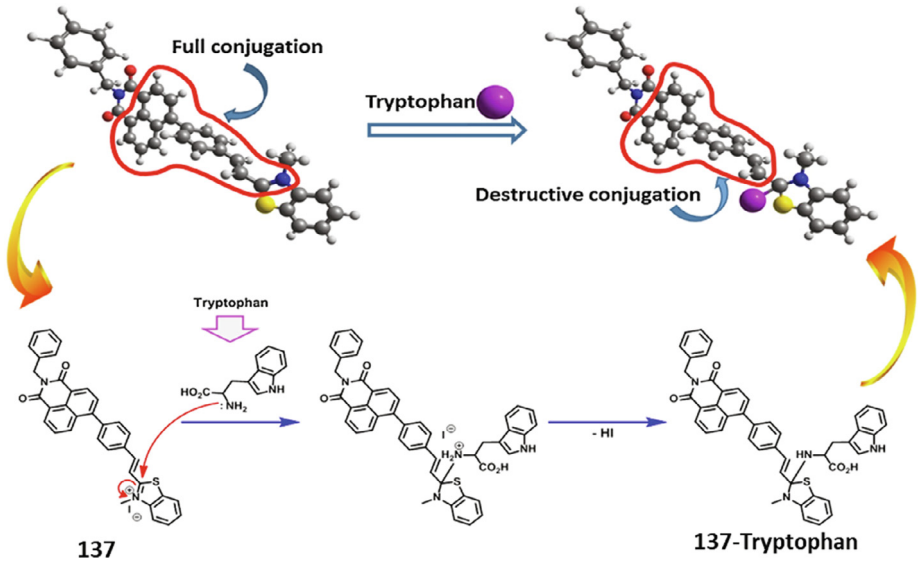

Fig. 115. Nucleophilic addition of tryptophan to **137** (Reproduced from Sens. Actuators B Chem. 273 (2018) 143–152 [191]).

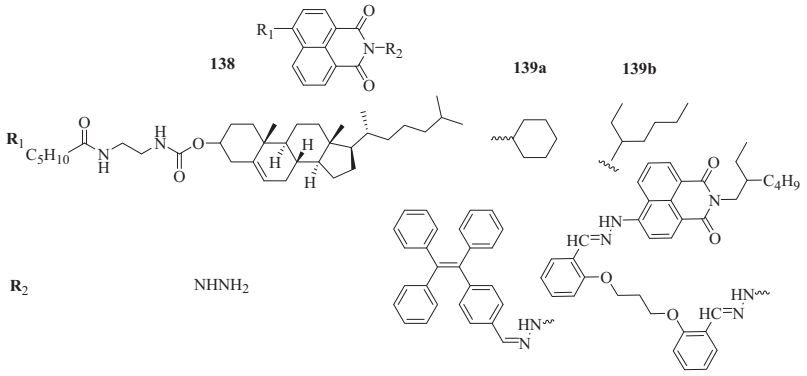

Fig. 116. Structures of chemosensors **138–139.**

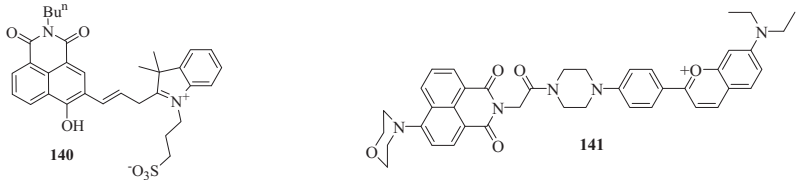

Fig. 117. Structures of chemosensors **140–141.**

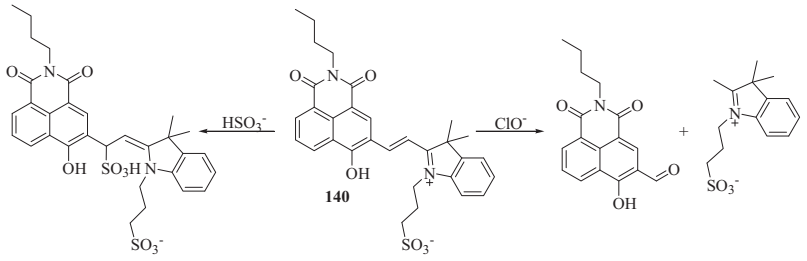

Fig. 118. Possible mechanism of sensing of HSO_3^- and ClO^- by **140.**

blue shifted to 351 nm. On the other hand, addition of F^- ions to **138** changed the fluorescence color from green to blue with 198-fold enhancement in fluorescence; while it changed from green to light blue in the presence of AcO^- ions with 132-fold fluorescence enhancement. Other competitive were found to exhibit no interference with the sensing of these ions. Furthermore, the sensor **138** also detected both the ions conveniently in the gel state. The association constants of **138**.F^- and **138**.AcO^- were measured to be 1.29×10^4 and 1.83×10^5 M^{-1}, respectively.

Two similar sensors showing mechanochromic luminescence (MCL) based on 1,8-naphthalimide **(139a** and **139b**) (Fig. 116) were able to detect F^- and AcO^- ions in THF solution [193]. The absorption spectrum of **139a** displayed bands at 457 and 570 nm, which shifted to 612 nm with addition of F^- and AcO^- ions. The fluorescence peak of **139a** at 570 nm underwent 91–93% quenching along with color change from yellow-green to dark blue in the presence of F^- and AcO^- ions. The possible reason for this quenching was the formation of hydrogen bonded adduct of **139a** with F^- ions (HF_2^- species) due to which lone pair of nitrogen got activated and PET process occurred. Similar results were obtained in case of **139b** on addition of F^- and AcO^- ions.

A ratiometric fluorescent probe based on 1,8-naphthalimide **140** (Fig. 117) was synthesized by **Wu** and group for the detection of HSO_3^- and ClO^- ions [194]. On addition of ClO^- ions to the (DMF/PBS = 1:99, v/v, pH = 7.4) solution of **140**, decrease was observed in the absorption peak at 550 nm along with naked eye color change from purple to pale yellow and in the fluorescence spectrum, emission peak at 620 nm decreased in intensity and a new peak appeared at 515 nm. These changes were ascribed to the cleavage and oxidation of C=C bond between naphthalimide and indole sulfonate, leading to the regeneration of raw material. Similar changes

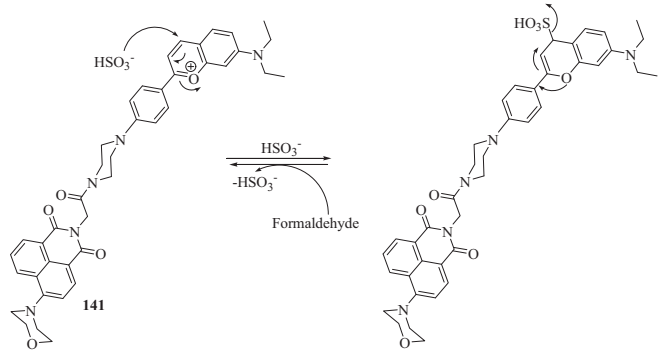

Fig. 119. Possible mechanism of sensing of HSO_3^- by **141** and formaldehyde by **141**. HSO_3^-**.**

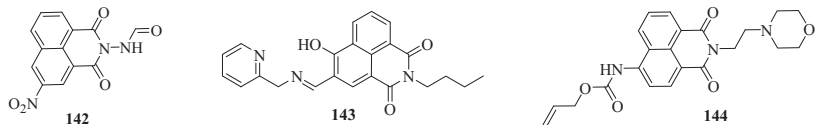

Fig. 120. Structures of chemosensors **142**–**144.**

in absorption and emission spectrum were observed in the presence of HSO_3^- ions. The sensing mechanism for the detection of HSO_3^- ions was found to be the 1,4-addition across C=C bond, which led to changes in the conjugation and thus spectral changes (Fig. 118). The practical applications exhibited by this probe include identification of tumor cells, exogenous and endogenous imaging of these analytes and also their detection in plasma.

Tan et al. synthesized a naphthalimide derived two-photon-FRET based probe, **141** (Fig. 117), for the detection of bisulfite ions and formaldehyde [195]. On addition of HSO_3^- ions to the phosphate buffered (PBS, pH 7.4, containing 1% DMSO) solution of **141**, the absorption peak at 590 nm was blue shifted to 400 nm with naked eye color change from purple to colorless. In the fluorescence spectrum, intensity of the emission peak at 630 nm decreased; while increase was observed at 535 nm along with fluorescence color change from bright red to bright green. Further, on addition of formaldehyde to the adduct **141**.HSO_3^-, spectrum similar to that of free sensor **141** was generated, which indicated the reversible nature of probe **141**. These changes were attributed to the Michael addition reaction of α,β-unsaturated bond (Fig. 119). The proposed sensor **141** was found to be highly selective towards HSO_3^- ions over other competitive anions and biothiols and detection limit of **141** towards HSO_3^- ions was measured to be 7.48 nM. Furthermore, the sensor **141** efficiently detected both the analytes in food and water samples. The sensor **141** was also used for their imaging in liver tissue, zebrafish and mice.

A trifunctional molecular sensor **142** (Fig. 120) based on 1,8-naphthalimide was synthesized by **Naha et al.** and was applied for the detection of CN^-, Fe^{3+} and H_2S [196]. Addition of CN^- ions to the 5% aqueous DMSO solution of **142** resulted in red coloration and orange *turn-on* emission, which could be ascribed to the deprotonation of the acidic hydrazide causing the attenuation of ESIPT and turning on the ICT mechanism. Further, **142**.CN^- complex was utilized for the relay detection of Fe^{3+} as its addition caused instant discoloration and quenched the fluorescence because of *turning off* of the ICT process due to protonation of the sensor. The proposed sensor **142** was also used for the detection of H_2S as it produced red coloration (similar to Fe^{3+}) in the solution of **142** after its addition due to conversion of nitro to amino group (Fig. 121). The changes produced by **142** in the UV–Vis and fluorescence spectrum were different than those produced by Fe^{3+} unlike the same color change. Binding ratio in **142**. CN^- and **142**.CN^-.Fe^{3+} was found to be 1:1 as indicated by the Job's plot. Job's plot construction was not applicable for finding the binding ratio in **142**. H_2S as it involved chemodosimetric reduction process. The proposed sensor **142** was also used for imaging of CN^- and Fe^{3+} in RAW264.7 cells and zebrafish.

A reversible, water-soluble, *on–off-on* naphthalimide-based chemosensor **143** (Fig. 120) was synthesized by **Guo et al.** for imaging of cellular Cu^{2+} and cysteine [197]. After addition of Cu^{2+} ions to aqueous buffer (5 mM HEPES, pH = 7.0) solution of **143**, the absorption peak at 400 nm and fluorescence band at 520 nm decreased in intensity. However, after addition of cysteine to the solution **143**.Cu^{2+}, these optical changes reappeared, indicating the reversible nature of **143** due to its release from the **143**.Cu^{2+} complex through the chelation of cysteine with the Cu^{2+} (Fig. 122). The detection limit of 7.11 nM and 0.18 μM was obtained for Cu^{2+} and cysteine, respectively. Fluorescence spectra titration and Job plot revealed the coordination ratio of 2:1 in **143** and Cu^{2+} ions. It was reported that lone pair of electrons on hydroxyl and amino functional groups could occupy the 3d, 4 s or 4p empty orbitals of Cu^{2+} leading to the formation of a bidentate or multidentate complex. Furthermore, it was found that **143** exhibited good cell permeability and successfully detected Cu^{2+} and cysteine in living cells (HeLa cells).

Xie et al. synthesized a dual analyte sensitive probe, **144** (Fig. 120), based on 1,8-naphthalimide for the detection of Pd (0) and pH involving morpholine group for pH and allylcarbamate group for Pd (0) sensing [198]. The sensitivity and selectivity of the proposed probe **144** towards pH was tested in PBS (10% DMSO; 10 mM) solution. In the absorption spectrum, the absorption peak at 370 nm was blue shifted to 365 nm and in the fluorescence spectrum, significant enhancement in the fluorescence intensity at 485 nm was observed as the pH was lowered down from 9.50 to 4.00. Good linearity was observed in the fluorescence enhancement at 485 nm and pH value in the range of 5.25 to 6.75. Anti-interference studies for the detection of pH were carried out in pH range 4.50 to 7.40 and it was found that other metal ions did not interfere with the pH sensing. Further, on addition of Pd $(PPh_3)_4$ (Pd^0 resource) to the PBS (10% DMSO; 10 mM; pH 7.4) solution of **144**, 36-fold enhancement in fluorescence intensity was

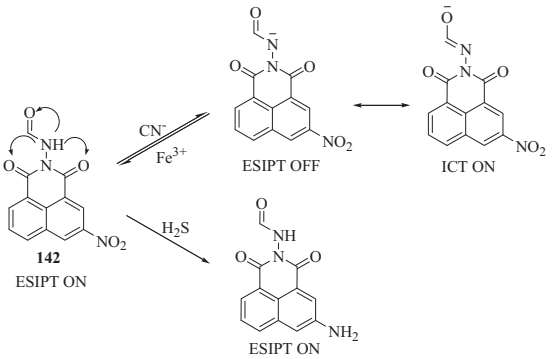

Fig. 121. Mode of sensing of CN^- and H_2S by **142** and Fe^{3+} by **142**.CN^-.

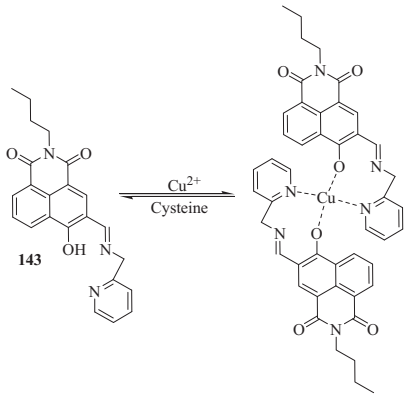

Fig. 122. Possible mode of sensing of Cu^{2+} by **143** and cysteine by **143**.Cu^{2+}.

observed at 545 nm and it was found that other metal ions including other variants of Pd did not show any interference with Pd (0) analysis. These changes were ascribed to the synergestic effects of PET and ICT processes. Furthermore, the proposed sensor **144** efficiently analysed pH and Pd (0) in the lysosome of HeLa cells and zebrafish.

6. Future perspectives and conclusions

Supramolecular chemistry offers a collection of particular yet non-permanent interactions that facilitate the creation of complex materials with tunable and reversible properties. The field of chemosensing has drawn a substantial attention, where the recognition process is coupled to the specific action of signalling. Monitoring the presence of contaminants in environment is of general interest in order to ensure safety of the environment and mankind. Among the several pollutants, sensing of ions (toxic metal ions and anions) is one of the most challenging fields owing to their use in physiology, medical diagnostics, catalysis and their subsequent impact on the biological system, environment and nature. Further, abnormal levels of the biomolecules eg. biothiols, amino acids, NADH, various enzymes and triphosphate based biomolecules etc. in the human body may lead to skin related problems, liver damage, brain injury and Parkinson's disease etc.

In this review, various 1,8-naphthalimide based derivatives and their potential applications in the field of chemosensing for the years 2017–2021 have been reported. 1, 8-naphthalimide has a very important place in the chemosensors owing to its superior features of strong absorption band in the visible region, outstanding photostability, high fluorescent quantum yield and large Stokes' shift besides the possibility of easy modification of its structure. 1, 8-naphthalimide contains a very strong naphthalene ring structure so that the interaction of its molecules with solvents or other solute molecules is reduced, making the external transfer of energy to be lowered, which is very beneficial to the emission of fluorescence. The presence of an electron donor conjugated system in its molecular structure allows for electrons in its system to be easily excited by the external light or electric field so as to produce a strong fluorescence. Furthermore, majority of the 1,8-naphthalimide based derivatives are less cytotoxic and biocompatible in nature, thus making them suitable candidates for bioimaging of analytes and cancer cells in living organisms without the destruction of sample.

Although, the literature of 1,8-naphthalimide is replete but still lot of advancements could be made in this research field and number of challenges such as achieving analyte detection in aqueous environments, demonstrating robust performance in biological environments etc. still remain unsolved due to their complexity and unpredictability. Therefore, efforts need to be done for strengthening the selectivity, environmental adaptability and sensor reusability. Other major issue is the non-green approach that for synthesis of majority of the chemosensors, which needs immediate attention for the welfare of environment. Also, scanty information with respect to 1,8-naphthalimide based bioconjugates is available which limits their application in clinical, molecular, cellular and translational fields. The greatest challenge in the field of chemosensing in present time is the practicality of the sensors, which is further associated with many factors such as cost, portability, operability etc. Due to lack of such attributes, the field of chemosensing is still limited to laboratory only, therefore, to take chemosensors beyond laboratory to commercial level, the crucial target is to develop simple, cost-effective, fast, easily operable and portable sensors. The perfect example of such practical and commercially available sensor possessing these attributes is a personal glucose meter, therefore attempts should to made to develop chemosensors of such kind. Simultaneously, we hope that gaining insights into the discussed literature reports will assist the research fraternity working in the area of sensing to refine their knowledge of the field and will facilitate to develop superlative chemosensors possessing improved practical applications in future.

Declaration of Competing Interest

The authors declare that they have no known competing financial interests or personal relationships that could have appeared to influence the work reported in this paper.

Acknowledgements

None to declare.

References

[1] J.H. Hartley, T.D. James, C.J. Ward, Synthetic receptors, J. Chem. Soc. Perkin Trans. 1 (2000) 3155–3184, https://doi.org/10.1039/A909641H.
[2] M. Takeuchi, M. Ikeda, A. Sugasaki, S. Shinkai, Molecular design of artificial molecular and ion recognition systems with allosteric guest responses, Acc. Chem. Res. 34 (11) (2001) 865–873, https://doi.org/10.1021/ar0000410.
[3] T.W. Bell, N.M. Hext, Supramolecular optical chemosensors for organic analytes, Chem. Soc. Rev. 33 (2004) 589–598, https://doi.org/10.1039/B207182G.
[4] G. Ghale, W.M. Nau, Dynamically analyte-responsive macrocyclic host-fluorophore systems, Acc. Chem. Res. 47 (7) (2014) 2150–2159, https://doi.org/10.1021/ar500116d.
[5] V. Schroeder, S. Savagatrup, M. He, S. Lin, T.M. Swager, Carbon nanotube chemical sensors, Chem. Rev. 119 (1) (2019) 599–663, https://doi.org/10.1021/acs.chemrev.8b00340.
[6] G. Fukuhara, Analytical supramolecular chemistry: Colorimetric and fluorimetric chemosensors, J. Photochem. Photobiol. C 42 (2020) 100340, https://doi.org/10.1016/j.jphotochemrev.2020.100340.
[7] A. Brzechwa-Chodzyńska, W. Drożdż, J. Harrowfield, A.R. Stefankiewicz, Fluorescent sensors: A bright future for cages, Coord. Chem. Rev. 434 (2021) 213820, https://doi.org/10.1016/j.ccr.2021.213820.
[8] M.-C. Ríos, N.-F. Bravo, C.-C. Sánchez, J. Portilla, Chemosensors based on N-heterocyclic dyes: Advances in sensing highly toxic ions such as CN^- and Hg^{2+}, RSC Adv. 11 (54) (2021) 34206–34234, https://doi.org/10.1039/D1RA06567J.
[9] F. Wang, K. Wang, Q. Kong, J. Wang, D. Xi, B. Gu, S. Lu, T. Wei, X. Chen, Recent studies focusing on the development of fluorescence probes for zinc ion, Coord. Chem. Rev. 429 (2021) 213636, https://doi.org/10.1016/j.ccr.2020.213636.
[10] K. Wang, Y. Liu, C. Liu, H. Zhu, X. Li, F. Zhang, N.a. Gao, X. Pang, W. Sheng, B. Zhu, A simple pyridine-based highly specific fluorescent probe for tracing hypochlorous acid in lysosomes of living cells, New J. Chem. 45 (32) (2021) 14548–14553, https://doi.org/10.1039/D1NJ02256C.
[11] A. Tigreros, J. Portilla, Recent progress in chemosensors based on pyrazole derivatives, RSC Adv. 10 (33) (2020) 19693–19712, https://doi.org/10.1039/D0RA02394A.
[12] C. Duan, M. Won, P. Verwilst, J. Xu, H.S. Kim, L. Zeng, J.S. Kim, In vivo imaging of endogenously produced $HClO^-$ in zebrafish and mice using a bright, photostable ratiometric fluorescent probe, Anal. Chem. 91 (6) (2019) 4172–4178, https://doi.org/10.1021/acs.analchem.9b0022410.1021/acs.analchem.9b00224.s001.
[13] L. Espinar-Barranco, P. Luque-Navarro, M.A. Strnad, P. Herrero-Foncubierta, L. Crovetto, D. Miguel, M.D. Giron, A. Orte, J.M. Cuerva, R. Salto, J.M. Alvarez-Pez, J.M. Paredes, A solvatofluorochromic silicon-substituted xanthene dye useful in bioimaging, Dyes Pigm. 168 (2019) 264–272, https://doi.org/10.1016/j.dyepig.2019.04.024.
[14] X. Bao, X. Wu, S.N. Berry, E.N.W. Howe, Y.-T. Chang, P.A. Gale, Fluorescent squaramides as anion receptors and transmembrane anion transporters, Chem. Commun. 54 (11) (2018) 1363–1366, https://doi.org/10.1039/C7CC08706C.
[15] X. Chen, T. Pradhan, F. Wang, J.S. Kim, J. Yoon, Fluorescent chemosensors based on spiroring-opening of xanthenes and related derivatives, Chem. Rev. 112 (3) (2012) 1910–1956, https://doi.org/10.1021/cr200201z.
[16] V.-N. Nguyen, J. Ha, M. Cho, H. Li, K.M.K. Swamy, J. Yoon, Recent developments of BODIPY-based colorimetric and fluorescent probes for the detection of reactive oxygen/nitrogen species and cancer diagnosis, Coord. Chem. Rev. 439 (2021) 213936, https://doi.org/10.1016/j.ccr.2021.213936.
[17] A.S. Oshchepkov, M.S. Oshchepkov, M.V. Oshchepkova, A. Al-Hamry, O. Kanoun, E.A. Kataev, Naphthalimide-based fluorescent polymers for molecular detection, Adv. Optical Mater. 9 (6) (2021) 2001913, https://doi.org/10.1002/adom.202001913.

[18] S. Zhou, Y. Rong, H. Wang, X. Liu, L. Wei, X. Song, A naphthalimide-indole fused chromophore-based fluorescent probe for instantaneous detection of thiophenol with a red emission and a large Stokes shift, Sens. Actuators B Chem. 276 (2018) 136–141, https://doi.org/10.1016/j.snb.2018.08.096.
[19] B. Du, F.-H. Zhang, W. Cao, P.-H. Wang, Z.-J. Li, Z.-J. Ding, A naphthalimide-based fluorescent turn-on sensor for the selective detection of diethyl chlorophosphate, ChemistrySelect 3 (47) (2018) 13470–13473, https://doi.org/10.1002/slct.201800544.
[20] J. Chung, H. Li, C.S. Lim, H.M. Kim, J. Yoon, Two-photon imaging of hydrogen polysulfides in living cells and hippocampal tissues, Sens. Actuators B Chem. 322 (2020) 128564, https://doi.org/10.1016/j.snb.2020.128564.
[21] L. Qian, L. Li, S.Q. Yao, Two-photon small molecule enzymatic probes, Acc. Chem. Res. 49 (4) (2016) 626–634, https://doi.org/10.1021/acs.accounts.5b00512.
[22] Y. Chen, R. Guan, C. Zhang, J. Huang, L. Ji, H. Chao, Two-photon luminescent metal complexes for bioimaging and cancer phototherapy, Coord. Chem. Rev. 310 (2016) 16–40, https://doi.org/10.1016/j.ccr.2015.09.010.
[23] H.M. Kim, B.R. Cho, Small-molecule two-photon probes for bioimaging applications, Chem. Rev. 115 (11) (2015) 5014–5055, https://doi.org/10.1021/cr5004425.
[24] H.M. Kim, B.R. Cho, Two-photon probes for intracellular free metal ions, acidic vesicles, and lipid rafts in live tissues, Acc. Chem. Res. 42 (7) (2009) 863–872, https://doi.org/10.1021/ar800185u.
[25] K.G. Leslie, D. Jacquemin, E.J. New, K.A. Jolliffe, Expanding the breadth of 4-amino-1, 8-naphthalimide photophysical properties through substitution of the naphthalimide core, Chem. Eur. J. 24 (21) (2018) 5569–5573, https://doi.org/10.1002/chem.201705546.
[26] M. Mahl, K. Shoyama, A.-M. Krause, D. Schmidt, F. Würthner, Base-assisted imidization: A synthetic method for the introduction of bulky imide substituents to control packing and optical properties of naphthalene and perylene imides, Angew. Chem. Int. Ed. 59 (32) (2020) 13401–13405, https://doi.org/10.1002/anie.202004965.
[27] H.-Q. Dong, T.-B. Wei, X.-Q. Ma, Q.-Y. Yang, Y.-F. Zhang, Y.-J. Sun, B.-B. Shi, H. Yao, Y.-M. Zhang, Q.i. Lin, 1,8-Naphthalimide-based fluorescent chemosensors: Recent advances and perspectives, J. Mater. Chem. C 8 (39) (2020) 13501–13529, https://doi.org/10.1039/D0TC03681A.
[28] W. Wang, Q. Wen, Y. Zhang, X. Fei, Y. Li, Q. Yang, X. Xu, Simple naphthalimide-based fluorescent sensor for highly sensitive and selective detection of Cd^{2+} and Cu^{2+} in aqueous solution and living cells, Dalton Trans. 42 (5) (2013) 1827–1833, https://doi.org/10.1039/C2DT32279J.
[29] S.M. Dimov, N.I. Georgiev, A.M. Asiri, V.B. Bojinov, Synthesis and sensor activity of a PET-based 1,8-naphthalimide probe for Zn^{2+} and pH determination, J. Fluoresc. 24 (6) (2014) 1621–1628, https://doi.org/10.1007/s10895-014-1448-2.
[30] N.I. Georgiev, M.D. Dimitrova, P.V. Krasteva, V.B. Bojinov, A novel water-soluble 1,8-naphthalimide as a fluorescent pH-probe and a molecular logic circuit, J. Lumin. 187 (2017) 383–391, https://doi.org/10.1016/j.jlumin.2017.03.049.
[31] S. Banerjee, E.B. Veale, C.M. Phelan, S.A. Murphy, G.M. Tocci, L.J. Gillespie, D.O. Frimannsson, J.M. Kelly, T. Gunnlaugsson, Recent advances in the development of 1,8-naphthalimide based DNA targeting binders, anticancer and fluorescent cellular imaging agents, Chem. Soc. Rev. 42 (2013) 1601–1618, https://doi.org/10.1039/c2cs35467e.
[32] J. Huang, D.i. Wu, H.-J. Ge, S.-H. Liu, J. Yin, Fluorinated 1,8-naphthalimides: Synthesis, solid structure and properties, Chin. Chem. Lett. 25 (10) (2014) 1399–1402, https://doi.org/10.1016/j.cclet.2014.04.017.
[33] J.-F. Lee, S.-C. Hsu, Green polymer-light-emitting-diodes based on polyfluorenes containing N-aryl-1,8-naphthalimide and 1,8-naphthoilene-arylimidazole derivatives as color tuner, Polymer 50 (24) (2009) 5668–5674, https://doi.org/10.1016/j.polymer.2009.10.010.
[34] P. Gautam, R. Sharma, R. Misra, M.L. Keshtov, S.A. Kuklin, G.D. Sharma, Donor–acceptor–acceptor (D–A–A) type 1,8-naphthalimides as non-fullerene small molecule acceptors for bulk heterojunction solar cells, Chem. Sci. 8 (3) (2017) 2017–2024, https://doi.org/10.1039/C6SC04461A.
[35] S. Liu, H. Bai, Q. Sun, W. Zhang, J. Qian, Naphthalimide-based fluorescent photoinduced electron transfer sensors for saccharides, RSC Adv. 5 (4) (2015) 2837–2843, https://doi.org/10.1039/C4RA13414A.
[36] R.M. Duke, T. Gunnlaugsson, 3-Urea-1,8-naphthalimides are good chemosensors: a highly selective dual colorimetric and fluorescent ICT based anion sensor for fluoride, Tetrahedron Lett. 52 (13) (2011) 1503–1505, https://doi.org/10.1016/j.tetlet.2011.01.099.
[37] C. Wang, D. Zhang, X. Huang, P. Ding, Z. Wang, Y. Zhao, Y. Ye, A ratiometric fluorescent chemosensor for Hg^{2+} based on FRET and its application in living cells, Sens. Actuators B Chem. 198 (2014) 33–40, https://doi.org/10.1016/j.snb.2014.03.032.
[38] P. Gopikrishna, N. Meher, P.K. Iyer, Functional 1,8-Naphthalimide AIE/AIEEgens: Recent advances and prospects, ACS Appl. Mater. Interfaces 10 (15) (2018) 12081–12111, https://doi.org/10.1021/acsami.7b14473.
[39] A. Kamal, N.R. Bolla, P.S. Srikanth, A.K. Srivastava, Naphthalimide derivatives with therapeutic characteristics: A patent review, Expert Opin. Ther. Patents 23 (3) (2013) 299–317, https://doi.org/10.1517/13543776.2013.746313.
[40] L. Roos, F.P. Malan, M. Landman, Naphthalimide-NHC complexes: Synthesis and properties in catalytic, biological and photophysical applications, Coord. Chem. Rev. 449 (2021) 214201, https://doi.org/10.1016/j.ccr.2021.214201.
[41] R. Martínez-Máñez, F. Sancenón, New advances in fluorogenic anion chemosensors, J. Fluoresc. 15 (3) (2005) 267–285, https://doi.org/10.1007/s10895-005-2626-z.
[42] K. Kaur, R. Saini, A. Kumar, V. Luxami, N. Kaur, P. Singh, S. Kumar, Chemodosimeters: An approach for detection and estimation of biologically and medically relevant metal ions, anions and thiols, Coord. Chem. Rev. 256 (17-18) (2012) 1992–2028, https://doi.org/10.1016/j.ccr.2012.04.013.
[43] L. Zhou, L. Xie, C. Liu, Y.i. Xiao, New trends of molecular probes based on the fluorophore 4-amino-1,8-naphthalimide, Chin. Chem. Lett. 30 (10) (2019) 1799–1808, https://doi.org/10.1016/j.cclet.2019.07.051.
[44] H. Zhu, C. Liu, M. Su, X. Rong, Y. Zhang, X. Wang, K. Wang, X. Li, Y. Yu, X. Zhang, B. Zhu, Recent advances in 4-hydroxy-1,8-naphthalimide-based small-molecule fluorescent probes, Coord. Chem. Rev. 448 (2021) 214153, https://doi.org/10.1016/j.ccr.2021.214153.
[45] H. Yu, Y. Guo, W. Zhu, K. Havener, X. Zheng, Recent advances in 1,8-naphthalimide-based small-molecule fluorescent probes for organelles imaging and tracking in living cells, Coord. Chem. Rev. 444 (2021) 214019, https://doi.org/10.1016/j.ccr.2021.214019.
[46] C. Geraghty, C. Wynne, R.B.P. Elmes, 1,8-Naphthalimide based fluorescent sensors for enzymes, Coord. Chem. Rev. 437 (2021) 213713, https://doi.org/10.1016/j.ccr.2020.213713.
[47] R.R. Crichton, Metal Toxicity-An Introduction, in: Metal Chelation in Medicine, The Royal Society of Chemistry (2016) 1–23, https://doi.org/10.1039/9781782623892-00001.
[48] J. Briffa, E. Sinagra, R. Blundell, Heavy metal pollution in the environment and their toxicological effects on humans, Heliyon 6 (9) (2020) e04691, https://doi.org/10.1016/j.heliyon.2020.e04691.
[49] P. Alam, N.L.C. Leung, J. Zhang, R.T.K. Kwok, J.W.Y. Lam, B.Z. Tang, AIE-based luminescence probes for metal ion detection, Coord. Chem. Rev. 429 (2021) 213693, https://doi.org/10.1016/j.ccr.2020.213693.
[50] L. Kang, Y.T. Liu, N.N. Li, Q.X. Dang, Z.Y. Xing, J.L. Li, Y. Zhang, A schiff-base receptor based naphthalimide derivative: Highly selective and colorimetric fluorescent turn-on sensor for Al^{3+}, J. Lumin. 186 (2017) 48–52, https://doi.org/10.1016/j.jlumin.2016.12.056.
[51] T. Tang, W. Guo, Y. Zhang, D. Xu, A novel 1,8-naphthalimide-based "turn-on" fluorescent sensor for Fe^{3+}, J. Fluoresc. 29 (2) (2019) 445–450, https://doi.org/10.1007/s10895-019-02354-8.
[52] B. Zhang, F. Qin, H. Niu, Y. Liu, D.i. Zhang, Y. Ye, A highly sensitive and fast responsive naphthalimide-based fluorescent probe for Cu^{2+} and its application, New J. Chem. 41 (23) (2017) 14683–14688, https://doi.org/10.1039/C7NJ02813J.
[53] C. Liu, X. Jiao, S. He, L. Zhao, X. Zeng, A highly selective and sensitive fluorescent probe for Cu^{2+} based on a novel naphthalimide–rhodamine platform and its application in live cell imaging, Org. Biomol. Chem. 15 (18) (2017) 3947–3954, https://doi.org/10.1039/C7OB00538E.
[54] Y. Fu, X.-X. Pang, Z.-Q. Wang, Q. Chai, F. Ye, A highly sensitive and selective fluorescent probe for determination of Cu (II) and application in live cell imaging, Spectrochim. Acta A Mol. Biomol. Spectrosc. 208 (2019) 198–205, https://doi.org/10.1016/j.saa.2018.10.005.
[55] M. Bahta, N. Ahmed, Naphthalimide-amino acid conjugates chemosensors for Hg^{2+} detection: Based on chelation mediated emission enhancement in aqueous solution, J. Photochem. Photobiol. A: Chem. 378 (2019) 85–93, https://doi.org/10.1016/j.jphotochem.2019.04.027.
[56] P.A. Panchenko, Y.V. Fedorov, O.A. Fedorova, Selective fluorometric sensing of Hg^{2+} in aqueous solution by the inhibition of PET from dithia-15-crown-5 ether receptor conjugated to 4-amino-1,8-naphthalimide fluorophore, J. Photochem. Photobiol. A: Chem. 364 (2018) 124–129, https://doi.org/10.1016/j.jphotochem.2018.06.003.
[57] M. Bahta, N. Ahmed, An AIEE active 1, 8-naphthalimide- sulfamethizole probe for ratiometric fluorescent detection of Hg^{2+} ions in aqueous media, J. Photochem. Photobiol. A: Chem. 391 (2020) 112354, https://doi.org/10.1016/j.jphotochem.2020.112354.
[58] L. Chen, S.J. Park, D.i. Wu, H.M. Kim, J. Yoon, A two-photon fluorescent probe for colorimetric and ratiometric monitoring of mercury in live cells and tissues, Chem. Commun. 55 (12) (2019) 1766–1769, https://doi.org/10.1039/C8CC08608G.
[59] F. Liu, P. Tang, R. Ding, L. Liao, L. Wang, M. Wang, J. Wang, A glycosylation strategy to develop a low toxic naphthalimide fluorescent probe for the detection of Fe^{3+} in aqueous medium, Dalton Trans. 46 (23) (2017) 7515–7522, https://doi.org/10.1039/C7DT01099K.
[60] S. Biswas, V. Sharma, P. Kumar, A.L. Koner, Selective sensing of lysosomal iron (III) via three-component fluorescence-based strategy in living cells, Sens. Actuators B Chem. 260 (2018) 460–464, https://doi.org/10.1016/j.snb.2018.01.011.
[61] S. Liang, Q. Tong, X. Qin, X. Liao, Q. Li, G. Yan, A hydrophilic naphthalimide-based fluorescence chemosensor for Cu^{2+} ion: Sensing properties, cell imaging and molecular logic behavior, Spectrochim. Acta A Mol. Biomol. Spectrosc. 230 (2020) 118029, https://doi.org/10.1016/j.saa.2020.118029.
[62] D. Liu, X. Yin, X. Deng, J. Shi, H. Zhu, Z. Shang, J. Chen, G. Yang, H. He, 1,8-Naphthalimide-based fluorescent sensor with highly selective and sensitive detection of Zn^{2+} in aqueous solution and living cells, Inorg. Chem. Commun. 106 (2019) 43–47, https://doi.org/10.1016/j.inoche.2019.05.026.
[63] D. Liu, X. Deng, X. Yin, Y. Wang, J. Guo, J. Chen, G. Yang, H. He, 1,8-Naphthalimide-based fluorescent sensor with high selectivity and sensitivity for Zn^{2+} and its imaging in living cells, Inorg. Chem. Commun. 101 (2019) 117–120, https://doi.org/10.1016/j.inoche.2019.01.023.

[64] D. Liu, T. Zhang, M. Zhang, J. Shi, L. Yin, Z. Shang, H. Zhu, G. Yang, H. He, Water-soluble fluorescent sensor for Zn^{2+} with high selectivity and sensitivity imaging in living cells, Bioorganic Med. Chem. Lett. 30 (8) (2020) 127073, https://doi.org/10.1016/j.bmcl.2020.127073.
[65] C.B. Bai, R. Qiao, J.X. Liao, W.Z. Xiong, J. Zhang, S.S. Chen, S. Yang, A highly selective and reversible fluorescence "off-on-off" chemosensor for Hg^{2+} based on rhodamine-6G dyes derivative and its application as a molecular logic gate, Spectrochim. Acta A Mol. Biomol. Spectrosc. 202 (2018) 252–259, https://doi.org/10.1016/j.saa.2018.05.050.
[66] S. Fernández-Alonso, T. Corrales, J.L. Pablos, F. Catalina, A Switchable fluorescence solid sensor for Hg^{2+} detection in aqueous media based on a photocrosslinked membrane functionalized with (benzimidazolyl)methyl-piperazine derivative of 1,8-naphthalimide, Sens. Actuators B Chem. 270 (2018) 256–262, https://doi.org/10.1016/j.snb.2018.05.030.
[67] D. Liu, H. Zhu, J. Shi, X. Deng, T. Zhang, Y. Zhao, P. Qi, G. Yang, H. He, 1, 8-Naphthalimide-based fluorescent sensor with high selectivity and sensitivity for Hg^{2+} in aqueous solution and living cells, Anal. Methods 11 (2019) 3150–3154, https://doi.org/10.1039/C9AY00711C.
[68] Y.-M. Zhang, K.-P. Zhong, J.-X. Su, X.-P. Chen, H. Yao, T.-B. Wei, Q.i. Lin, A novel histidine-functionalized 1,8-naphthalimidebased fluorescent chemosensor for the selective and sensitive detection of Hg^{2+} in water, New J. Chem. 41 (9) (2017) 3303–3307, https://doi.org/10.1039/C6NJ03930H.
[69] H. Wu, J. Jia, Y. Xu, X. Qian, W. Zhu, A reusable bifunctional fluorescent sensor for the detection and removal of silver ions in aqueous solutions, Sens. Actuators B Chem. 265 (2018) 59–66, https://doi.org/10.1016/j.snb.2018.01.241.
[70] P.A. Panchenko, A.S. Polyakova, Y.V. Fedorov, O.A. Fedorova, Chemoselective detection of Ag^{+} in purely aqueous solution using fluorescence 'turn-on' probe based on crown-containing 4-methoxy-1,8-naphthalimide, Mendeleev Commun. 29 (2) (2019) 155–157, https://doi.org/10.1016/j.mencom.2019.03.012.
[71] Y. Xu, S. Mao, H. Peng, F. Wang, H. Zhang, S.O. Aderinto, H. Wu, A fluorescent sensor for selective recognition of Al^{3+} based on naphthalimide Schiff-base in aqueous media, J. Lumin. 192 (2017) 56–63, https://doi.org/10.1016/j.jlumin.2017.06.023.
[72] H. Peng, K. Shen, S. Mao, X. Shi, Y. Xu, S.O. Aderinto, H. Wu, A highly selective and sensitive fluorescent turn-on probe for Al^{3+} based on naphthalimide Schiff base, J. Fluoresc. 27 (3) (2017) 1191–1200, https://doi.org/10.1007/s10895-017-2056-8.
[73] F. Wang, Y. Xu, S.O. Aderinto, H. Peng, H. Zhang, H. Wu, A new highly effective fluorescent probe for Al^{3+} ions and its application in practical samples, J. Photochem. Photobiol. A: Chem. 332 (2017) 273–282, https://doi.org/10.1016/j.jphotochem.2016.09.004.
[74] K. Shen, S. Mao, X. Shi, F. Wang, Y. Xu, S.O. Aderinto, H. Wu, Characterization of a highly Al^{3+}- selective fluorescence probe based on naphthalimide-Schiff base and its application to practical water samples, Luminescence 33 (1) (2018) 54–63, https://doi.org/10.1002/bio.3372.
[75] N.-N. Li, S. Zeng, M.-Q. Li, Y.-Q. Ma, X.-J. Sun, Z.-Y. Xing, J.-L. Li, A highly selective naphthalimide-based chemosensor: "Naked-eye" colorimetric and fluorescent turn-on recognition of Al^{3+} and its application in practical samples, test paper and logic gate, J. Fluoresc. 28 (1) (2018) 347–357, https://doi.org/10.1007/s10895-017-2197-9.
[76] S.K. Dwivedi, R.C. Gupta, R. Ali, S.S. Razi, S.K. Hira, P.P. Manna, A. Misra, Smart PET based organic scaffold exhibiting bright "turn–on" green fluorescence to detect Fe^{3+} ion: Live cell imaging and logic implication, J. Photochem. Photobiol. A: Chem. 358 (2018) 157–166, https://doi.org/10.1016/j.jphotochem.2018.03.011.
[77] D. Jothi, S. Munusamy, S. Sawminathan, S. Kulathu Iyer, Highly sensitive naphthalimide based Schiff base for the fluorimetric detection of Fe^{3+}, RSC Adv. 11 (19) (2021) 11338–11346, https://doi.org/10.1039/D1RA00345C.
[78] G. Huang, C. Li, X. Han, S.O. Aderinto, K. Shen, S. Mao, H. Wu, Sensitive and selective detection of Cu(II) ion: A new effective 1,8-naphthalimide-based fluorescence 'turn off' sensor, Luminescence 33 (4) (2018) 660–669, https://doi.org/10.1002/bio.3461.
[79] S.O. Aderinto, Y. Xu, H. Peng, F. Wang, H. Wu, X. Fan, A highly selective fluorescent sensor for monitoring Cu^{2+} ion: Synthesis, characterization and photophysical properties, J. Fluoresc. 27 (1) (2017) 79–87, https://doi.org/10.1007/s10895-016-1936-7.
[80] Z. Bao, C. Qin, J.J. Wang, J. Sun, L. Dai, G. Chen, F. Mei, A sensitive and selective probe for visual detection of Cu^{2+} based on 1, 8-naphthalimide derivative, Sens. Actuators B Chem. 265 (2018) 234–241, https://doi.org/10.1016/j.snb.2018.03.050.
[81] Z. Xu, P. Deng, J. Li, S. Tang, Fluorescent ion-imprinted sensor for selective and sensitive detection of copper (II) ions, Sens. Actuators B Chem. 255 (2018) 2095–2104, https://doi.org/10.1016/j.snb.2017.09.007.
[82] J. Wei, H. Sun, Y. Jiang, B. Miao, X. Han, Y. Zhao, Z. Ni, A novel 1,8-naphthalimide-based Cu^{2+} ion fluorescent probe and its bioimaging application, Spectrochim. Acta A Mol. Biomol. Spectrosc. 261 (2021) 120037, https://doi.org/10.1016/j.saa.2021.120037.
[83] N.Z. Xu, M.M. Liu, M.A. Ye, Y.W. Yao, Y. Zhou, G.Z. Wu, C. Yao, A Rhodamine-naphthalimide conjugated chemosensor for ratiometric detection Hg^{2+} in actual aqueous samples, J. Lumin. 188 (2017) 135–140, https://doi.org/10.1016/j.jlumin.2017.03.067.
[84] X. Yuan, T.H. Leng, Z.Q. Guo, C.Y. Wang, J.Z. Li, W.W. Yang, W.H. Zhua, A FRET-based dual-channel turn-on fluorescence probe for the detection of Hg^{2+} in living cells, Dyes Pigments 161 (2019) 403–410, https://doi.org/10.1016/j.dyepig.2018.09.078.
[85] F. Lv, Y. Chen, T. Tang, Y. Chen, D. Xu, A new reactive 1,8-naphthalimide derivative for highly selective and sensitive detection of Hg^{2+}, J. Fluoresc. 27 (4) (2017) 1285–1292, https://doi.org/10.1007/s10895-017-2061-y.
[86] Y. Liu, J. Zhang, T. Feng, Y. Li, Synthesis, structure–fluorescence relationships and density functional theory studies of novel naphthalimide–piperazine–pyridine-based polystyrene sensors for Hg(II) detection, RSC Adv. 10 (2020) 25281–25289, https://doi.org/10.1039/D0RA04557H.
[87] X. Zhang, W. Shi, X. Chen, Z. Xie, Isocyano-functionalized, 1,8-naphthalimide-based chromophore as efficient ratiometric fluorescence probe for Hg^{2+} in aqueous medium, Sens. Actuators B Chem. 255 (2018) 3074–3084, https://doi.org/10.1016/j.snb.2017.09.132.
[88] H. Zhang, C. Yin, T. Liu, Y. Zhang, F. Huo, "Turn-on" fluorescent probe detection of Ca^{2+} ions and applications to bioimaging, Spectrochim. Acta A Mol. Biomol. Spectrosc. 180 (2017) 211–216, https://doi.org/10.1016/j.saa.2017.03.023.
[89] Z. Li, W. Chen, L. Dong, Y. Song, R. Li, Q. Li, D. Qu, H. Zhang, Q. Yang, Y. Li, A novel ratiometric and reversible fluorescent probe based on naphthalimide for the detection of Al^{3+} and pH with excellent selectivity, New J. Chem. 44 (8) (2020) 3261–3267, https://doi.org/10.1039/C9NJ06309A.
[90] D. Sarkar, M. Chowdhury, P.K. Das, Naphthalimide based fluorescent organic nanoparticles in selective sensing of Fe^{3+} and as a diagnostic probe for Fe^{2+}/Fe^{3+} transition, J. Mater. Chem. B 9 (2) (2021) 494–507, https://doi.org/10.1039/D0TB02450C.
[91] Y. Wang, P.D. Mao, W.N. Wu, X.J. Mao, X.L. Zhao, Z.Q. Xu, Y.C. Fan, Z.H. Xu, A novel colorimetric and ratiometric fluorescent Cu^{2+} sensor based on hydrazone bearing 1,8-naphthalimide and pyrrole moieties, Sens. Actuators B Chem. 251 (2017) 813–820, https://doi.org/10.1016/j.snb.2017.05.134.
[92] S. Anbu, A. Paul, K. Surendranath, A. Sidali, A.J.L. Pombeiro, Naphthalimide-phenanthroimidazole incorporated new fluorescent sensor for "turn-on" Cu^{2+} detection in living cancer cells, J. Inorg. Biochem. 220 (2021) 111466, https://doi.org/10.1016/j.jinorgbio.2021.111466.
[93] D. Liu, M. Zhang, S. Fang, J. Shi, J. Zhang, L. Yin, G. Yang, H. Zhu, H. He, Naphthalimide based fluorescent sensor for Zn^{2+} with high selectivity and sensitivity and its imaging in living cells, Inorg. Chem. Commun. 113 (2020) 107798, https://doi.org/10.1016/j.inoche.2020.107798.
[94] S. Adhikari, S. Ta, A. Ghosh, S. Guria, A. Pal, M. Ahir, A. Adhikary, S.K. Hira, P.P. Manna, D. Das, A 1,8 naphthalimide anchor rhodamine B based FRET probe for ratiometric detection of Cr^{3+} ion in living cells, J. Photochem. Photobiol. A: Chem. 372 (2019) 49–58, https://doi.org/10.1016/j.jphotochem.2018.12.010.
[95] Y.L. Liu, L. Yang, L. Li, Y.Q. Guo, X.X. Pang, P. Li, F. Ye, Y. Fu, A new fluorescent chemosensor for cobalt(II) ions in living cells based on 1,8-naphthalimide, Molecules 24 (2019) 3093, https://doi.org/10.3390/molecules24173093.
[96] H. Zhang, T. Liu, C. Yin, Y. Wen, J. Chao, Y. Zhang, F. Huo, A novel ratiometric fluorescent probe based on 1, 8-naphthalimide for the detection of Ho^{3+} and its bioimaging, Spectrochim. Acta A Mol. Biomol. Spectrosc. 174 (2017) 230–235, https://doi.org/10.1016/j.saa.2016.11.039.
[97] L. Li, H. Li, G. Liu, S. Pu, A novel fluorescent sensor for Al^{3+} based on a new diarylethene with a naphthalimide unit, J. Photochem. Photobiol. A: Chem. 338 (2017) 192–200, https://doi.org/10.1016/j.jphotochem.2017.02.011.
[98] I.J. Chang, M.G. Choi, Y.A. Jeong, S.H. Lee, S.-K. Chang, Colorimetric determination of Cu^{2+} in simulated wastewater using naphthalimide-based Schiff base, Tetrahedron Lett. 58 (5) (2017) 474–477, https://doi.org/10.1016/j.tetlet.2016.12.066.
[99] H. Zhang, C. Yin, T. Liu, J. Chao, Y. Zhang, F. Huo, Selective "off-on" detection of magnesium (II) ions using a naphthalimide-derived fluorescent probe, Dyes Pigments 146 (2017) 344–351, https://doi.org/10.1016/j.dyepig.2017.07.033.
[100] X.L. Yue, C.R. Li, Z.Y. Yang, A novel Schiff-base fluorescent probe based on 1,8-naphthyridine and naphthalimide for Al^{3+}, Inorganica Chim. Acta. 464 (2017) 167–171, https://doi.org/10.1016/j.ica.2017.05.032.
[101] J.-C. Qin, Z.-H. Fu, L.-M. Tian, Z.-Y. Yang, Study on synthesis and fluorescence property of rhodamine–naphthalene conjugate, Spectrochim. Acta A Mol. Biomol. Spectrosc. 229 (2020) 117868, https://doi.org/10.1016/j.saa.2019.117868.
[102] A. Yildirim, M.B. Kocer, A.D. Demir, E. Arslan, M. Yilmaz, A bi-modal, cellulose-based sensor for fluorometric detection of Fe(III) and antimicrobial studies of its silver-loaded form, Int. J. Biol. Macromol. 183 (2021) 35–44, https://doi.org/10.1016/j.ijbiomac.2021.04.134.
[103] S. Hladysh, A. Murmiliuk, J. Vohlídal, J. Zedník, Attachment of a 1,8-naphthalimide moiety to a conjugated polythiophene efficiently improves the sensing abilities of naphthalimide-based materials, Macromol. Chem. Phys. 220 (3) (2019) 1800436, https://doi.org/10.1002/macp.201800436.
[104] S.O. Aderinto, A. New, Highly potent 1,8-naphthalimide-based fluorescence "turn off" chemosensor capable of Cu^{2+} detection in China's Yellow river water samples, J. Chin. Chem. Soc. 64 (2017) 1432–1445, https://doi.org/10.1002/jccs.201700308.
[105] Y. Xu, S.O. Aderinto, H. Wu, H. Peng, H. Zhang, J. Zhang, X. Fan, A highly selective fluorescent chemosensor based on naphthalimide and Schiff base units for Cu^{2+} detection in aqueous medium, Z. Naturforsch. B. 72 (2017) 35–41, https://doi.org/10.1515/znb-2016-0138.
[106] F. Ye, Q. Chai, X.M. Liang, M.Q. Li, Z.Q. Wang, Y. Fu, A highly selective and sensitive fluorescent turn-off probe for Cu^{2+} based on a guanidine derivative, Molecules 22 (2017) 1741. https://dx.doi.org/10.3390%2Fmolecules22101741.

[107] C.R. Li, Z.Y. Yang, S.L. Li, 1,8-Naphthalimide derived dual-functioning fluorescent probe for "turn-off" and ratiometric detection of Cu^{2+} based on two distinct mechanisms in different concentration ranges, J. Lumin. 198 (2018) 327–336, https://doi.org/10.1016/j.jlumin.2018.02.031.
[108] Y. Qu, Y. Wu, C. Wang, K. Zhao, H. Wu, A new 1,8-naphthalimide-based fluorescent "turn-off" sensor for detecting Cu^{2+} and sensing mechanisms, J. Chem. Res. 44 (1-2) (2020) 121–127, https://doi.org/10.1177/1747519819886540.
[109] H. Zhang, Y. Qu, K. Zhao, C. Wang, Y. Wu, H. Wu, A fluorescence "on–off" sensor for the highly selective and sensitive detection of Cu^{2+} ion, J. Chin. Chem. Soc. 67 (6) (2020) 1062–1069, https://doi.org/10.1002/jccs.201900337.
[110] G. Wenxun, Z. Yaqing, L.i. Botian, T. Liming, Fluorescent sensor of copper (II) ions based on PMBA microtubes with 4-methoxy-1,8-naphthalimide groups, React. Funct. Polym. 146 (2020) 104400, https://doi.org/10.1016/j.reactfunctpolym.2019.104400.
[111] G.R.C. Hamilton, S. Kaur, S. Kamila, B. Callan, J.F. Callan, A low affinity nanoparticle based fluorescent ratiometric probe for the determination of Zn (II) concentrations in living cells, New J. Chem. 42 (2018) 14986–14993, https://doi.org/10.1039/C7NJ04520D.
[112] P.A. Panchenko, P.A. Ignatov, M.A. Zakharko, Y.V. Fedorov, O.A. Fedorova, A fluorescent PET chemosensor for Zn^{2+} cations based on 4-methoxy-1,8-naphthalimide derivative containing salicylideneamino receptor group, Mendeleev Commun. 30 (1) (2020) 55–58, https://doi.org/10.1016/j.mencom.2020.01.018.
[113] P.A. Panchenko, Y.V. Fedorov, A.S. Polyakova, O.A. Fedorova, Fluorimetric detection of Ag^{+} cations in aqueous solutions using a polyvinyl chloride sensor film doped with crown-containing 1,8-naphthalimide, Mendeleev Commun. 31 (4) (2021) 517–519, https://doi.org/10.1016/j.mencom.2021.07.027.
[114] Y. Fu, X.X. Pang, Z.Q. Wang, H.T. Qu, F. Ye, Synthesis and fluorescent property study of novel 1,8-naphthalimide-based chemosensors, Molecules 23 (2018) 376, https://doi.org/10.3390/molecules23020376.
[115] A. Pal, M. Karmakar, S.R. Bhatta, A. Thakur, A detailed insight into anion sensing based on intramolecular charge transfer (ICT) mechanism: A comprehensive review of the years 2016 to 2021, Coord. Chem. Rev. 448 (2021) 214167, https://doi.org/10.1016/j.ccr.2021.214167.
[116] Y. Lou, Y. Zhao, J.-J. Zhu, Ultrasensitive optical detection of anions by quantum dots, Nanoscale Horiz. 1 (2) (2016) 125–134, https://doi.org/10.1039/C5NH00039D.
[117] Z. Xu, X. Chen, H.N. Kim, J. Yoon, Sensors for the optical detection of cyanide ion, Chem. Soc. Rev. 39 (1) (2010) 127–137, https://doi.org/10.1039/B907368J.
[118] S. Dhawan, H. Devnani, J. Babu, H. Singh, M.A. Haider, T.S. Khan, P.P. Ingole, V. Haridas, Supersensitive detection of anions in pure organic and aqueous media by amino acid conjugated Ellman's reagent, ACS Appl. Bio Mater. 4 (3) (2021) 2453–2464, https://doi.org/10.1021/acsabm.0c0143110.1021/acsabm.0c01431.s001.
[119] C. Li, C. Tang, L. Xing, B. Sun, S. Cheng, Q. Liao, B. Zhu, A highly selective colorimetric and fluorescent dual-modal probe for the rapid determination of fluoride anions, Luminescence 32 (6) (2017) 1051–1055, https://doi.org/10.1002/bio.3290.
[120] R. Shen, Y. Qian, A mitochondria-oriented fluorescent probe for ultrafast and ratiometric detection of HSO_3^- based on naphthalimide–hemicyanine, New J. Chem. 43 (43) (2019) 7606–7612, https://doi.org/10.1039/C9NJ01467E.
[121] K.R. Everitt, H.C. Schmitz, A. Macke, J. Shan, E. Jang, B.E. Luedtke, K.A. Carlson, H. Cao, Investigation of a sensing strategy based on a nucleophilic addition reaction for quantitative detection of bisulfite (HSO_3^-), J. Fluoresc. 30 (5) (2020) 977–983, https://doi.org/10.1007/s10895-020-02599-8.
[122] Y. Fu, H. Nie, R. Zhang, F. Xin, Y. Tian, J. Jing, X. Zhang, An ESIPT based naphthalimide chemosensor for visualizing endogenous $ONOO^-$ in living cells, RSC Adv. 8 (4) (2018) 1826–1832, https://doi.org/10.1039/C7RA11774D.
[123] L. Wang, W.T. Li, W.J. Qu, Y.Q. Fan, H. Yao, Q. Lin, T.B. Wei, Y.M. Zhang, A water soluble naphthalimide-based chemosensor for fluorescent detection CN^- in pure water and its application in practical samples, J. Braz. Chem. Soc. 29 (2018) 1563–1569, https://doi.org/10.21577/0103-5053.20180030.
[124] S.C. Lee, C. Kim, Naphthalimide-based probe for the detection of hypochlorite in a near-perfect aqueous solution, Anal. Sci. 35 (11) (2019) 1189–1193.
[125] A.S. Oshchepkov, R.R. Mittapalli, O.A. Fedorova, E.A. Kataev, Naphthalimide-based polyammonium chemosensors for anions: Study of binding properties and sensing mechanisms, Chem. Eur. J. 23 (40) (2017) 9657–9665, https://doi.org/10.1002/chem.201701515.
[126] A. Oshchepkov, M. Oshchepkov, S. Kamagurov, A. Redchuk, M. Oshchepkova, K. Popov, E. Kataev, Fluorescence detection of phosphonates in water by a naphthalimide-based receptor and its derived cryopolymers, New J. Chem. 44 (28) (2020) 12113–12121, https://doi.org/10.1039/D0NJ01734E.
[127] P. Yadav, H. Laddha, M. Agarwal, R. Gupta, Colorimetric assay of fluoride goes digital: On the spot testing of F^- ions in water using smartphone's digital imaging and test strip assay by a novel chromofluorogenic receptor based on 1,8-naphthalimide, J. Mol. Liq. 324 (2021) 114690, https://doi.org/10.1016/j.molliq.2020.114690.
[128] L. Yang, Y.-L. Liu, C.-G. Liu, Y. Fu, F. Ye, A naked-eye visible colorimetric and ratiometric chemosensor based on Schiff base for fluoride anion detection, J. Mol. Struct. 1236 (2021) 130343, https://doi.org/10.1016/j.molstruc.2021.130343.
[129] P. Yadav, H. Laddha, M. Agarwal, H.S. Kushwaha, R. Gupta, Studies on 1,8-naphthalimide derivative as a robust multi-responsive receptor for an array of low cost microanalytical techniques for selective prompt and on-site recognition of duplicitous fluoride in semi-aqueous medium, J. Fluor. Chem. 249 (2021) 109858, https://doi.org/10.1016/j.jfluchem.2021.109858.
[130] X. Yuan, X. Xu, C. Zhao, F. Zhang, Y. Lu, Y. Shen, C. Wang, A novel colorimetric and fluorometric fluoride ion probe based on photoinduced electron transfer signaling mechanism, Sens. Actuators B Chem. 253 (2017) 1096–1105, https://doi.org/10.1016/j.snb.2017.07.044.
[131] S. Lohar, A. Maji, S. Pal, S.K. Mukhopadhyay, D. Nag, N. Demitri, P. Chattopadhyay, Naphthalimide-based turn-on fluorosensor for aqueous sulfide ions for staining in living cells, ChemistrySelect 2 (31) (2017) 9977–9983, https://doi.org/10.1002/slct.201701351.
[132] Z. Zhang, J. Fan, Y. Zhao, Y. Kang, J. Du, X. Peng, Mitochondria-accessing ratiometric fluorescent probe for imaging endogenous superoxide anion in live cells and Daphnia magna, ACS Sensors 3 (3) (2018) 735–741, https://doi.org/10.1021/acssensors.8b0008210.1021/acssensors.8b00082.s001.
[133] S. Ma, Y. Ma, Q. Liu, W. Lin, A two-photon fluorescent probe with lysosome targetability for imaging endogenous superoxide anion in living cells, zebrafish and pneumonia tissue, Sens. Actuators B Chem. 332 (2021) 129523, https://doi.org/10.1016/j.snb.2021.129523.
[134] X. Yuan, C.X. Zhao, Y.X. Lu, Y.J. Shen, C.Y. Wang, A novel naphthalimide-based probe for highly sensitive and selective recognition of fluoride ion, J. Photochem. Photobiol. A: Chem. 361 (2018) 41–47, https://doi.org/10.1016/j.jphotochem.2018.05.005.
[135] L. Xiao, L. Ren, X. Jing, Z. Li, S. Wu, D. Guo, A selective naphthalimide-based colorimetric and fluorescent chemosensor for "naked-eye" detection of fluoride ion, Inorganica Chim. Acta 500 (2020) 119207, https://doi.org/10.1016/j.ica.2019.119207.
[136] X. Chen, T. Leng, C. Wang, Y. Shen, W. Zhu, A highly selective naked-eye and fluorescent probe for fluoride ion based on 1,8-naphalimide and benzothizazole, Dyes Pigm. 141 (2017) 299–305, https://doi.org/10.1016/j.dyepig.2017.02.008.
[137] C. Pati, K. Ghosh, A 1,8-naphthalimide–pyridoxal conjugate as a supramolecular gelator for colorimetric read out of F^- ions in solution, gel and solid states, New J. Chem. 43 (6) (2019) 2718–2725, https://doi.org/10.1039/C8NJ05626A.
[138] J. Kongwutthivech, T. Tuntulani, V. Promarak, B. Tomapatanaget, Naked-eye optical sensor based on imidazolium cation and napthalamide for specific detection of fluoride, J. Fluoresc. 30 (2020) 259–267, https://doi.org/10.1007/s10895-020-02494-2.
[139] T. Sheshashena Reddy, H. Moon, M.-S. Choi, Turn-on fluorescent naphthalimide-benzothiazole probe for cyanide detection and its two-mode aggregation-induced emission behavior, Spectrochim. Acta A Mol. Biomol. Spectrosc. 252 (2021) 119535, https://doi.org/10.1016/j.saa.2021.119535.
[140] S.C. Lee, C. Kim, Naphthol-naphthalimide based 'turn-on' fluorescent sensor for ClO^- in aqueous media and test kit, Inorg. Chem. Commun. 108 (2019) 107545, https://doi.org/10.1016/j.inoche.2019.107545.
[141] H.-L. Wu, S.O. Aderinto, Y.-L. Xu, H. Zhang, X.-Y. Fan, A highly selective fluorescent chemosensor for the detection of picrate anion based on 1,8-naphthalimide derivatives, J. Appl. Spectrosc. 84 (1) (2017) 25–30, https://doi.org/10.1007/s10812-017-0421-7.
[142] H. Liu, Y.u. Lei, A critical review: Recent advances in "digital" biomolecule detection with single copy sensitivity, Biosens. Bioelectron. 177 (2021) 112901, https://doi.org/10.1016/j.bios.2020.112901.
[143] X. Hou, Z. Li, Y. Li, Q. Zhou, C. Liu, D. Fan, J. Wang, R. Xu, Z. Xu, ICT-modulated NIR water-soluble fluorescent probe with large Stokes shift for selective detection of cysteine in living cells and zebrafish, Spectrochim Acta A Mol Biomol Spectrosc. 246 (2021) 119030, https://doi.org/10.1016/j.saa.2020.119030.
[144] Y. Zhuo, Y. Zhang, Y. Feng, Y. Xu, Q. You, L. Zhang, H. Huang, L. Lin, A 3,5-dinitropyridin-2yl substituted naphthalimide based fluorescent probe for the selective detection of biothiols and its application in cell-imaging, RSC Adv. 11 (16) (2021) 9290–9295, https://doi.org/10.1039/D1RA00010A.
[145] Y. Rong, C. Wang, P. Chuai, Y. Song, S. Zhou, P. Hou, X. Liu, L. Wei, X. Song, A naphthalimide-indole fused chromophore-based fluorescent probe for the detection of biothiol with red emission and a large Stokes shift, New J. Chem. 43 (33) (2019) 13212–13216, https://doi.org/10.1039/C9NJ02709B.
[146] Y. Tian, F. Xin, C. Gao, J. Jing, X. Zhang, Ratiometric fluorescence imaging of endogenous selenocysteine in cancer cell matrix, J. Mater. Chem. B 5 (33) (2017) 6890–6896, https://doi.org/10.1039/C7TB01558E.
[147] Z. Wang, C. Hao, X. Luo, Q. Wu, C. Zhang, W. Dessie, Y. Jiang, A FRET-ICT dual-modulated ratiometric fluorescence sensor for monitoring and bio-imaging of cellular selenocysteine, Molecules 25 (2020) 4999, https://doi.org/10.3390/molecules25214999.
[148] X. Zhao, G. Yuan, H. Ding, L. Zhou, Q. Lin, A TP-FRET-based fluorescent sensor for ratiometric visualization of selenocysteine derivatives in living cells, tissues and zebrafish, J. Hazard. Mater. 381 (2020) 120918, https://doi.org/10.1016/j.jhazmat.2019.120918.
[149] D. Aydin, S.N. Karuk Elmas, G. Akin Geyik, A. Bostanci, F.N. Arslan, T. Savran, G. Sadi, I. Yilmaz, 1,8-Naphthalimide appended propiolate-based fluorescent sensor for selective detection of cysteine over glutathione and homocysteine in living cells, New J. Chem. 45 (36) (2021) 16617–16624, https://doi.org/10.1039/D1NJ03317D.

[150] M. Verma, N. Kaur, N. Singh, Naphthalimide-based DNA-coupled hybrid assembly for sensing dipicolinic acid: A biomarker for Bacillus anthracis spores, Langmuir 34 (22) (2018) 6591–6600, https://doi.org/10.1021/acs.langmuir.8b0034010.1021/acs.langmuir.8b00340.s001.
[151] A.K. Ghosh, P. Choudhury, P.K. Das, Fabrication of orange-emitting organic nanoparticle-protamine conjugate: Fluorimetric sensor of heparin, Langmuir 35 (47) (2019) 15180–15191, https://doi.org/10.1021/acs.langmuir.9b0241410.1021/acs.langmuir.9b02414.s001.
[152] H. Zhu, H. Zhang, C. Liang, C. Liu, P. Jia, Z. Li, Y. Yu, X. Zhang, B. Zhu, W. Sheng, A novel highly sensitive fluorescent probe for bioimaging biothiols and its applications in distinguishing cancer cells from normal cells, Analyst 144 (23) (2019) 7010–7016, https://doi.org/10.1039/C9AN01760G.
[153] J. Zheng, J. Cao, Y. Tu, S. Wang, Detection of heparin by fluorescent sensor based on naphthalimide derivatives in human serum, Dyes Pigm. 181 (2020) 108632, https://doi.org/10.1016/j.dyepig.2020.108632.
[154] Y. Yu, J. Yang, X. Xu, Y. Jiang, B. Wang, A novel fluorescent probe for highly sensitive and selective detection of cysteine and its application in cell imaging, Sens. Actuators B Chem. 251 (2017) 902–908, https://doi.org/10.1016/j.snb.2017.05.150.
[155] J. Singh Sidhu, A. Singh, N. Garg, N. Kaur, N. Singh, A highly selective naphthalimide-based ratiometric fluorescent probe for the recognition of tyrosinase and cellular imaging, Analyst 143 (18) (2018) 4476–4483, https://doi.org/10.1039/C8AN01136B.
[156] J.S. Sidhu, N. Singh, FRET and PET paired dual mechanistic carbon dots approach for tyrosinase sensing, J. Mater. Chem. B 6 (24) (2018) 4139–4145, https://doi.org/10.1039/C8TB00512E.
[157] A. Podder, V.P. Murali, S. Deepika, A. Dhamija, S. Biswas, K.K. Maiti, S. Bhuniya, NADH-activated dual-channel fluorescent probes for multicolor labeling of live cells and tumor mimic spheroids, Anal. Chem. 92 (18) (2020) 12356–12362, https://doi.org/10.1021/acs.analchem.0c0204910.1021/acs.analchem.0c02049.s001.
[158] J.S. Sidhu, A. Singh, N. Garg, N. Singh, Carbon dot based, naphthalimide coupled FRET pair for highly selective ratiometric detection of thioredoxin reductase and cancer screening, ACS Appl. Mater. Interfaces 9 (31) (2017) 25847–25856, https://doi.org/10.1021/acsami.7b0704610.1021/acsami.7b07046.s001.
[159] L. Feng, P. Li, J. Hou, Y.-L. Cui, X.-G. Tian, Z.-L. Yu, J.-N. Cui, C. Wang, X.-K. Huo, J. Ning, X.-C. Ma, Identification and isolation of glucosytransferases (GT) expressed fungi using a two-photon ratiometric fluorescent probe activated by GT, Anal. Chem. 90 (22) (2018) 13341–13347, https://doi.org/10.1021/acs.analchem.8b0285710.1021/acs.analchem.8b02857.s001.
[160] S. Mondal, K. Ghosh, Naphthalimide-linked bispyridinium clefts in selective aqueous sensing of triphosphate and triphosphate-based biomolecules, Anal. Methods 11 (46) (2019) 5864–5871, https://doi.org/10.1039/C9AY01588D.
[161] S. Mangalath, S. Abraham, J. Joseph, pH-Responsive fluorescence enhancement in graphene oxide-naphthalimide nanoconjugates: A fluorescence turn-on sensor for acetylcholine, Chem. Eur. J. 23 (47) (2017) 11404–11409, https://doi.org/10.1002/chem.201702198.
[162] D. Staneva, E. Vasileva-Tonkova, P. Bosch, I. Grabchev, A new green fluorescent tripod based on 1,8-naphthalimide. Detection ability for metal cations and protons and antimicrobial activity, J. Photochem. Photobiol. A: Chem. 344 (2017) 143–148, https://doi.org/10.1016/j.jphotochem.2017.04.037.
[163] H.J. Jang, J.H. Kang, D. Yun, C. Kim, A multi-responsive naphthalimide-based "turn-on" fluorescent chemosensor for sensitive detection of trivalent cations Ga^{3+}, Al^{3+} and Cr^{3+}, J. Fluoresc. 28 (3) (2018) 785–794, https://doi.org/10.1007/s10895-018-2240-5.
[164] F. Ye, N. Wu, P. Li, Y.-L. Liu, S.-J. Li, Y. Fu, A lysosome-targetable fluorescent probe for imaging trivalent cations Fe^{3+}, Al^{3+} and Cr^{3+} in living cells, Spectrochim. Acta A Mol. Biomol. Spectrosc. 222 (2019) 117242, https://doi.org/10.1016/j.saa.2019.117242.
[165] X. Cao, N.a. Zhao, A. Gao, Q. Ding, Y. Li, X. Chang, Terminal molecular isomer-effect on supramolecular self-assembly system based on naphthalimide derivative and its sensing application for mercury(II) and iron(III) ions, Langmuir 34 (25) (2018) 7404–7415, https://doi.org/10.1021/acs.langmuir.8b0099110.1021/acs.langmuir.8b00991.s001.
[166] N.I. Georgiev, M.D. Dimitrova, A.T. Mavrova, V.B. Bojinov, Synthesis, fluorescence-sensing and molecular logic of two water-soluble 1,8-naphthalimides, Spectrochim. Acta A Mol. Biomol. Spectrosc. 183 (2017) 7–16, https://doi.org/10.1016/j.saa.2017.04.016.
[167] Q.i. Lin, K.-P. Zhong, J.-H. Zhu, L. Ding, J.-X. Su, H. Yao, T.-B. Wei, Y.-M. Zhang, Iodine controlled pillar[5]arene-based multiresponsive supramolecular polymer for fluorescence detection of cyanide, mercury, and cysteine, Macromolecules 50 (20) (2017) 7863–7871, https://doi.org/10.1021/acs.macromol.7b0183510.1021/acs.macromol.7b01835.s001.
[168] R. Kavitha, T. Stalin, Dual emission and pH based naphthalimide derivative fluorescent sensor for the detection of Bi^{3+}, Sens. Actuators B Chem. 247 (2017) 632–640, https://doi.org/10.1016/j.snb.2017.03.043.
[169] L.i. Wang, W.-T. Li, W.-J. Qu, J.-X. Su, Q.i. Lin, T.-B. Wei, Y.-M. Zhang, A highly selective fluorescent chemosensor for successive detection of Fe^{3+} and CN^- in pure water, Supramol. Chem. 29 (7) (2017) 489–496, https://doi.org/10.1080/10610278.2016.1277586.
[170] Y.-M. Zhang, B.-B. Han, P.-P. Mao, J.-F. Chen, H. Yao, T.-B. Wei, Q.i. Lin, A novel fluorescent sensor based on 4-(diethylamino)-2-(hydroxy)-phenyl imine functionalized naphthalimide for highly selective and sensitive detection of CN^- and Fe^{3+}, Can. J. Chem. 97 (8) (2019) 597–602, https://doi.org/10.1139/cjc-2018-0138.
[171] Y.-M. Zhang, X.-P. Chen, G.-Y. Liang, K.-P. Zhong, H. Yao, T.-B. Wei, Q.i. Lin, A water-soluble fluorescent chemosensor based on Asp functionalized naphthalimide for successive detection Fe^{3+} and $H_2PO_4^-$, Can. J. Chem. 96 (4) (2018) 363–370, https://doi.org/10.1139/cjc-2017-0451.
[172] P.X. Liu, H. Chen, N. Xu, H.N. Wang, X. Meng, Z.Y. Zhou, Z.M. Su, A new "turn-on" fluorescent sensor for highly selective sensing of $H_2PO_4^-$, Inorg. Chem. Commun. 79 (2017) 60–64, https://doi.org/10.1016/j.inoche.2017.03.015.
[173] S. Zhang, Y. Gu, Z. Shi, N. Lu, H. Xu, A novel reversible fluorescent probe based on naphthalimide for sequential detection of aluminum (Al^{3+}) and fluoride (F^-) ions and its applications, Anal. Methods 13 (44) (2021) 5360–5368, https://doi.org/10.1039/D1AY01545A.
[174] G. Kumar, I. Singh, R. Goel, K. Paul, V. Luxami, Dual-channel ratiometric recognition of Al^{3+} and F^- ions through an ESIPT-ESICT signalling mechanism, Spectrochim. Acta A Mol. Biomol. Spectrosc. 247 (2021) 119112, https://doi.org/10.1016/j.saa.2020.119112.
[175] S.K. Dwivedi, R.C. Gupta, P. Srivastava, P. Singh, B. Koch, B. Maiti, A. Misra, Dual fluorophore containing efficient photoinduced electron transfer based molecular probe for selective detection of Cr^{3+} and PO_4^{3-} ions through fluorescence "turn–on–off" response in partial aqueous and biological medium: Live cell imaging and logic application, Anal. Chem. 90 (18) (2018) 10974–10981, https://doi.org/10.1021/acs.analchem.8b0257010.1021/acs.analchem.8b02570.s001.
[176] X.J. Sun, T.T. Liu, H. Fu, N.N. Li, Z.Y. Xing, F. Yang, A naphthalimide-based fluorescence "off-on-off" chemosensor for relay detection of Al^{3+} and ClO^-, Front. Chem. 7 (2019) 1–13, https://doi.org/10.3389/fchem.2019.00549.
[177] S. Wang, H. Ding, Y. Wang, C. Fan, Y. Tu, G. Liu, S. Pu, An "off–on–off" sensor for sequential detection of Cu^{2+} and hydrogen sulfide based on a naphthalimide–rhodamine B derivative and its application in dual-channel cell imaging, RSC Adv. 8 (58) (2018) 33121–33128, https://doi.org/10.1039/C8RA05963B.
[178] K.B. Li, W.P. Jia, D.M. Han, D.X. Liang, X.P. He, G.R. Chen, Fluorogenic bis-triazolyl galactoprobe-metal complex for full-aqueous analysis of sulfide ion, Sens. Actuators B Chem. 246 (2017) 197–201, https://doi.org/10.1016/j.snb.2017.02.082.
[179] M.V. Oshchepkova, M.S. Oshchepkov, O.A. Fedorova, Y.V. Fedorov, V.I. Lozinskii, New copolymer gels based on N, N-dimethylacrylamide and crown-containing allyl derivative of 1,8-naphthalimide as optical sensors for metal cations in an organic medium, Dokl. Phys. Chem. 476 (2) (2017) 181–185, https://doi.org/10.1134/S0012501617100050.
[180] A. Narula, C.P. Rao, Fluorophoric conjugate of N alkyl naphthalimide in sodium dodecyl sulfate as a tunable and sustainable sensing system: Differential sensing of Zn^{2+} and Al^{3+} and the application of its Zn^{2+} complex in detecting dipicolinic acid, a component of anthrax bacterial endospores, J. Phys. Chem. C 123 (34) (2019) 21271–21280, https://doi.org/10.1021/acs.jpcc.9b0534910.1021/acs.jpcc.9b05349.s001.
[181] A.J. Blok, M.R. Johnston, C.E. Lenehan, Insights into the complexation of N-Allyl-4-(4-(N-phenylureido) benzylamino)-1,8-naphthalimide with various anions, Sci. Rep. 7 (2017) 2512, https://doi.org/10.1038/s41598-017-02470-0.
[182] X. Yan, H. Lan, Y. Li, X. Yan, Q. Xing, W. Wang, J. Zhang, S. Xiao, High-contrast colourimetric probes for fluoride and trace water based on tautomerization of naphthalimide and application in fingerprint imaging, Spectrochim. Acta A Mol. Biomol. Spectrosc. 254 (2021) 119674, https://doi.org/10.1016/j.saa.2021.119674.
[183] S. Ghosh, N. Baildya, N.N. Ghosh, K. Ghosh, Naphthalimide-decorated imino-phenol: supramolecular gelation and selective sensing of Fe^{3+} and Cu^{2+} ions under different experimental conditions, New J. Chem. 45 (11) (2021) 5213–5220, https://doi.org/10.1039/D1NJ00259G.
[184] Y. Fu, C. Fan, G. Liu, S. Pu, A colorimetric and fluorescent sensor for Cu^{2+} and F^- based on a diarylethene with a 1,8-naphthalimide Schiff base unit, Sens. Actuators B Chem. 239 (2017) 295–303, https://doi.org/10.1016/j.snb.2016.08.020.
[185] N. Saini, N. Prigyai, C. Wannasiri, V. Ervithayasuporn, S. Kiatkamjornwong, Green synthesis of fluorescent N, O-chelating hydrazone Schiff base for multi-analyte sensing in Cu^{2+}, F^- and CN^- ions, J. Photochem. Photobiol. A: Chem. 358 (2018) 215–225, https://doi.org/10.1016/j.jphotochem.2018.03.018.
[186] N. Wu, L.-X. Zhao, C.-Y. Jiang, P. Li, Y. Liu, Y. Fu, F. Ye, A naked-eye visible colorimetric and fluorescent chemosensor for rapid detection of fluoride anions: Implication for toxic fluorine-containing pesticides detection, J. Mol. Liq. 302 (2020) 112549, https://doi.org/10.1016/j.molliq.2020.112549.
[187] C. Jiang, X. Ye, N. Wu, P. Li, L. Yang, Y. Liu, Y. Fu, F. Ye, Development and application of fluorescent probes for the selective and sensitive detection of F^- and oxyfluorfen, Inorg. Chim. Acta 522 (2021) 120362, https://doi.org/10.1016/j.ica.2021.120362.
[188] R. Goel, S. Sharma, K. Paul, V. Luxami, Naphthalimide based chromofluorescent sensor and DNA intercalator: Triggered by Hg^{2+}/HSO_4^- cleavage reaction, Sens. Actuators B Chem. 246 (2017) 776–782, https://doi.org/10.1016/j.snb.2017.02.090.
[189] S.K. Dwivedi, R. Ali, M. Singh, T. Gupta, A.K. Kar, V. Prakash, A. Sadasivam, S. Patnaik, A. Misra, A simple naphthalimide based PET probe for Fe^{3+} and selective detection of pyrophosphate through displacement approach: Cell imaging studies and logic interpretation, J. Photochem. Photobiol. A: Chem. 403 (2020) 112854, https://doi.org/10.1016/j.jphotochem.2020.112854.

[190] M. Li, H. Ge, V. Mirabello, R.L. Arrowsmith, G. Kociok-Köhn, S.W. Botchway, W. Zhu, S.I. Pascu, T.D. James, Lysosomal tracking with a cationic naphthalimide using multiphoton fluorescence lifetime imaging microscopy, Chem. Commun. 53 (81) (2017) 11161–11164, https://doi.org/10.1039/C7CC05166B.

[191] N. Mergu, J.H. Moon, H. Kim, G. Heo, Y.A. Son, Highly selective naphthalimide-benzothiazole hybrid-based colorimetric and turn on fluorescent chemosensor for cyanide and tryptophan detection in aqueous media, Sens. Actuators B Chem. 273 (2018) 143–152, https://doi.org/10.1016/j.snb.2018.05.165.

[192] X. Pang, J. Ge, X. Yu, Y. Li, F. Shen, Y. Wang, J. Ren, An "off–on" fluorescent naphthalimide-based sensor for anions: Its application in visual F^- and AcO^- discrimination in a self-assembled gel state, New J. Chem. 43 (26) (2019) 10554–10559, https://doi.org/10.1039/C9NJ01687B.

[193] S. Shi, P.-Y. Gu, S. Zhou, Y. Zhu, J. He, Q. Xu, J. Lu, Naphthalimide-based hydrazone derivatives: synthesis, mechanochromism in the solid state and response to ions in dilute solutions, ChemPlusChem 86 (1) (2021) 103–109, https://doi.org/10.1002/cplu.202000764.

[194] L. Wu, S. Qi, Y. Liu, X. Wang, L. Zhu, Q. Yang, J. Du, H. Xu, Y. Li, A novel ratiometric fluorescent probe for differential detection of HSO^{3-} and ClO^- and application in cell imaging and tumor recognition, Anal. Bioanal. Chem. 413 (4) (2021) 1137–1148, https://doi.org/10.1007/s00216-020-03077-7.

[195] L. Tan, H. Ding, S. Chanmungkalakul, L. Peng, G. Yuan, Q. Yang, X. Liu, L. Zhou, A smart TP-FRET-based ratiometric fluorescent sensor for bisulfite/formaldehyde detection and its imaging application, Sens. Actuators B Chem. 345 (2021) 130331, https://doi.org/10.1016/j.snb.2021.130331.

[196] S. Naha, S.-P. Wu, S. Velmathi, Naphthalimide based smart sensor for CN^-/Fe^{3+} and H_2S. Synthesis and application in RAW264.7 cells and zebrafish imaging, RSC Adv. 10 (15) (2020) 8751–8759, https://doi.org/10.1039/C9RA07998J.

[197] B. Guo, X. Pan, Y. Liu, L. Nie, H. Zhao, Y. Liu, J. Yahoo, X. Zhang, A reversible water-soluble naphthalimide-based chemosensor for imaging of cellular copper (II) ion and cysteine, Sens. Actuators B Chem. 256 (2018) 632–638, https://doi.org/10.1016/j.snb.2017.09.196.

[198] Z. Xie, Y. Zhou, M. Fu, L. Ni, Y. Tong, Y. Yu, N.a. Li, Z. Yang, Q. Zhu, J. Wang, A 1,8-naphthalimide-based lysosome-targeting dual-analyte fluorescent probe for the detection of pH and palladium in biological samples, Talanta 231 (2021) 122365, https://doi.org/10.1016/j.talanta.2021.122365.